DELFT UNIVERSITY OF TECHNOLOGY

ARUP

Time-Dependent Capacity of Driven Displacement Piles in Sand

Erik Beutick

TUDelft

ARUP

Time-Dependent Capacity of Driven Displacement Piles in Sand

by

Erik Beutick

in partial fulfillment of the requirements for the degree of

Master of Science

at Delft University of Technology

November 21, 2017

Graduation committee:

Prof. dr. K.G. Gavin	TU Delft
Dr. C. Reale	TU Delft
Ing. H.J. Everts	TU Delft
Dr. ing. M.Z. Voorendt	TU Delft
Ir. J. Oudhof	Arup

An electronic version of this thesis is available at
`https://repository.tudelft.nl/`

TUDelft

ARUP

Preface

This thesis is the final product of my graduation research, performed in order to complete the master degree in Civil Engineering with a specialization in Geo-Engineering at Delft University of Technology. I would like to use this opportunity to thank some people for their contribution.

First of all I would like to thank the graduation committee. Their support, knowledge and experience challenged me to give my utmost best and improved the value of this final product. In special I would like to thank Jessica Oudhof for her support during the entire process of the research.

Further I would like to thank the infrastructure department of the Arup Amsterdam office for the pleasant work environment. The relaxed and positive atmosphere at the office contributed to the joy I had while working on my thesis.

I would also like to thank Patrick IJnsen for his enthusiasm and for providing me with the opportunity to be involved in a pile test program. Being involved from start to end gave great knowledge and insight in pile testing and helped understanding the data.

Last but not least I would like to thank my parents for their support during my entire studies and for providing me with the opportunities to achieve my goals.

Erik Beutick
Amsterdam, November '17

Abstract

A time-dependent capacity *increase* has often been observed for driven displacement piles in sand. Long-term bearing capacity increase after dissipation of excess pore water pressure is referred to as set-up. Significant increases in axial capacity have been reported where the rate of set-up varied between 15 and 75% per log cycle of time. The time-dependent capacity increase is attributed to an increase in shaft capacity. The tip capacity was found to be constant in time.

More economic foundation designs are feasible when set-up is incorporated in pile design methods. The objective of this thesis is to expand knowledge on time-dependent capacity of driven displacement piles and make way for a pile design method that incorporates time dependency of pile bearing capacity.

The time dependency of virgin pile capacity has been assessed in a database study and a scaled test program. 4 scaled closed-ended steel piles were driven in a man made sand deposit. The virgin capacity of a pile was assessed 2, 16, 31 and 70 days after installation. The 3 m long, 0.15 m diameter piles were statically tested in compression. Strain was measured at multiple locations along the shaft during the load tests. The applied load and pile displacement were measured at the pile head.

The contribution of the pile shaft and pile tip was determined from the strain distribution over the pile length at failure. A trend for capacity increase with time has been found in the database study and the test program. A capacity increase of 13% per log cycle of time was found for the closed-ended piles tested. Both an increase in shaft and tip resistance was found with respect to the reference capacity determined 2 days after installation. The shaft capacity increased on average 18.5% per log cycle of time and an average increase of 9% per log cycle of time has been found for the pile tip capacity.

The measured capacity was compared with the calculated capacity determined by the Dutch design code. Considering the measured capacity normalized by the calculated capacity the influence of time is even stronger on the tip capacity than on the shaft capacity for the piles tested. As discussed in the report, there are some uncertainties with the interpretation of the strain distributions over the pile shafts.

The accuracy of the CPT-based design method available in the Dutch design code, method Koppejan, has been assessed from the pile test results in the database. The results were compared with other design methods available. The accuracy of all methods was low. The calculated capacity exceeded the measured capacity up to a factor 3.

Time-dependent capacity increase is a potential mechanism to incorporate in designs of axially loaded driven displacement piles. A trend for time-dependent increase of virgin capacity was found for all the test results considered in literature as well as for the test program conducted. However, the rate of capacity increase was highly variable. More research is required on the mechanism(s) for a better understanding of time-dependent capacity increase. Understanding of the mechanisms will also help understand what factors, and how these factors, influence the rate of increase. Research by a standardized method will reduce the scatter in the database and better indicate the time-dependent bearing capacity of axially loaded driven displacement piles.

Keywords:
Time-dependent, bearing capacity, set-up, driven, piles, sand, fresh deposit, closed-ended piles, steel piles, virgin capacity, test program, static load test, database

Contents

List of Figures

List of Tables

List of Symbols and Abbreviations

α_p	Calculation factor for tip resistance [-]
α_s	Calculation factor for shaft resistance [-]
β	Dimensionless shaft capacity factor [-]
δ	Interface friction angle [°]
ϵ	strain [-]
γ	Volume weight [kN/m^3]
ϕ	Soil friction angle [°]
σ_h	Stress in horizontal direction [kPa]
σ_v	Stress in vertical direction [kPa]
A	Surface area [m^2]
A_b	Tip surface [m^2]
A_s	Shaft surface [m^2]
D	Pile diameter [m]
D_{eq}	Equivalent pile diameter [m]
E	Young's modulus [kPa]
F	Force [kN]
f_b	Empirical factor for installation effects, soil type, pile type and geometry [-]
f_s	Empirical factor for installation effects, soil type, pile type and geometry [-]
h	Relative height above pile tip [m]
K	Lateral earth pressure coefficient [-]
K_0	At rest earth pressure coefficient [-]
K_p	Passive earth pressure coefficient [-]
L	Pile length [m]
n	porosity [-]
N_q	Dimensionless tip capacity factor [-]
Q_0	Pile capacity at reference time t_0 [kN]
q_b	Tip resistance [kPa]
q_s	Shaft resistance [kPa]
Q_t	Pile capacity at time t [kN]
Q_u	Ultimate capacity with 100% of setup realized [kN]

$q_{c;avg}$	Average cone resistance [kPa]
Q_c	Calculated capacity[kN]
Q_{EOID}	Pile capacity at End Of Initial Driving [kN]
Q_m	Measured capacity [kN]
R	Pile radius [m]
R_b	Calculated tip capacity [kN]
R_s	Calculated shaft capacity [kN]
s	horizontal displacement [m]
t	Time after the end of initial driving [days]
t_0	Initial reference time elapsed since end of driving [days]
z	Depth [m]
API	American Petroleum Institute
CPT	Cone Penetration Test
EOID	End Of Initial Driving
ICP	Imperial College Pile
NGI	Norwegian Geotechnical Institute
PDA	Pile Driving Analysis
UWA	University of Western Australia

1 | Introduction

Past studies have indicated that the axial bearing capacity of driven displacement piles in sand may increase significantly over time (Axelsson, 2000; Chow et al., 1998; Gavin et al., 2013; Karlsrud et al., 2014). For piles installed below the groundwater level the capacity increases for some period of time after installation due to dissipation of excess pore water pressure. In sand this process is expected to take no more than several hours after installation while capacity increases have been observed for weeks up to years after installation. Time-dependent capacity increase after dissipation of excess pore water pressure is the topic of this thesis and is often referred to as set-up.

Motivation

Generally piles are not loaded directly after installation. Especially pile foundations of large structures (e.g. bridges, high rise buildings) will not experience their full design load prior than several weeks up to months after installation. This makes inclusion of time effects on the pile capacity appealing for foundation designs. Incorporating time-dependent capacity in foundation designs might lead to more economic designs due to less piles, lighter material and/or reduced construction time.

For decades time-dependent changes in bearing capacity have been acknowledged for driven displacement piles in sand. In recent years time-dependent pile capacity gained more attention in both on- and offshore foundation designs.

With the rise of offshore renewable energy more and more offshore foundations are constructed. Incorporating capacity dependency of time in the foundation designs might lead to more economic foundations.

The interest in time dependency of capacity for onshore foundations increased in the Netherlands after the introduction of the new Dutch code for foundation design, Eurocode NEN9997-1 (2016). Validation of the Dutch method for calculating tip resistance proved that the Dutch calculation method overestimated the actual tip resistance. The measured resistance was on average only 67% of the calculated resistance (CUR B&I, 2010; Van Tol et al., 2010). With the introduction of the new code the calculation factor for tip resistance (α_p) was reduced from 1.0 to 0.7 for driven displacement piles. Thus, the new code prescribed a more conservative calculation method than previous editions. Research by Deltares (Stoevelaar et al., 2012) on potential unconsidered contributions to pile capacity indicated set-up as a potential effect to compensate for the reduced calculation factor.

Scope

The objective of this thesis is to expand knowledge on time-dependent capacity of driven displacement piles and make way for a pile design method that incorporates time dependency of pile capacity.

The research consists of three parts:

1. Evaluating time-dependent capacity, and pile capacity in general, in an extensive literature review.
2. Collect available test results and assess set-up and the accuracy of common pile design methods.
3. Conduct tests to determine the time-dependent capacity of scaled closed-ended steel piles in a fresh sand deposit.

In this study the focus is on time-dependent capacity of vertically installed displacement piles, driven in sand and axially loaded. The load might be applied either in tension, or compression. In the database and test program the virgin capacity of piles is evaluated. This means that the piles had not been subjected to significant loads prior to the load test where the pile is loaded to failure.

Definition

There are different understandings of the term "set-up", sometimes the term is used in combination with an object like "pile set-up" or "soil set-up". When set-up is mentioned in this thesis it refers to the long-term pile bearing capacity increase after dissipation of excess pore water pressure.

Report Outline

This thesis consists of three parts. The first part, Chapter 2 and 3, consists of the theoretical background considering (time-dependent) pile capacity and pile design methods. The second part, Chapter 4 and 5 consists of a database study. A database is compiled from the results of static load test on driven displacement piles in sand. The accuracy of pile design methods is assessed as well as the development of pile capacity with time. The last and main part, Chapter 6 and 7, elaborates a scaled test program on time-dependent capacity. Four instrumented closed-ended steel piles are driven in a man made sand deposit and tested at different moments after installation. A section with concluding remarks is provided at the end of each part. The conclusions and recommendations are elaborated in the last Chapter, Chapter 8.

2 | Pile Foundations

Pile foundations represent the most general and widespread method of deep foundations in the Netherlands. In delta areas, like the Netherlands, the soil often consists of layers of soft soil (peat and/or clay) on top of a stiff sand layer. The sand layer is commonly a suitable foundation layer due to its high density and friction angle. Figure 2.1 illustrates various examples of pile foundations both on land and offshore.
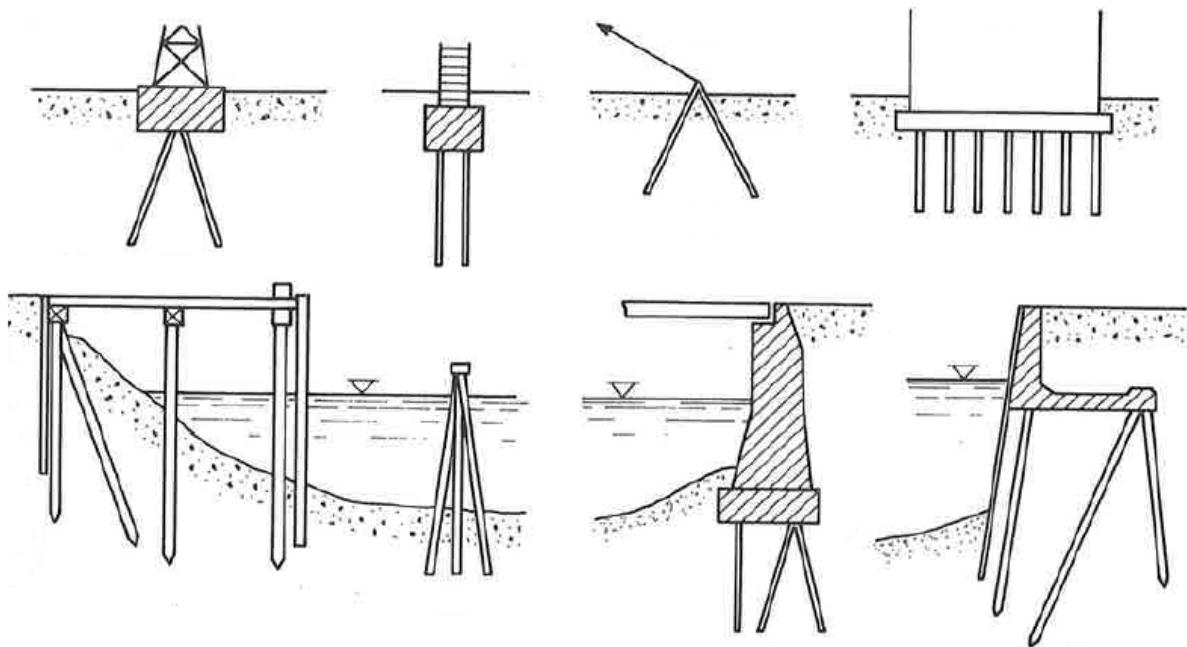
Figure 2.1: Examples of pile foundations (Winterkorn and Fang, 1975), *modified*

Piles can be installed vertical or slanting and can be loaded axially and/or horizontally. Loads on a pile consist of permanent and variable loads transferred to the piles by the superstructure. These loads are generally transferred to the subsurface by frictional forces at the pile shaft a reaction force at the pile tip.

There are various pile types, all have a relative small cross sectional dimension compared to their length. Historically wooden piles were used, modern materials are steel and (reinforced) concrete. Generally piles have a uniform or tapered cross section, common shapes are circular, octagonal, hexagonal, square or H-shaped. The pile surface may either be smooth or rough and the pile tip is flat or conical and might have an enlarged cross section compared to the pile shaft. Other, less common, configurations are also practicable (Winterkorn and Fang, 1975).

Like pile types there is also a large selection of installation methods available. Distinction is made between piles installed by soil replacement and piles installed by soil displacement. For replacement piles the soil is removed prior to installation using a wide range of drilling techniques. For displacement piles there is no soil removal, instead the soil is displaced into the surrounding soil mass. Displacement piles are generally jacked, driven or vibrated into the ground (Tomlinson and Woodward, 2015).

2.1 Pile Bearing Capacity

The capacity of a pile is generally defined by the resistance of the pile to a set displacement at the pile tip. The total bearing capacity of an axially loaded pile in compression is determined by the sum of the base and shaft resistance. Base, or tip resistance is the resistance formed at the base of the pile, determined by the soil bearing resistance and the pile tip surface and shape. The bearing capacity of an axially loaded pile in tension is usually only determined by its shaft resistance. The base contribution is generally negligible in tension. Shaft resistance is the resistance derived by soil-shaft interaction. Friction generated at the pile shaft does not always contribute to the pile bearing capacity. Consolidation may cause an opposite effect and increase the load on a pile due to soil layers "hanging" on the pile. The left image in Figure 2.2 demonstrates a positive contribution of the shaft resistance to the total bearing capacity and the right image demonstrates a negative contribution due to consolidation. Consolidation is likely to occur when the pile crosses a compressible soil layer. The geological history of the Netherlands generally cause piles to cross a stratified soil profile where the pile tip is driven into a dense sand layer.

The capacity of a pile in sand depends on multiple factors (Tomlinson and Woodward, 2015; Winterkorn and Fang, 1975):

Soil characteristics

- Friction angle
- Density
- Stress state
- Strength and uniformity of sand particles

Pile characteristics

- Pile surface roughness
- Pile geometry
- Relative installation depth (L/D ratio)

Installation

- Installation method

Load characteristics

- Load type
- Loading rate
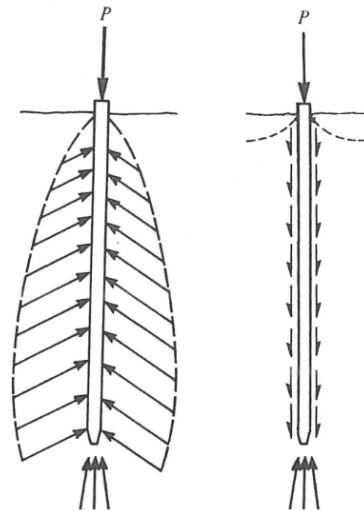
Figure 2.2: **Left**: Positive contribution of shaft resistance to the pile bearing capacity - **Right**: Negative contribution of shaft resistance to the pile bearing capacity (Winterkorn and Fang, 1975), *modified*

The method of installation and loading rate are expected to have a dominant role in the shaft capacity of a pile and will be further elaborated.

Installation Effects

Installation of a pile affects the initial soil stress state. The stress state of the soil surrounding a pile partly determines the pile shaft capacity, thereby the installation method has a strong influence on the pile shaft capacity.

A reduced soil stress state (relaxation) at the pile shaft is generally found after installation of a replacement pile, for displacement piles the opposite effect is often observed. During installation of a displacement pile soil is predominantly displaced outward into the surrounding soil mass increasing local soil stresses. The extend of the influenced zone surrounding the pile depends on the soil conditions, pile geometry and installation method. Piles driven in medium dense sand usually drag along a thin layer of sand and compress the lateral soil mass as presented in Figure 2.3. When stresses are very high soil particles might be crushed. Lateral displacement of the soil causes a decrease in porosity and an increase in friction angle as presented in Figure 2.4. Often a stress arch surrounding the pile is formed. Figure 2.3 and Figure 2.4 present the results for specific test conditions and not a general law. For this specific test the horizontal displacement decreased according to a parabolic law and the diameter of the disturbed zone around the pile was approximately 6 times the diameter of the pile (Winterkorn and Fang, 1975).
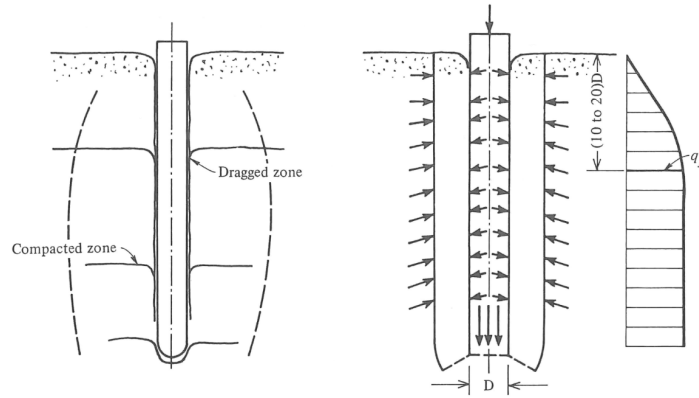
Figure 2.3: Deformation zone for a pile driven in medium dense sand (Winterkorn and Fang, 1975)
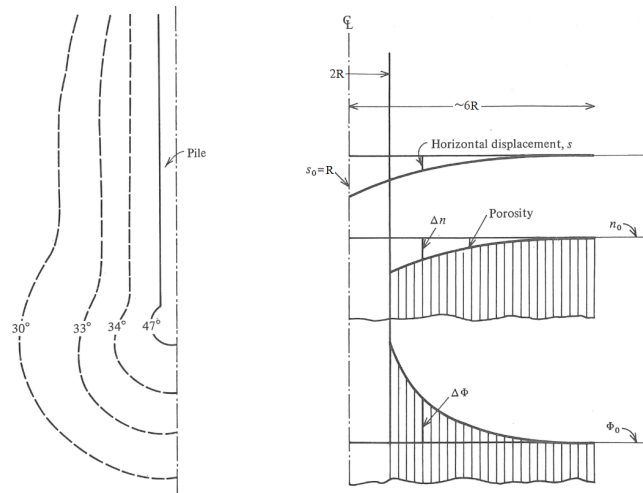
Figure 2.4: Change in soil parameters in the vicinity of a pile due to driving (Winterkorn and Fang, 1975)

The general view is that the stress distribution along the shaft after pile installation is dependent on pile bedding depth. For piles with an installation depth of less than 10 to 15 times the diameter the stresses increase rapidly with depth. The distribution is assumed linear over the pile length as presented in the left image of Figure 2.5. The distribution linear with depth is described by the relation presented in Equation 2.1 (Winterkorn and Fang, 1975).

$$\sigma_h = K_p z \gamma \qquad (2.1)$$

With:

σ_h	=	Horizontal stress on the pile shaft	kPa
K_p	=	Passive earth pressure coefficient	-
z	=	Depth	m
γ	=	Volume weight	kN/m^3

The passive earth pressure coefficient is in the order of 3 to 4, depending on the angle of internal friction. The volume weight of dry sand is in the order of 17 to 20 kN/m^3, for wet sand this is 19 to 22 kN/m^3.

For piles with an installation depth larger than 15 to 20 times the pile diameter the stress distribution is presented in the right image of Figure 2.5. Starting from ground surface the same initial tangent as the $L < 15D$ distribution is found, then a transitional curve and a constant increase with respect to the at rest stress diagram. The initial soil stress state depends on the soil load history. For a normally consolidated situation the at rest stress state is indicated by K_0 in Figure 2.5 (Winterkorn and Fang, 1975).

The representations provided in Figure 2.5 are only rough approximations of horizontal stress distribution with depth on a pile shaft.
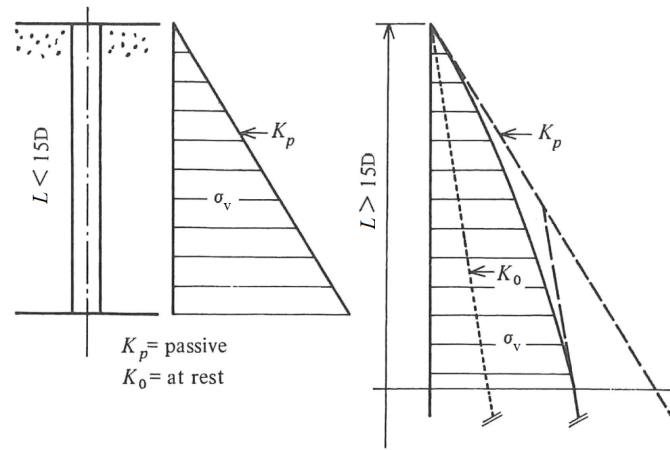
Figure 2.5: General assumption of stress distribution along pile shaft (Winterkorn and Fang, 1975), *modified*

Loading Rate and Sequence

When a pile is subjected to a progressively increasing load in compression shaft and base resistance will develop when the pile moves relative to the soil mass. Initially the resistance by the pile-soil mass interaction is elastic. If the load is released in the elastic zone the pile head would rebound to its original level (Tomlinson and Woodward, 2015).

Shear stresses along the pile shaft are mobilized by settlement of the pile when loaded. The relative displacement required to mobilize maximum shaft friction is very small, approximately a few millimeters and rarely exceeds a value of about 10 mm. This displacement is practically independent of the pile diameter. On the contrary, the deformation required to mobilize a given percentage of the maximum tip resistance is a function of the soil characteristics and increases with the diameter of the pile. The ultimate pile capacity is reached when an ongoing settlement is found for a constant load (Tomlinson and Woodward, 2015; Winterkorn and Fang, 1975).

Shaft resistance is built up of frictional forces due to horizontal earth pressure and adhesion. Stress arching affects the amount of lateral friction that can be mobilized through vertical loading. The loading rate influences the shear stress mobilized, as a higher loading rate will provide a stiffer response. When load is applied in cycles the pile moves up and down relative to the soil causing the stress direction to change. The changing stress directions cause a degradation of the shaft resistance (Fellenius, 2002).

The relation between shaft and tip resistance contribution for a pile with given length is presented in Figure 2.6. For small loads shaft resistance is predominant; then, as mobilization of skin friction proceeds, the relative value of tip resistance increases. Where shaft friction is fully mobilized, a turning point occurs. Figure 2.6 represents the relation for a homogeneous soil. The true ratio tip/shaft contribution depends on the stratification, soil characteristics and pile geometry (Winterkorn and Fang, 1975).
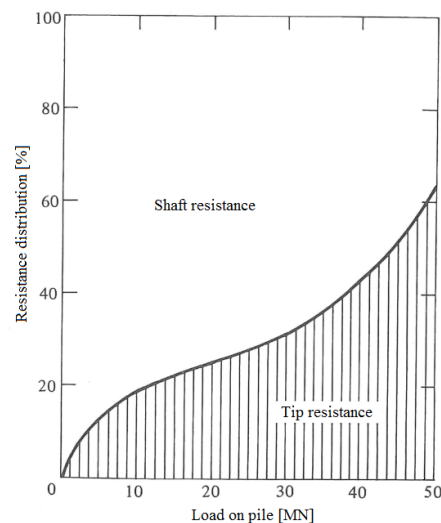
Figure 2.6: Contribution of tip and shaft resistance to the total bearing capacity for an increasing compressive load (Winterkorn and Fang, 1975)

2.2 Pile Design Methods

The bearing capacities of piles should be determined such that the foundation ensures adequate safety against structural failure. Structural failure implies impairing the structures efficiency due to excessive deformation, deflection, rotation or vibration.

There are various methods available to determine pile capacity. These methods can roughly be divided in three categories; empirical-, analytical- and numerical methods. Empirical methods are often used methods that are based on in-situ tests like the Cone Penetration Test (CPT). Analytical methods are predominantly based on effective vertical stress or load test results as obligated in some countries. Fully numerical methods are rarely used. Numerical methods are still under development and commonly experience problems implementing installation effects on the soil and pile characteristics (Van Tol et al., 2010). Direct CPT methods are most often used, for instance in the Dutch code.

Direct CPT Methods

A direct CPT method is an empirical method where a direct relation between measured cone end resistance and pile tip- and shaft capacity is considered. Estimation of pile tip resistance based on CPT data was developed in the Netherlands over 80 years ago. Over the years a number of (derived) methods have developed, examples of recent empirical methods are (Xu et al., 2008):

- Fugro method
- Imperial College Pile (ICP) method
- University of Western Australia (UWA) method
- Norwegian Geotechnical Institute (NGI) method
- Method provided by the Dutch code (NEN 9997-1), also known as Koppejan method

All methods employ a direct relationship between the pile tip resistance and the average cone end resistance in the vicinity of the pile tip. The methods, with exception of the Koppejan method, were initially developed for steel piles. Non of the methods include time effects on pile capacity. The methods are further elaborated in Appendix A.

Most methods have a comparable format for calculating the total capacity (Van Tol et al., 2010):

$$Q_c = R_b + R_s \tag{2.2}$$

$$R_b = A_b * q_b \tag{2.3}$$

$$R_s = \sum A_s * q_s \tag{2.4}$$

$$q_b = f_b * q_{c;avg} \tag{2.5}$$

$$q_s = f_s * q_{c;avg} \tag{2.6}$$

with:

Q_c	=	Calculated pile capacity	kN
R_b	=	Calculated tip capacity	kN
R_s	=	Calculated shaft capacity	kN
A_b	=	Tip surface	m^2
A_s	=	Shaft surface	m^2
q_b	=	Tip resistance	kPa
$q_{c;avg}$	=	Average cone resistance	kPa
q_s	=	Shaft resistance	kPa
f_b, f_s	=	Empirical factors for installation effects, soil type, pile type and geometry	-

Determination of q_b differs strongly per method, determination of q_s is more or less consistent in all methods presented above. Generally additional method specific factors are considered. The Dutch method (NEN 9997-1) for instance prescribes limit values for q_b and q_s as well as a cone resistance reduction when working in overconsolidated sand or gravel, see Appendix A.

7

Comparison and validation of the Dutch, French and Belgian calculation method revealed that these empirical calculation methods based on CPT data predict the actual bearing capacity with limited accuracy. The coefficient of variation in this research was in the order of 30% (Van Tol, 2012). Empirical methods are generally highly approximate. The methods are often based on results of field tests on either driven prefab concrete piles or closed ended steel piles. For other pile types these calculation methods are generally adjusted by adding a pile type factor.

Analytical Method

The American Petroleum Institute (API) method designed for calculation of offshore steel cylindrical (pipe) piles in cohesionless soils is an often used analytical method. The method assumes that local tip and shaft resistance increase in proportion with the vertical effective stress as outlined in Equation 2.7 and Equation 2.8 (American Petroleum Institute, 2014; Yang et al., 2016). The predicted unit friction and end bearing values are predominantly based on soil classification and estimated relative densities.

$$q_b = N_q \sigma'_v \tag{2.7}$$

$$q_s = \beta \sigma'_v \tag{2.8}$$

With:

q_b	=	Tip resistance	kPa
q_s	=	Shaft resistance	kPa
N_q	=	Dimensionless tip capacity factor	-
β	=	Dimensionless shaft capacity factor	-
σ'_v	=	Local effective vertical stress	kPa

Equation 2.7 and Equation 2.8 do not recognize any relative pile tip depth dependency, the methods specifies upper limits to the unit tip ($q_{b,lim}$) and shaft ($q_{s,lim}$) resistance.

The β factor in Equation 2.8 is equal to $K * \tan \delta$ where K is the coefficient of lateral earth pressure and δ the interface friction angle. β, N_q and the limit values depend on soil type description and relative density. Parameters intended as guidelines are tabulated in the API guideline (American Petroleum Institute, 2014), see Appendix A.

3 | Set-Up

Set-up is long-term time-dependent bearing capacity increase of a pile. The time-dependent increase and rate of increase is influenced by soil characteristics and stratification as well as by pile type, dimensions and installation method. The phenomenon of capacity increase is predominantly caused by an increase in shaft capacity, increase in tip resistance with time is very limited (Axelsson, 2000). Set-up was observed under saturated and unsaturated conditions with concrete, steel and timber piles of various lengths and with various cross sections. Total capacity increases with a factor 4 or more have been found in researches on set-up in non-cohesive soils (Alawneh et al., 2009). Set-up has not been implemented in standard design practise yet due to distinct variability observed in various case histories and a general lack of understanding of the basic mechanisms controlling set-up (Gavin et al., 2015).

3.1 Magnitude

Tavenas and Audy (1972) were one of the first to mention time-dependent capacity increase of piles in cohesionless soil. For static load tests (compression) at a single site where pile type, soil conditions and loading type were constant Tavenas and Audy (1972) found an average capacity increase of about 70% over a 15 to 20 day period after assessing the reference capacity. The reference capacity of the concrete piles was determined at t_0 equal to half a day after installation (Tavenas and Audy, 1972). Many cases of time-dependent capacity increase for piles installed in non-cohesive soils have been reported since then.

Chow et al. (1998) and Axelsson (2000) collected and visualized the results of field tests on time-dependent pile capacity. Chow et al. (1998) constructed two graphs, one with the total pile capacity in time (Figure 3.1) and one with solely shaft capacity in time (Figure 3.2). Axelsson (2000) excluded the effect of excess pore water dissipation (short-term capacity gain) on the total capacity increase by only selecting tests with a reference time (t_0) of 0.5 to 4 days after installation, often referred to as end of initial driving (EOID) (Figure 3.3).

The pile capacities found in the test programs available in literature were obtained in different manners. Pile capacities were determined by static testing or dynamic testing, see Appendix B. Static testing is more time consuming than dynamic testing but the results are generally more reliable since the capacity is measured directly instead of back-calculated.

An often used but controversial method to determine time-dependent capacity is testing one and the same pile at different moments in time. Previous tests will influence the results of successive tests, this accounts for both static and dynamic tests. Bullock et al. (2005) state that repeated dynamic tests overestimate the pile capacity while repeated static load testing a pile to failure provides a lower capacity than first time (virgin) testing (Jardine et al., 2006). Evident is that re-testing of the same pile at different ages can lead to misleading trends for ageing effects. It could also introduce false biases between compression and tension capacities, or between cyclic and static behaviour. Most valuable results for a research on set-up are obtained when multiple piles are installed within a homogeneous site and tested at different moments in time. In this case the results of first time test can be compared.

Like the method of testing and the test sequence the method of installation is also likely to influence the set-up rate. Lim and Lehane (2014) tested both jacked and driven piles in a sand deposit. The jacked piles showed little to no gain in capacity over a 72 day period while for the driven piles a significant gain was observed (Lim and Lehane, 2014). Both closed-ended and open-ended piles were tested and a relation was found between the pile geometry and the set-up rate. The general observation was that more soil displacement equaled more set-up.

Figure 3.1 to 3.3 reveal that gain in pile capacity at a given time after installation is highly variable.
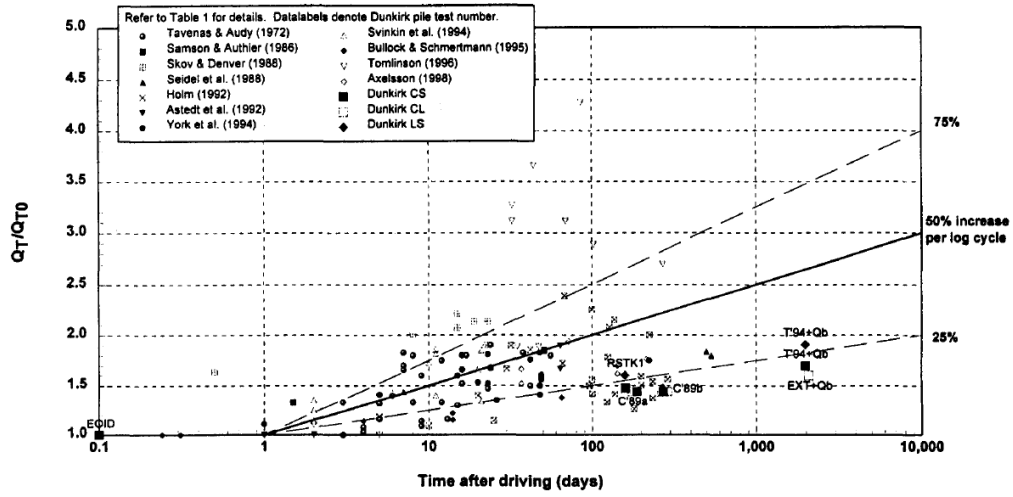
Figure 3.1: Case histories of total pile capacity increase with time (Chow et al., 1998)
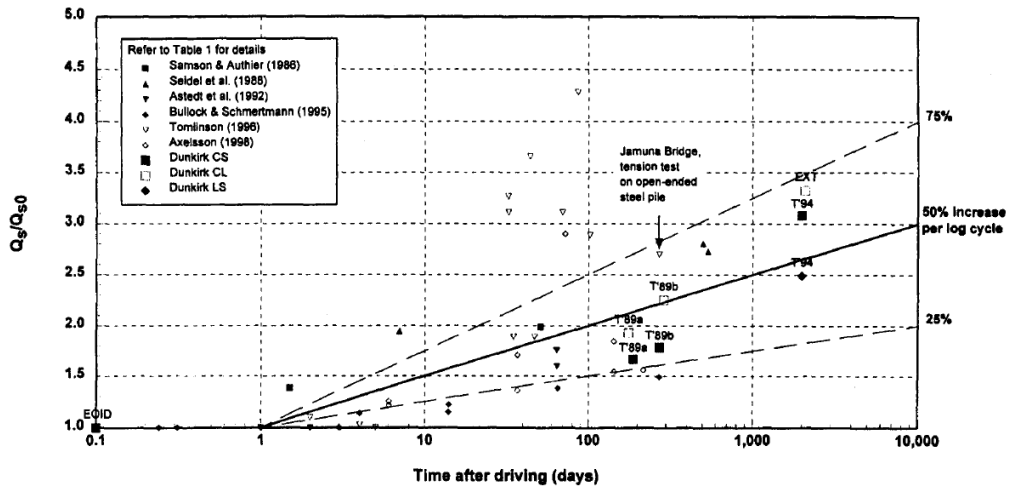
Figure 3.2: Case histories of shaft capacity increase with time (Chow et al., 1998)
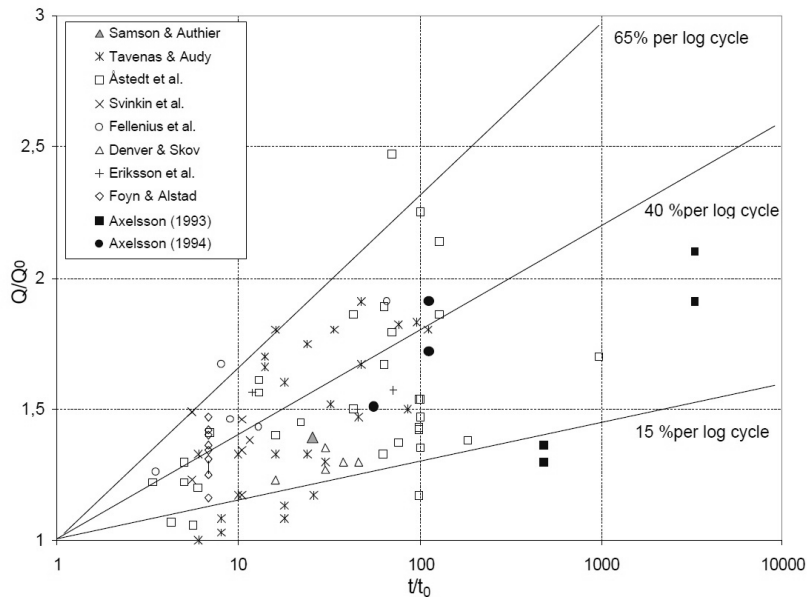
Figure 3.3: Case histories of total pile capacity increase with time for t_0 between 0.5 and 4 days after pile installation (Axelsson, 2000)

However, general observations can be made. Chow et al. (1998) found that, while base resistance gains are relatively small, shaft capacity increases by around 50% ($\pm$25%) per log cycle of time (Chow et al., 1998). Axelsson (2000) displayed two lines representing 15 and 65% increase in bearing capacity per log cycle of time. The average set-up is approximately 40% per log cycle of time. In contrast to Axelsson (2000), Chow et al. (1998) included the results of tests with a reference time less than half a day. Thereby pore water dissipation might have contributed to the increase in capacity. The contribution of excess pore pressure dissipation is further elaborated in section 3.3.

Long et al. (1999) produced a comparable graph considering the results of pile tests conducted in different soil types. All piles in sand showed at least 30% set-up 10 days after end of initial driving and some showed even as much as 100% gain in capacity (Long et al., 1999).

Many researchers (amongst others, York et al. (1994), Svinkin (1996) and Bullock et al. (2005)) found time-dependent capacity increase compared to the dynamic capacities at the end of initial driving and hence included short-term effects. The short-term component may be very large, zero or negative depending on the permeability and dilation characteristics of the sand (Chow et al., 1998).

Cases of relaxation (capacity reduction in time) of driven piles in sand do occasionally occur, primarily due to dissipation of negative pore pressures created during pile installation (driving) (Bullock et al., 2005). Chow et al. (1998) noted that relaxation cases were related to:

1. Short-term pore pressure effects
2. Piles founded on rock
3. Closely spaced piles

3.2 Duration

The time span over which pile capacity increases is likely to vary with the installation method and the soil characteristics. Although delayed set-up was observed (Axelsson, 2000) it will generally start directly after installation. At what point in time the ultimate pile capacity is reached is variable. Various time spans after installation were suggested in literature. Most authors suggested that for open and closed-ended displacement piles the capacity tends to a maximum about a year after installation (Gavin et al., 2015; Karlsrud et al., 2014). However, Long et al. (1999) determined that although the largest set-up occurred in the first 10 days after driving, set-up appeared to continue for up to 500 days (Long et al., 1999). Axelsson (2000) and Zhang and Wang (2014) suggest that set-up can even last for as long as several years.

Chow et al. (1998) found that capacity increase between 0.5 and 5 years after installation is still significant. Re-tests on two open-ended steel pipe piles revealed 72% and 85% capacity increase over this 4.5 year time span (Chow et al., 1998). This indicates that the process causing capacity increase continues far on.

Pile capacity increases rapidly directly after installation. This increase is related to dissipation of excess pore pressure (see section 3.3). After dissipation of excess pore pressure the rate of (shaft) capacity increase is approximately constant with the logarithm of time (Axelsson, 2000; Bullock et al., 2005; Skov and Denver, 1988). Most authors confirm the log-linear increase in capacity. However, other distributions have been found. York et al. (1994) found a set-up rate approximately constant with time 15 to 25 days after pile installation. While Karlsrud et al. (2014) suggest a non-linear capacity increase with the logarithm of time. The best fit for the open-ended steel pipe piles installed in sand was a S-curve where the increase flattens after about 10 months (Karlsrud et al., 2014).

White & Zhao (2006) fastened the process of set-up by cyclic changes in groundwater table (De Lange et al., 2015). Jardine et al. (2006) conducted tests with a dynamic load applied to the pile of approximately 20% of the failure load. After a study period of 1.5 years a larger capacity increase was found in the dynamically loaded pile than in the reference pile where no load was applied (Jardine et al., 2006). Karlsrud et al. (2014) tested a steel pipe pile with a sustained tension load of about 60% of the assumed failure load and found less set-up than for reference piles which aged without any external load applied. It is unknown whether the reduction also applies for sustained compressive loads (Karlsrud et al., 2014).

3.3 Mechanism

The mechanism(s) causing set-up are not yet fully understood. There are multiple hypotheses concerning the mechanisms contributing to set-up of piles in sand, as elaborated below.

Distinction is often made between short-term capacity gain (excess pore water dissipation) and long-term capacity gain (set-up). Installation of ground displacement piles generally induces high pore pressures in the zone surrounding the pile. The excessive pore pressures generated during the installation process will dissipate over time. The time required depends on the amount of disturbance caused during pile installation and on the permeability of the soil. Dissipation of excess pore pressure is fast in non-cohesive soils. Excess pore pressures in sand will generally dissipate within a few minutes to hours and for silty sand it might take up to a few days after installation (Stoevelaar et al., 2012). For non-cohesive soils short-term capacity gain is often defined as the increase in capacity that takes place within the first 24 hours after installation.

With the dissipation of the excess pressure in the pores the effective stress on the pile increases. Set-up is a substantial increase in bearing capacity of driven piles in sand over a long period of time as elaborated in section 3.1 and 3.2. A substantial increase in the ultimate bearing capacity of piles driven into sand over a long period of time cannot be attributed to dissipation of excess pore pressure.

Set-up in sand is generally attributed to one or more of the mechanisms listed below. The different mechanisms may depend on each other or act at the same time.

- Horizontal creep (relaxation of radial stress) causing an increased horizontal effective stress on the pile shaft.
- Particle rearrangement causing increased resistance to dilatancy
- Inter-particle binding causing increased stiffness

The mechanisms are predominantly related to change in shaft capacity since time-dependent change in base capacity is limited and has thereby a minor contribution to set-up. This result was found in pile tests where the contribution of base and shaft capacity were separated (Axelsson, 2000).

Piles installed in a uniform sand are likely to have a shaft resistance increasing with depth. Generally the highest stresses are mobilized at the bottom part of the pile. Shear stresses stabilize with decreasing distance to the surface due to the reduction in radial stress towards surface level (Lehane et al., 1993).

Stress dependency of installation depth was found in a research where 7 m long concrete 275 mm square piles were load tested dynamically at different pile tip depths. Relatively large shear stresses were mobilized between 2 and 3 m depth when the pile tip was at 3 m below ground level. When the tip reached its final depth, 7 m below ground level, there was hardly any shear resistance between 2 and 3 m depth. The shear stress mobilized along the pile shaft was concentrated to the bottom 4 m. The left image of Figure 3.4 illustrates the interpreted shaft shear stress from the dynamic load tests performed at three different pile tip levels. The right image illustrates an increase in shaft shear resistance 24 hours after installation. No stress increase was found for the upper section of the pile (Gavin et al., 2015).
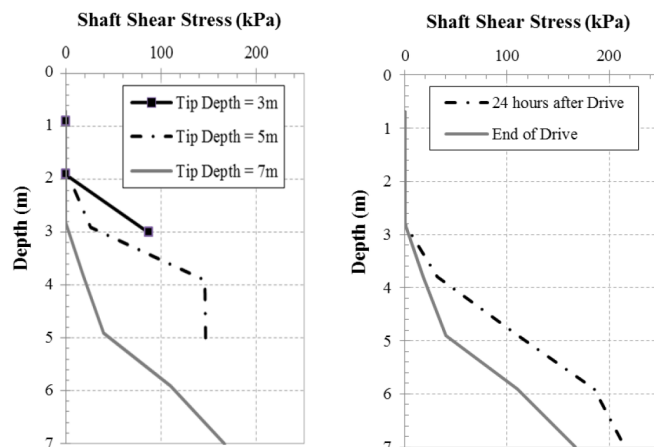
Figure 3.4: Interpreted shear stress from dynamic load tests performed on driven concrete piles (Gavin et al., 2015)

This finding was in accordance with Lehane et al. (1993) who found a decreasing radial stress acting on the pile with increasing h/R. Where h is the length from pile tip to the location along the shaft and R is the pile radius. Bullock et al. (2005) measured the stresses on a pile and found no depth dependency of the stresses over the 25 m shaft length in a dynamic load tests.

Horizontal Effective Stress

Soil is displaced in a downward and outward direction while driving a pile. Along the shaft the movement is predominant in the radial direction, some vertical displacement may also occur. At the pile tip soil moves in both vertical and radial direction (Komurka et al., 2003). Figure 3.5 illustrates a schematic representation of the stress and particle movement during installation of a displacement pile in sand. Outward particle movement will cause a stress increase and compaction of the soil surrounding the pile. A stress arch will develop (cross section B-B') depending on the in-situ stress state.
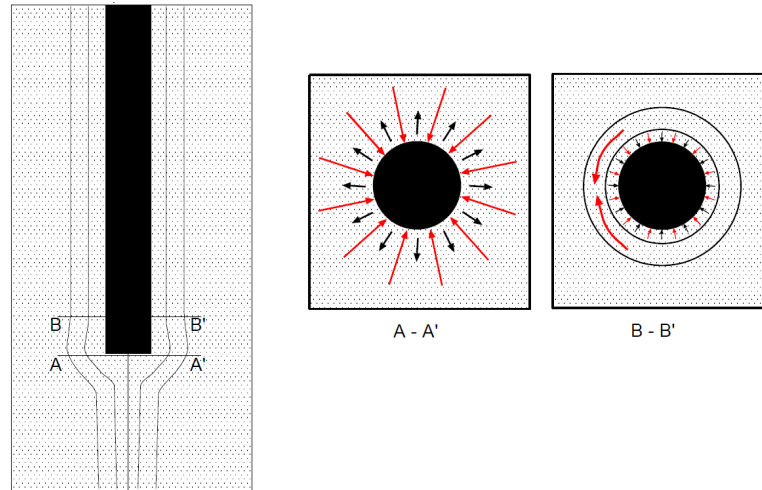
Figure 3.5: Schematic representation of particle (black) and stress (red) movement during installation of a displacement pile in sand (Stoevelaar et al., 2012)

Over time the stress arch will vanish. Creep is likely to be the dominant mechanism causing breakdown (relaxation) of the stress arch over time. Peak stresses are redistributed over time, increasing the horizontal effective stress on the pile shaft.

Development of a stress arch is only expected for driven displacement piles. See section 3.1 for the relation between installation method and set-up. Contradicting results have been found considering the influence of radial stress on set-up. Set-up has been found for piles where the horizontal effective stress increased over time (Axelsson, 2000), decreased over time (Gavin et al., 2015) and for piles with a more or less constant horizontal effective stress level over time (Zhang and Wang, 2014).

Friction Angle and Dilatancy

Pile driving changes the soil fabric in the close vicinity of the pile. Particles rearrange and might be crushed. Over time the soil recovers and a stiffer fabric develops. This process is sometimes referred to as 'soil healing'. The friction angle increases as the soil particles set and the resistance to dilatancy increases. Increase in friction angle and constrained dilatancy is closely related to the previous discussed stress redistribution. Both mechanisms require change in the micro structure. The processes are visualized in Figure 3.6
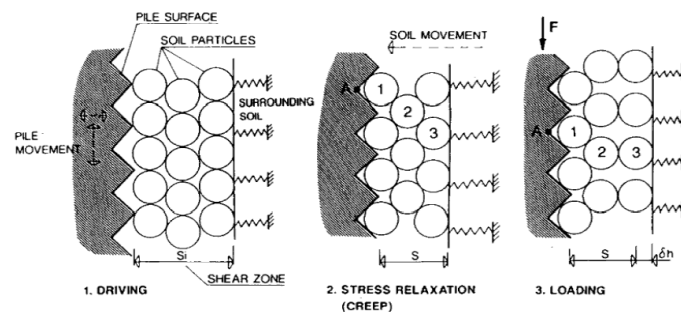
Figure 3.6: Increase in effective stress and constrained dilation (Stoevelaar et al., 2012)

Chemical Processes

Chemical processes relate to inter-particle binding and particle binding to the pile shaft, also referred to as cementation. Bindings between particles are formed by dissolved substances in the pore water. For instance the formation of silica acid gel at particle contacts. Bindings between particles increase the stiffness of the soil fabric.

Particles binding to the pile shaft will form a crust. Chow et al. (1998) found a rust-sand crust up to 5 mm for a steel pile extracted 5 years after installation. The crust caused the failure surface to migrate into the soil mass. Thereby the interface friction angle changes from a soil-pile value to a soil-soil value leading to increased resistance to dilatancy (Lehane et al., 1993). Rust itself induces a volume increase that causes an increased effective stress on the pile shaft (Chow et al., 1998).

Friction induced by pile driving causes temperature increases at the pile-soil interface. The increased temperature might stimulate chemical binding. On the other hand, a crust does not always develop and similar degrees of set-up have been observed for piles of corroding and non-corroding materials installed above and below the water table (Chow et al., 1998).

3.4 Calculation Methods

Long delays between installation and the first testing occasion are often impractical. For this reason researchers tried to describe long-term capacity from short-term measurements. Many equations have been proposed to calculate the long-term capacity. All calculation methods found in literature are summarized in Table 3.1, a comprehensive elaboration of the different methods is provided in Appendix C. All equations have at least one fitting factor. The ranges of the fitting factors proposed in literature are presented in the last column of Table 3.1.

Method	Equation	t_0	Remarks
Skov and Denver (1988)	$Q_t = Q_0(1 + A * \log \frac{t}{t_0})$	0.5 day	$A = 0.2$
Svinkin (1996)	$Q_t = B * Q_{EOID} * t^{0.1}$	EOID	Designed to calculate the capacity up to 25 days after installation. $B = 1.025$ to 1.4
Chun et al. (1999)	$Q_t = C(1 - (\frac{C-1}{C})e^{-\frac{t}{B}}) * Q_{EOID}$	EOID	$B = 0.11$ to 4.33 $C = 1.41$ to 2.08
Tan et al. (2004)	$Q_t = Q_u(\alpha + (1 - \alpha)(\frac{\frac{t}{T_{50}}}{1 + \frac{t}{T_{50}}}))$	EOID	$\alpha = 0.2$ to 0.5 $T_{50} = 0.7$ to 10 days
Yan and Yuen (2010)	$Q_t = Q_0(1 + C \log(1 + t)$	not specified	$C = 0.418$
Reddy and Stuedlein (2014)	$Q_t = \frac{Q_0 * A \log \frac{t}{t_0}}{k_1 + k_2 * Q_0 * A \log \frac{t}{t_0}} + Q_0$	EOID	$A = 0.7$ to 1.72 $k1 = 0.12$ to 0.17 $k2 = 0.00044$ to 0.00078
Karlsrud et al. (2014)	$Q_t = Q_0 + a * \tanh(b * (t - t_0))$	2 to 7 months	$a = 260$ to 1150 $b = 0.2$ to 0.4

Table 3.1: Set-up calculation methods

Most methods are designed from the results of either dynamic or static pile tests, see Appendix B. The method proposed by Karlsrud et al. (2014) is the only method designed from solely the results of static tension load tests on virgin piles. For all other methods staged tests were included in the databases. As discussed in section 3.1 re-testing a pile at different moments in time will provide a misleading trend for the development of capacity over time.

All methods describe a decreasing capacity increase with time described by a parabolic function on a linear time scale and a linear relation on a logarithmic time scale. All methods were either specially designed for piles in sand or adjustable by fitting parameter to sand conditions.

The reference capacity used in the different methods is either determined in a load test or back calculated from Pile Driving Analysis (PDA) data. The reference time (t_0) determines the reference capacity (Q_0) of the pile. The rate of set-up is critically dependent on the reference time. When for the same case a different reference time is considered a different Q_0 will be found and thereby a different set-up rate. Short-term capacity gain caused by dissipation of excess pore water pressure is included in the total capacity gain when the reference capacity is determined from pile driving data or a dynamic load test shortly after installation.

A set reference time is thought to be impractical, therefore a set-up rate compared to a calculated capacity will be analyzed in the database study of chapter 4 and chapter 5.

Concluding Remarks Literature Review

The bearing capacity of piles fully embedded in sand is determined by the tip resistance and shaft resistance. A time-dependent increase in capacity is often observed for driven displacement piles in sand. The magnitude differs strongly per site and even within one site with homogeneous soil properties, constant pile geometry, installation- and test method. The set-up rate in sand is generally in the range of 15 to 75% per log cycle of time. Non linear relations with the logarithm of time have also been proposed but stagnation of capacity increase over time was always observed. Time-dependent capacity increase is predominantly attributed to shaft capacity increase, the influence of time on the base capacity is limited.

Depending on the pile geometry, soil characteristics and installation method set-up will start within 2 days after installation and will continue for several weeks up to two years after installation. In particular the installation method is thought to have a strong influence on the set-up period of a pile. The division between set-up and short term capacity gain by dissipation of excess pore water pressure is not always acknowledged. Dissipation of excess pore water pressure may cause a significant increase in horizontal effective stress and thus in pile capacity.

Capacity increase after dissipation of excess pore pressure in sand is expected to be related to change in stress state and soil properties. An increased horizontal stress is related to creep-induced breakdown of a driving-induced stress arch. When present, chemicals or salts establishing inter-particle bindings or bindings between particles and pile shaft are also expected to contribute to set-up. These mechanisms elaborated in section 3.3 lack experimental evidence and could be considered no more than hypotheses for potential mechanisms. Inter-particle binding and rearrangement of particles are both suggested as mechanisms causing set-up but seem to contradict one another. The first mechanism describes cohesive behaviour due to cementation of particles, the second mechanism describes increase in frictional behaviour due to interlocking. Particle movement will destroy inter-particle bindings.

Generally CPT-based design methods are used to calculate pile capacity. The current design codes do not recognize time-dependency of the capacity. Multiple methods have been proposed to quantify time-dependent behaviour. The Skov and Denver (1988) method is most common used, this method predicts capacity increase on the assumption that the rate of increase is linearly proportional to the logarithm of time. In general, all calculation methods exhibit significant uncertainty without site-specific calibration and specified reference time.

The databases used to design the equation predicting time-dependent pile capacity are constructed from load test results of different test types. Dynamic testing and static testing are common used methods. Dynamic load tests are cheaper but the results are less reliable. Static load tests could be in tension or in compression, compressive tests can be top-loaded or bottom-loaded. Comparison of different pile capacities determined by dynamic load tests on different piles is hard. Often the capacities found in dynamic load tests at different moments in time are calibrated with one or more static load tests. A distinction should also be made between capacity increase found with staged pile testing and virgin capacity increase. Generally capacity increases are found when one and the same pile is loaded to failure at different moments in time. However, the set-up rate is lower compared to virgin capacity increase.

The information found in the literature review was used to design the test program on time-dependent pile capacity and to compile a database of the results for virgin pile tests, axially loaded to failure in a static load test.

4 | Database Study

Research on set-up is often done by testing (scaled) piles at different moments in time, either by dynamic or static testing. Centrifuge tests dedicated to analyze set-up have not provided satisfying results (De Lange et al., 2015) and a numerical analysis of time-dependent pile capacity is doubtful since the mechanism(s) causing set-up are not fully understood.

Most calculation methods presented in section 3.4 were designed from the results of pile load tests. Combining all the test results presented in literature would provide a large database which could be used to asses the development of capacity over time. However, no test is the same. Different pile types, diameters, lengths and materials were used at sand sites with different characteristics. Besides the different pile geometries and soil characteristics different installation and test methods were used.

All available data was filtered and a database was compiled of test results for statically tested virgin displacement piles driven in sand. Both piles tested in tension and compression were included. To research the effect of time on the axial capacity of driven displacement piles the results of re-test were eliminated and only virgin capacity in time was assessed.

4.1 Data Availability and Quality

There was a large amount of data available of load tests on displacement piles in sand. However, when assessing time-dependent virgin pile capacity the amount of available load test results was limited. There were two main causes. In order to assess time-dependent capacity the time elapsed between installation and testing is required. And, when assessing virgin pile capacity multiple (similar) piles have to be tested within a site with limited spatial variability.

The majority of the entries in the database assembled for this thesis originate from the ZJU-ICL database (Yang et al., 2016). This is a free accessible database with load test data on axially loaded piles driven in sand compiled by the Zhejiang University in collaboration with Imperial College London. The ZJU-ICL database is partly assembled of data collected by Imperial College London and University of Western Australia which used the data to develop the ICP- and UWA-method for pile foundation design (see Appendix A). For the ZJU-ICL database new pile load test results were added and the load test results in the ICP and UWA databases were re-examined on quality and documentation. In the ZJU-ICL database all entries met the quality requirements presented below:

1. More than 65% of the shaft capacity must be developed in silica sand strata
2. Full tip capacity must be developed in silica sand strata
3. A complete CPT profile from a nearby location and soil description must be available
4. Information on the groundwater level and particle size distribution must be available
5. Ideally, good measurements of in-situ density and interface shearing angles should also be available
6. The test is a high-quality (ideally load controlled) first time axial test to failure on a virgin pile. A load-displacement curve must be included that continues until either a peak load or an axial displacements of $0.1 * D_{eq}$ developed.
7. Successive tests on the same pile were generally not included, exceptions being cases where piles were tested shortly after driving to more than one depth, where the depth intervals are sufficiently different to reduce possible interactions between successive tests.
8. Piles must be installed by driving
9. Information on pile material and geometry must be available

Two additional requirements for this thesis were:

10. Information on the time elapsed between installation and testing
11. Multiple piles per site with different ages

4.2 Database Characteristics

The database consisted of a total of 57 load tests divided over 15 sites in Europe, Asia, Northern America and the Middle East. 5 pile types were present in the database as presented in Table 7.1.

Pile type	Tested in tension	Tested in compression	Total
Circular open-ended concrete	-	2	2
Square open-ended concrete	-	1	1
Square closed-ended concrete	1	8	9
Circular open-ended steel	30	9	39
Circular closed-ended steel	3	3	6

Table 4.1: Pile types in database

In total 34 piles were tested in tension, the characteristics of the tension tests are provided in Table 4.2. The average age of the piles before testing was 73 days when ignoring 2 tests conducted 730 days after installation. 23 piles were tested in compression, the characteristics of the compression tests are provided in Table 4.3.

Tension	Min	Max	Mean
Age	2 days	730 days	116 days
L	7 m	47 m	18.6 m
D_{eq}	0.305 m	1.22 m	0.558 m
L/D_{eq}	14.9	61.6	32.9

Table 4.2: Tension test characteristics

Compression	Min	Max	Mean
Age	1 day	89 days	34 days
L	5.3 m	79.1 m	28.3 m
D_{eq}	0.265 m	1.22 m	0.559 m
L/D_{eq}	14.9	86.5	48.3

Table 4.3: Compression test characteristics

4.3 Pile Capacity

The capacity of the pile equaled the load at a set displacement. The Dutch code considers a pile to be failed when there is significant upward or downward movement of a pile without noticeable change in applied load (NEN9997-1, 2016). For piles tested in tension the failure point is more evident than for piles tested in compression. In tension the max capacity is the force for which a constant displacement is found. For displacement piles in compression the max capacity is often defined by the load for which $0.1 * D_{eq}$ tip displacement is measured. The equivalent diameter (D_{eq}) is used to define a diameter for rectangular piles, see Appendix A. The equivalent diameter of circular piles is equal to the diameter ($D_{eq} = D$).

Generally the $0.1 * D_{eq}$ tip displacement failure criterion works. But there are some limitations to the diameter dependency of the failure criterion:

- For piles with very large diameters the displacement required to meet the failure criterion is enormous. The large displacement often causes intolerable deformation for the super structure.
- In turn, for piles with very small diameters the failure criterion could be met before failure is reached. Especially for long, small diameter piles there is significant difference between $0.1 * D_{eq}$ pile head displacement and $0.1 * D_{eq}$ pile tip displacement. When analyzing pile head displacement the elastic shortening of a pile should be considered (Xu et al., 2008).
- Large open-ended piles in compression often require a larger displacement than $0.1 * D_{eq}$ before failure is reached.

4.4 Database

Full database is available with Yang et al. (2016), a summary is presented in Appendix D. This Appendix provides information on the pile type, geometry, location, age, test type and capacity.

4.5 Calculation Methods

Yang et al. (2016) used the database to assess the accuracy of different pile calculation methods. A representative CPT-profile was available for each test site in the database. The methods assessed by Yang et al. (2016) were:

- Fugro method
- American Petroleum Institute (API) method
- Imperial College Pile (ICP) method
- University of Western Australia (UWA) method
- Norwegian Geotechnical Institute (NGI) method

The CPT-based design method, method Koppejan, elaborated in the Dutch design method NEN9997-1 (2016) was added to this list.

5 | Results Database Study

A database was compiled with the results of static load tests on driven piles in sand. Within some test sites different embedded lengths or pile geometries were used. In order to eliminate the effect of embedded length and geometry the measured pile capacities (Q_m) were normalized by the calculated capacity (Q_c) (Koppejan method).
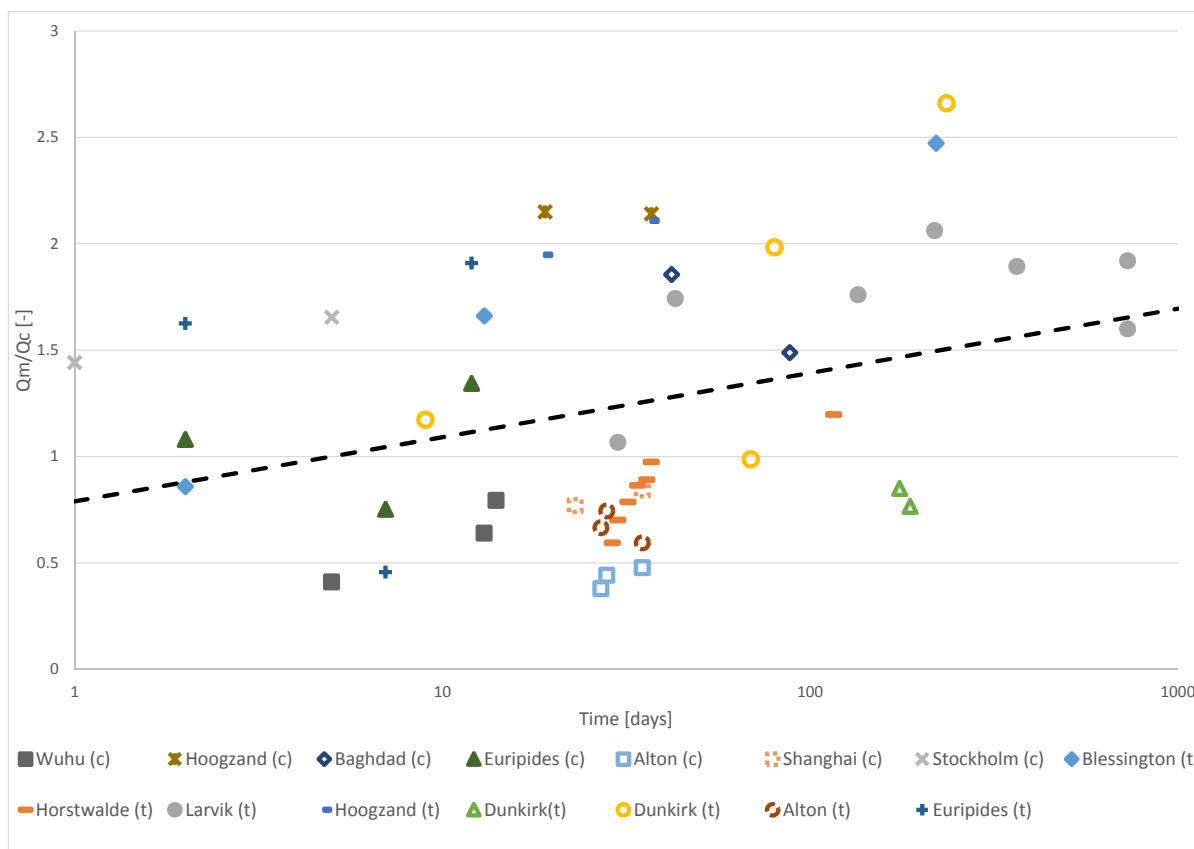
Figure 5.1: Normalized capacity in time

The results were classified per test site. The legend presents the location of the test site and, between brackets, the test method. Where (t) indicates load tests in tension and (c) compression. A general trend for capacity increase with time for virgin test was observed. Set-up is attributed to shaft capacity increase, a stronger trend for capacity increase was found for the piles tested in tension.

5.1 Accuracy Calculation Methods

For the piles in the database Yang et al. 2016 determined the capacity considering the first 5 methods listed below. The capacity considering the Dutch (Koppejan) method was added to this list. All methods are CPT-based methods with exception of the API method. The calculation methods are elaborated in Appendix A.

- Fugro method
- American Petroleum Institute (API) method
- Imperial College Pile (ICP) method
- University of Western Australia (UWA) method
- Norwegian Geotechnical Institute (NGI) method
- Method provided by the Dutch code (NEN 9997-1), also known as Koppejan method
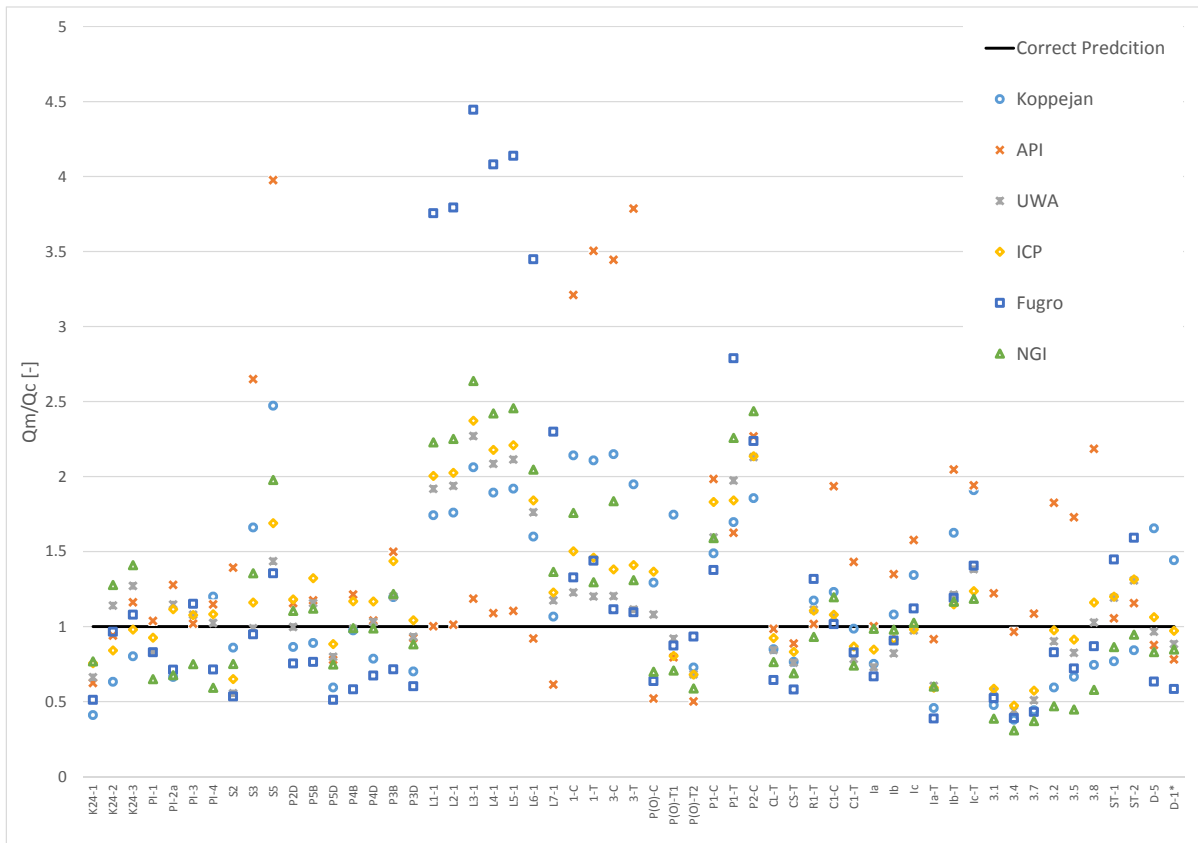
Figure 5.2: Comparison of different calculation methods

Figure 5.2 visualizes the accuracy of the different methods. The horizontal axes provides all piles in the database. On the vertical axes the measured capacity is divided by the calculated capacity. The thick black line indicates a correct prediction, for all entries above this line the measured capacity was larger than the calculated capacity and indicates a factor of safety. More concerning are the entries below this line where the measured capacity is smaller than the capacity predicted by the specific calculation method. Up to 3 times higher capacities have been predicted than measured. The results of the individual methods are provided in Table 5.1

	Koppejan	API	UWA	ICP	Fugro	NGI
Mean	1.209	1.446	1.136	1.209	1.295	1.153
Standard deviation	0.562	0.820	0.440	0.455	1.050	0.612
Coefficient of variation	0.465	0.567	0.387	0.376	0.811	0.531

Table 5.1: Accuracy of calculation methods

The scatter in figure Figure 5.2 is disturbingly large. The best performing method is the UWA method, the least performing method is the API method. The Fugro method fits surprisingly well. This method was only designed for driven steel pipe piles in the following field of application:

- Wall thickness / Outer diameter $> 1/60$
- Single open and closed piles
- Static and quasi-static loads
- Open piles with and without a driving shoe
- Loads applied within 10 to 50 days after installation (before 10 days the capacity might be less, after 50 days the capacity might be larger)
- Pile diameter: 0.25 to 3.00 m
- Pile length: 5 to $80 * (L/D)$
- Sand conditions: Silica sand with relative densities from 10 to 100%

The results of the Fugro method presented in Table 5.1 is for all piles in the database.

5.2 Capacity Prediction in Time

The previous section indicated that the accuracy of the calculated virgin capacity with the CPT-based design methods as well as the API method is low. The capacity was calculated from a CPT profile that was representative for the complete test site. Therefore some variation in result was to be expected.

In order to use a calculated capacity as reference capacity for set-up the day after installation of correct prediction is required. In Figure 5.3 the measured capacity normalized by the calculated capacity (Koppejan) is illustrated for the different virgin tests at different moments after installation. An indication of the moment after installation where the calculated capacity equaled the measured capacity could be determined from the log-linear regression line. The results for the Koppejan method are illustrated in Figure 5.3, the results for all methods are summarized in Table 5.2.
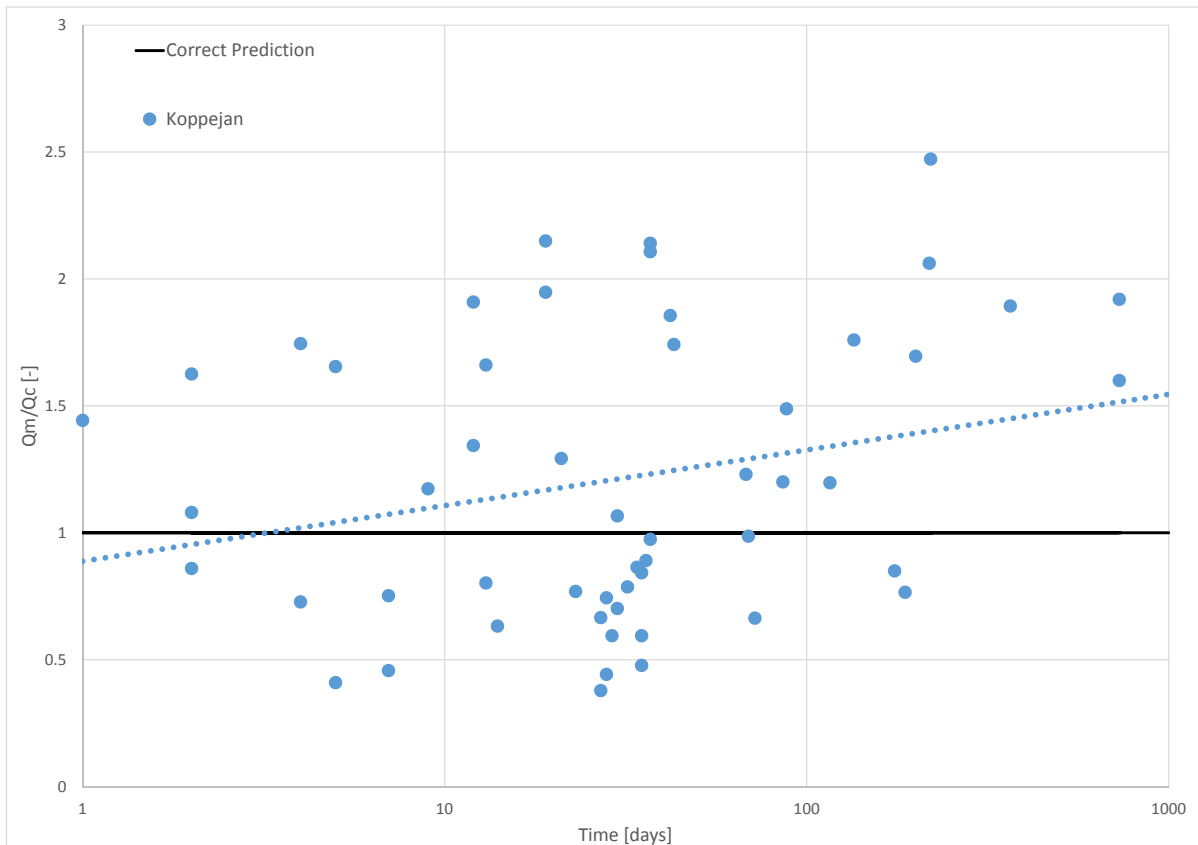
Figure 5.3: Koppejan method in time

	Koppejan	API	UWA	ICP	Fugro	NGI
Predict capacity at day	3	-	14	10	14	14
R^2	0.0617	0.0072	0.3141	0.3533	0.2973	0.2299

Table 5.2: Accuracy of calculation methods in time

All CPT-based methods showed an increase in normalized capacity with time but had a poor fit to the data. All log-linear trends intersect with the correct prediction line with exception of the API method. The log-linear trend line had a slight increase in time but stayed above the correct prediction line.

5.3 Set-Up

For the individual test sites visualized in Figure 5.1 the gain in capacity was not always evident. Looking only at test sites with constant pile geometry 3 sites remained. From literature 1 test site was added. A test site in Dunkirk, France where 3 piles were tested in tension (Jardine et al., 2006), these pile were not included in the database since the piles were not virgin. The piles had been loaded up to 60% of their calculated capacity. The results illustrated in Figure 5.4 are all for circular open-ended steel piles in tension with various diameters. The piles within 1 of the 4 sites all have the same diameter, the embedded length might differ by up to a few centimeters, see Appendix D.
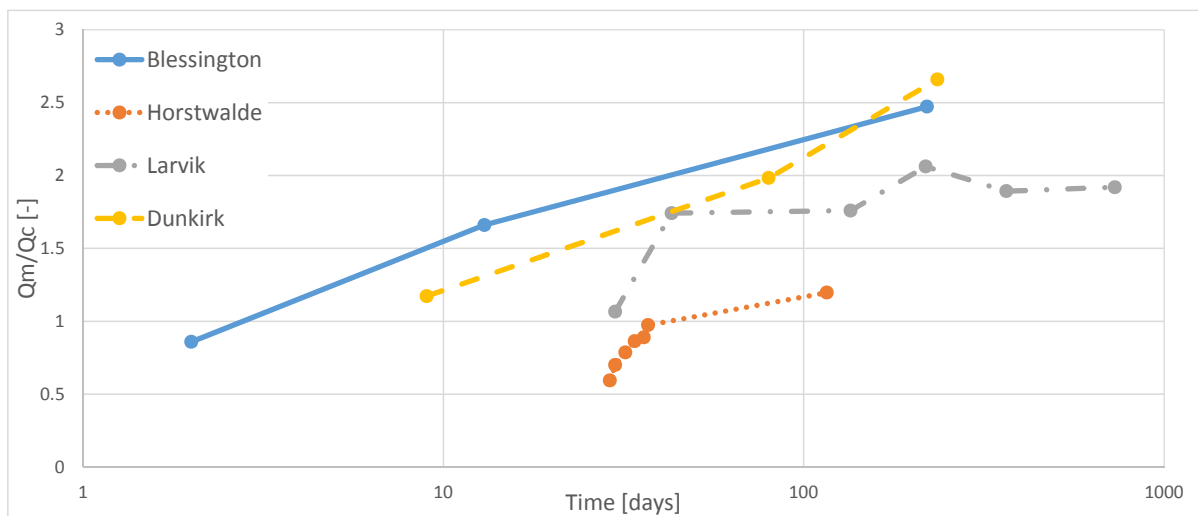
Figure 5.4: Capacity development in time for circular open-ended steel piles in tension

Concluding Remarks Database Study

A large amount of load test results was available in literature. However, only very little test sites were available where the virgin capacity of multiple piles was statically assessed at different moments after installation. In order to compare the results of sites where different pile geometries were used the measured capacity was normalized by the calculated capacity.

A general trend for capacity increase with time was found for the measured capacity normalized by the calculated capacity. However, normalization by the calculated capacity for sites where different pile geometries were used did not show a consistent trend for capacity increase with time. This might be due to a geometry dependency of capacity increase. Also, the calculation methods might not predict pile capacity with the same accuracy for all pile geometries and materials.

The accuracy of the CPT-based design methods available was disturbingly low. No single method predicted the capacity well. The calculated capacity exceeded the measured capacity up to 3 times. It should be noted that each test site came with 1 representative CPT for the complete site. Therefore, some variation was to be expected. In the test program elaborated in the coming chapters CPTs were made at the center line location of each pile prior to installation.

Only 4 test sites were identified where multiple piles with a constant geometry were installed and tested to failure at different moments after installation. At all sites open-ended steel piles were used that were tested statically in tension. Convincing increases in capacity with time were found at these test sites.

A database study is a suitable method to get an indication of the time-dependent behaviour of piles. However, data must be selected carefully. The wide range of variables between test sites and even within a test site makes comparison of the results inaccurate.

6 | Test Program

The influence of time on pile capacity was examined in a scaled field test. As part of a larger test program 4 scaled closed-ended steel piles were statically tested at different moments in time. The length of the piles was 3 m and the diameter equaled 0.15 m. The piles were installed in a man made sand deposit, the maximum ageing period was 70 days. During the static load tests the load applied at the pile head was recorded with a load cell and strain was measured at multiple locations along the shaft by means of strain sensor equipped fibre optic strings. The test pit was located in Zuid-Oost Beemster, next to the head office of Van 'T Hek Foundations. Appendix E provides a photographic visualization of the test program.

6.1 Site Layout

The scaled test program consisted of 8 instrumented piles in total. The piles were installed in a sand fill enclosed with sheet piles, see Figure 6.1. The size of the pit was roughly 16 x 9 m and surface level was at approximately -3.5 m NAP. Sheet piles of 13 m length were installed before excavating the stiff clay in the pit up to -7.5 m NAP. The 4 m sheet piled excavation was back-filled with sand, which was deposited and compacted in layers to create a homogeneous soil profile in the pit, see Figure 6.2.
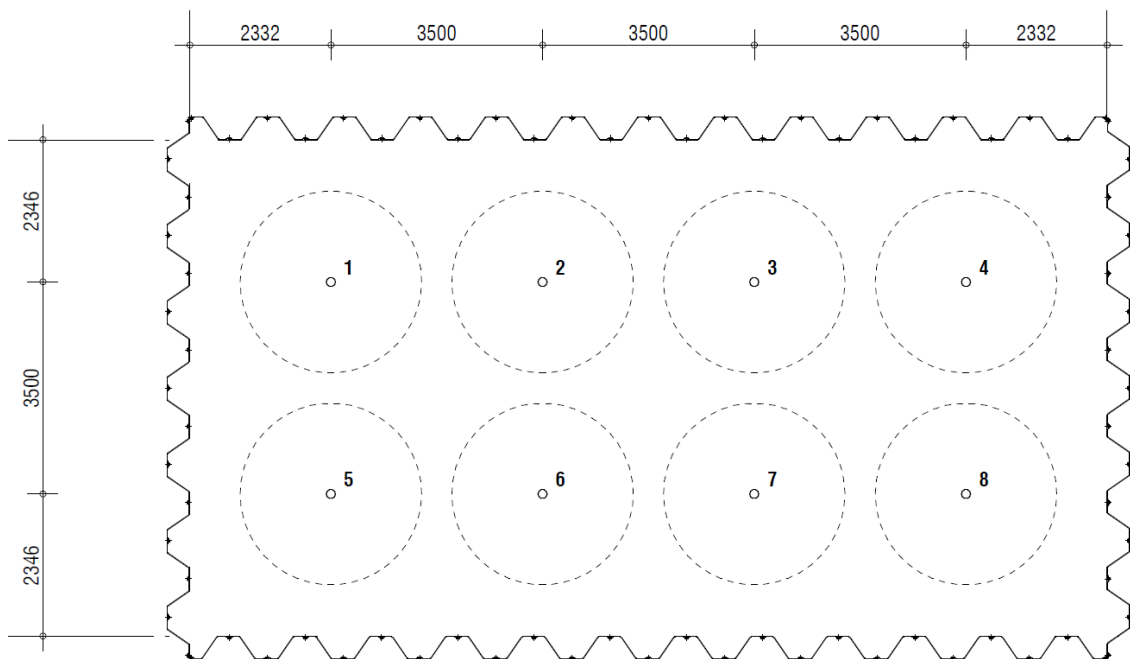
Figure 6.1: Schematic site layout with pile numbers and influence zone $(10 * D)$ of the piles (dimensions in millimeters)

The pile locations were determined such that the influence of adjacent piles and the sheet piled wall of the test pit were minimized. The size of the slip surface is a function of the equivalent pile diameter and the friction angle of the sand. The distance between the pile tip and the bottom of the sand fill largely exceeded the max theoretical slip surface length of $4 * D$ (600 mm) below the pile tip.
The horizontal zone of influence was expected to be less than $10 * D$ for a sand with an angle of internal friction up to 40°. After the virgin tests new CPTs were made between the piles and close to the piles to determine the zone of influence. The theoretical slip surface up on failure is provided in Figure 6.3.
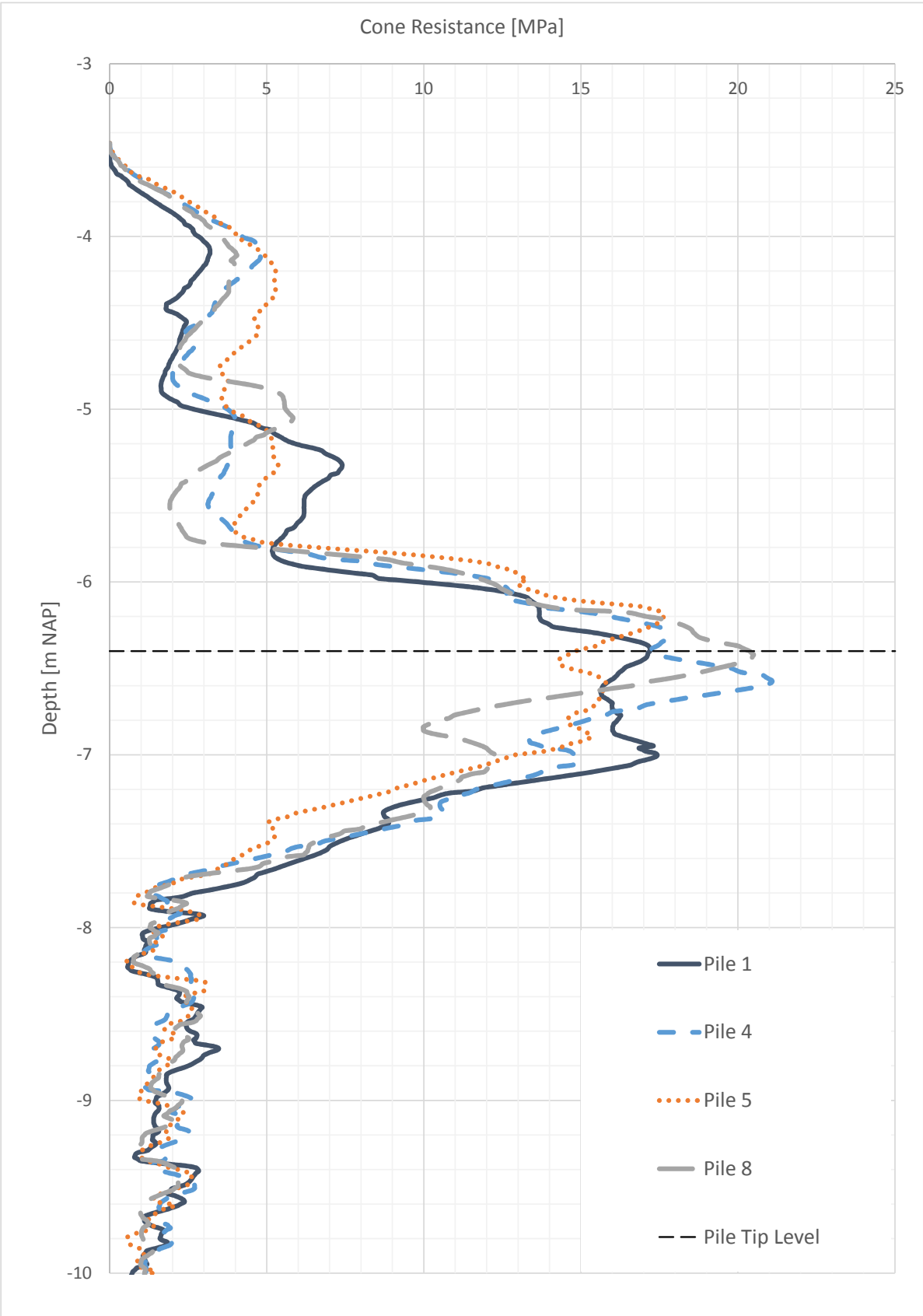
Figure 6.2: Cone resistance at pile locations
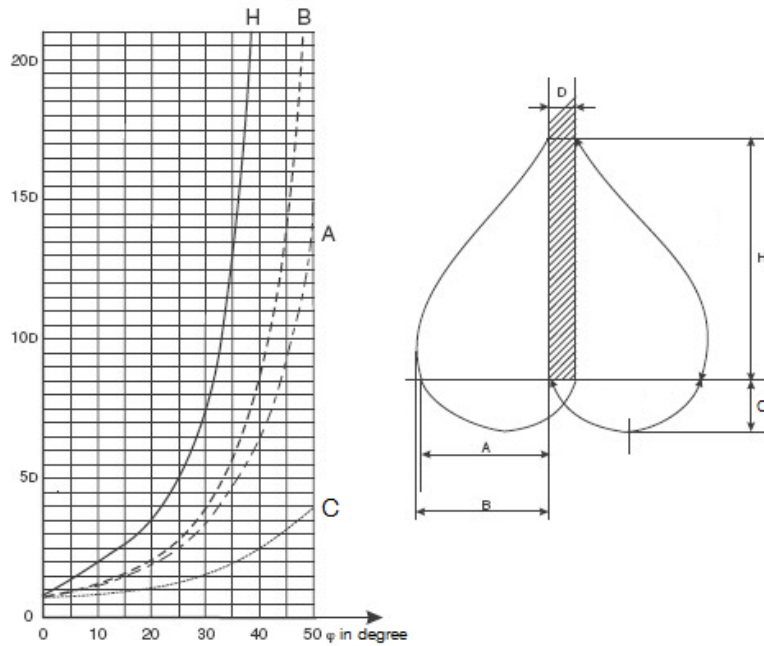
Figure 6.3: Slip surface size as function of friction angle and pile diameter (SBRCURnet, 2010), *modified*

Soil Characteristics

A fine sand was selected to reduce potential scaling effects with the small diameter piles. By applying and densifying the fill in layers a homogeneous compaction rate was created within the test pit. Prior to installation of the piles CPTs were conducted at the exact pile locations. The CPT profiles at the locations of the closed-ended steel piles are provided in Figure 6.2.

The sand fill was unsaturated. The bottom of the test pit consisted of a clay layer with a very low permeability that sealed the fill from groundwater inflow. Rainwater was drained out of the test pit during the complete time span of the test program. A standpipe was present in the test pit to monitor a potential water table in the sand fill.

A sample of the sand was characterized in the lab, the results are provided in Table 6.1. The porosity, angle of response, structure and gradation of the sand were determined as well as the substances in the sample. Figure 6.4 presents the sieve curve of the uniform distributed sand. The results illustrated in Table 6.1 are the average of the two sieve analysis by the different institutions. A small portion of the sand was photographed under the microscope to determine the angularity and sphericity of the grains, see Figure 6.5.

Characteristic	Value/Description	Unit	Method	Processed by
Structure	Closed	-	EN 14955	Kiwa ISA Sport
Shape	spherical, angular and moderate angular	-	EN 14955	Kiwa ISA Sport
Max porosity	0.88	-	JIS A1224	TU Delft Lab
Min porosity	0.60	-	JIS A1224	TU Delft Lab
Angle of response	31	°	JIS A1202	TU Delft Lab
Calcium carbonate content	3	%	DIN 18129	Kiwa ISA Sport
Organic content	< 0.2	%	NEN 5754	Kiwa ISA Sport
pH (CaCl)	7.4	-	MN/G2.1	Kiwa ISA Sport
Sieve analysis				
Fines	0	%	EN 933	Kiwa ISA Sport
D_{50}	0.30	mm	&	&
D_{10}	0.20	mm	BS410	TU Delft Lab
D_{60}	0.33	mm		
C_u	1.6	-		

Table 6.1: Sand characteristics
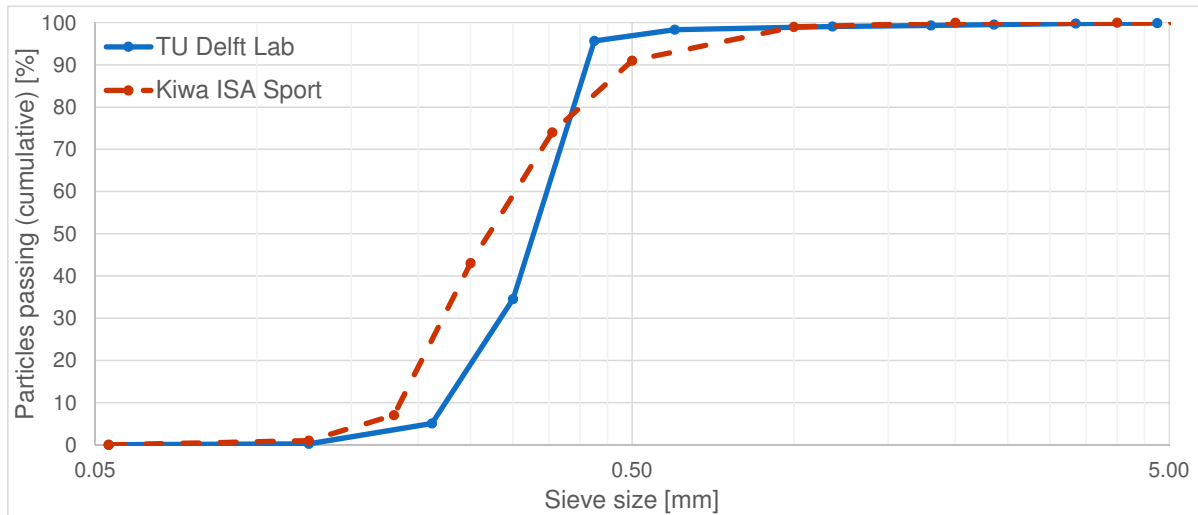
Figure 6.4: Sieve curves
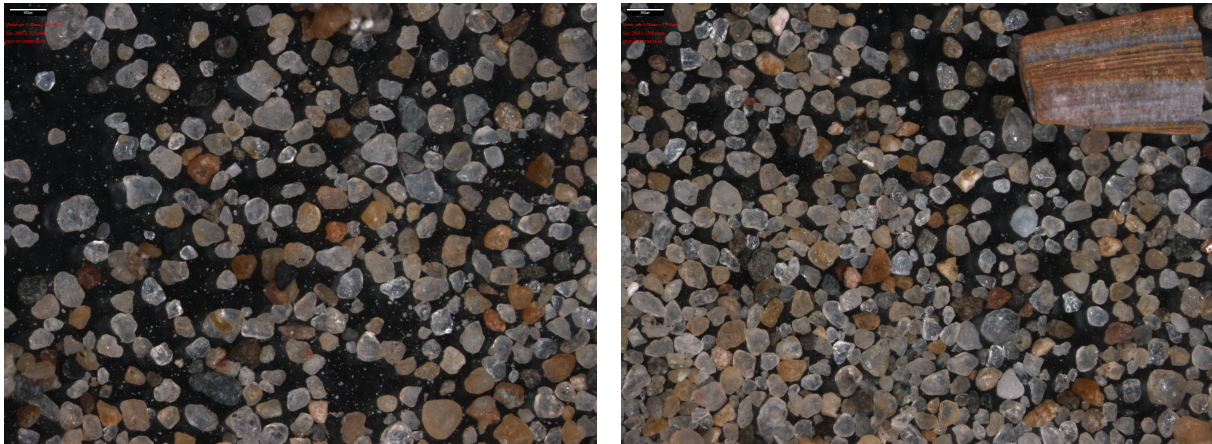
Figure 6.5: Microscopic pictures of sand sample

6.2 Pile Types

In total 8 instrumented piles were installed and tested. Pile 1, 4, 5 and 8 were driven closed-ended steel piles (Figure 6.7) designated for this research on time-dependent capacity. Piles 2, 3, 6 and 7 were screwed displacement piles designated for a different research on the influence of pile tip shape on tip bearing capacity. Piles 2 and 6 had a conical tip and piles 3 and 7 were flat tipped screw displacement piles, see Figure 6.6.
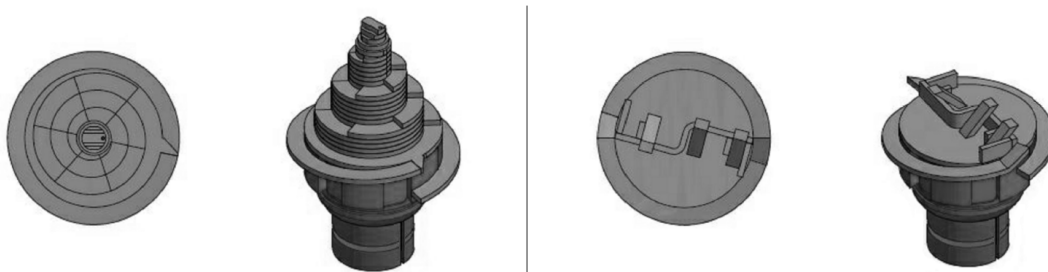
Figure 6.6: Screw displacement pile tips

A comprehensive description and the results of the research on the influence of pile tip shape on the tip bearing capacity of screwed displacement piles was not included in this thesis. A description of the test was published in the Dutch journal *Civiele Techniek nr. 7 - 2017* (IJnsen and Admiraal, 2017). The results will be published soon.

The piles were about 3 m long and the embedded length was approximately 2.9 m. For the closed-ended steel piles the outer diameter equaled 152 mm and the wall thickness was 9.5 mm. The footplate was welded to the pile over the complete outer circumference and grinded off to create a smooth edge. No enlarged footplate was used.

|← 0.15 m →| |← 3.00 m →|
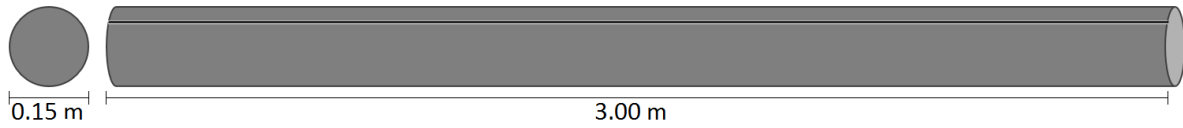
Figure 6.7: Closed-ended steel pile

Pile Instrumentation

The piles were instrumented with strain sensors along the pile shaft. Strain was measured with fibre optic strings. On opposite sides, along the length of the shaft, a small trench was cut to facilitate the fibre optic strings. At each side (A and B) 2 strings were glued in the trench, the sensors were located close to the pile tip, up to about 2 m above the tip (see Table 6.2). The interval between two sensors positions on the strings equaled 1 m. The strings were glued in with half an interval length difference in order to measure strain every 0.5 m. In total 10 strain sensors were installed at each pile. The sensor locations are visualized in Figure 6.8 where A and B indicate the side of the sensor and the number indicates the approximate distance of the sensor with respect to the pile tip. For protection the sensors were covered in silicone kit and the string was covered with epoxy hardener. Using two fibre optic strings per side not only reduced the recording interval along the shaft but also made the test more robust.

To check the response of the sensors prior to installation the piles were tested in a test frame, see Appendix E. In the frame 5 load steps were applied with an hydraulic jack while recording load and strain. Strain recordings up to 1000 Hz were possible.
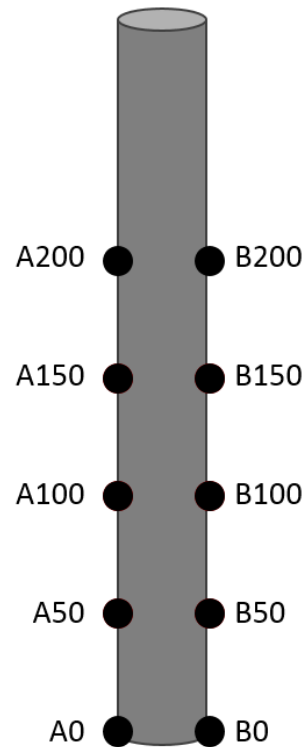
Figure 6.8: Sensor location and numbering

The strain measurements were used to determine the distribution of forces and thereby resistance over the pile. By multiplying the strain with the Young's modulus of steel ($210 * 10^6$ kPa) and the cross sectional area of the pile the force was calculated, see Equation 6.1.

$$F = \epsilon E A \qquad (6.1)$$

With:

F	=	Force	kN
ϵ	=	Strain	-
E	=	Young's modulus	kPa
A	=	Surface area	m^2

	A0	B0	A50	B50	A100	B100	A150	B150	A200	B200
Pile 1	25	45	525	525	1025	1040	1520	1520	2020	2040
Pile 4	25	30	530	525	1025	1030	1530	1525	2025	2030
Pile 5	25	25	535	515	1020	1025	1530	1515	2030	2025
Pile 8	30	30	530	525	1030	1025	1525	1525	2030	2025

Table 6.2: Sensor location with respect to pile tip in millimeter

6.3 Installation

The closed-ended steel piles were driven with a 400 kg ram in combination with a small drop height. The piles were driven by a mini rig which was located on drag line mats, see Figure 6.9 and Appendix E. The mats were supported by the sheet piles surrounding the sand fill in order to have no direct contact between equipment and sand fill.

A casing hosting the ram was placed on top of the steel pile. The impact of the ram was at the bottom of the casing transferring the impact to the pile head. The last meter was driven with a steel extension piece between the pile head and casing in order to drive the pile up to ground surface level.
During installation of the closed-ended steel piles the blows per 100 mm were counted and strain was recorded with 1000 Hz. The blows counted over the last meter and the total blows counted during installation are presented in Table 6.3.

A Ram
B Casing
C Drag line mat
D Pile
E Sand fill
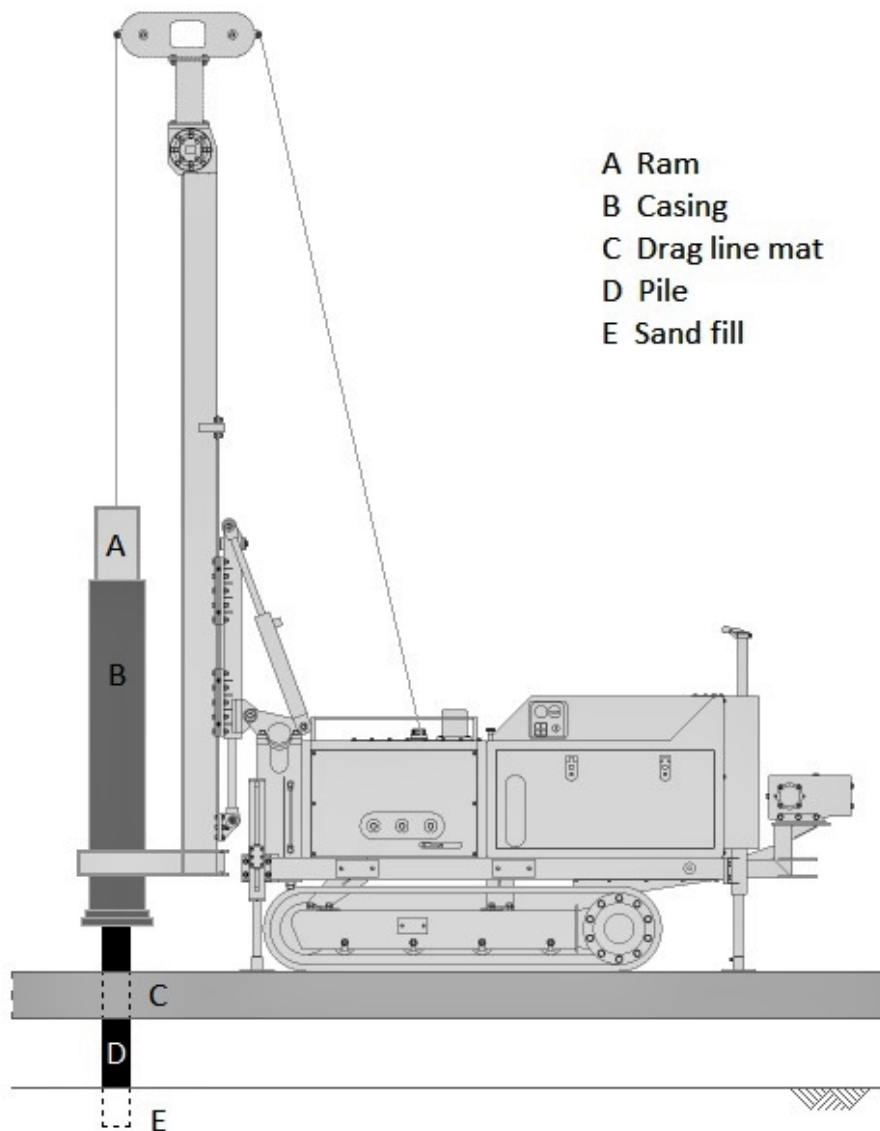
Figure 6.9: Mini rig used for installation

The steel piles were installed prior to installation of the screw displacement piles. This sequence was chosen to not affect the grout while hardening.

	Pile tip level [m NAP]	Embedded length [m]	Total blow count	Blow count last meter
Pile 1	-6.4	2.9	197	132
Pile 4	-6.4	2.9	207	146
Pile 5	-6.3	2.8	168	113
Pile 8	-6.4	2.9	212	167

Table 6.3: Installation depth and blow count

6.4 Load Test

The piles were statically tested in compression, a schematized test setup is provided in Figure 6.10. The load was applied to the pile head with a hydraulic jack where the counter force was provided by the self weight of a stack of steel drag line mats. During the load test strain was measured with a constant interval of 10 Hz. The force applied at the pile head was measured with a load cell at the pile head and by pressure gauges at the jack and near the pump. The load measurements were processed and recorded with the highest possible interval which equaled on average about 5 measurements per minute. All tests have been documented in time lapse from multiple angles.

First time, so called, virgin tests were conducted 2, 16, 32 and 70 days after installation. Virgin testing means that no significant load has been applied to a pile prior to testing it up to failure.
The test protocol and load scheme of the virgin tests were based on the Dutch guideline for load tests (NPR7201, 2017). The load scheme for the test program was designed to reach the average calculated capacity of 275 kN in 8 magnifying load cycles. For the last pile (pile 8) a lower theoretical capacity of 230 kN was considered since the previous tested piles did not reach the theoretical capacity. The loads applied are provided in Table 7.2 and visualized in Figure 7.1 presented in the next chapter.
The designed zero load equaled 10 kN. The zero load is the minimum load applied to the pile head during a load cycle, the pile was never fully unloaded during the test. Starting from the zero load, the load was increased in steps up to the intended load which would be kept constant for at least 1 hour. During build up and release of pressure the previous load steps were called for 10 minutes. The zero load between two load steps was kept constant for 15 minutes.
When a pile head movement of 0.1 mm or more was measured over the last 20 minutes of a load step the load step was extended until the creep was less than 0.1 mm over a 20 minute period. When the total duration of a load test was more than 4 hours the protocol continued to the next load step.

Failure Criteria

The piles were loaded up to a continuous downward movement of the pile head without noticeable change in the capacity. The pile capacity was determined as the force required for $0.1 * D$ pile displacement.
Displacement of the pile head was recorded by 3 probes measuring the distance between a reference frame and smooth horizontal steel plates attached to the pile head. The reference frame was supported by 3 legs situated outside the $10 * D$ influence zone. Movement by bending or displacement of the support frame was monitored with a wire sensor. Tents were on site to cover the frame and thereby reduce undesired weather influences like the influence of direct sun on the frame. The displacement transducers and the reference frame are indicated in the schematized test setup in Figure 6.10. Due to elastic shortening of the pile the difference between pile head and tip displacement increases with the applied load. For the 3 m long piles the difference between pile head and tip displacement increases 0.1 mm for every 30 kN capacity increase.
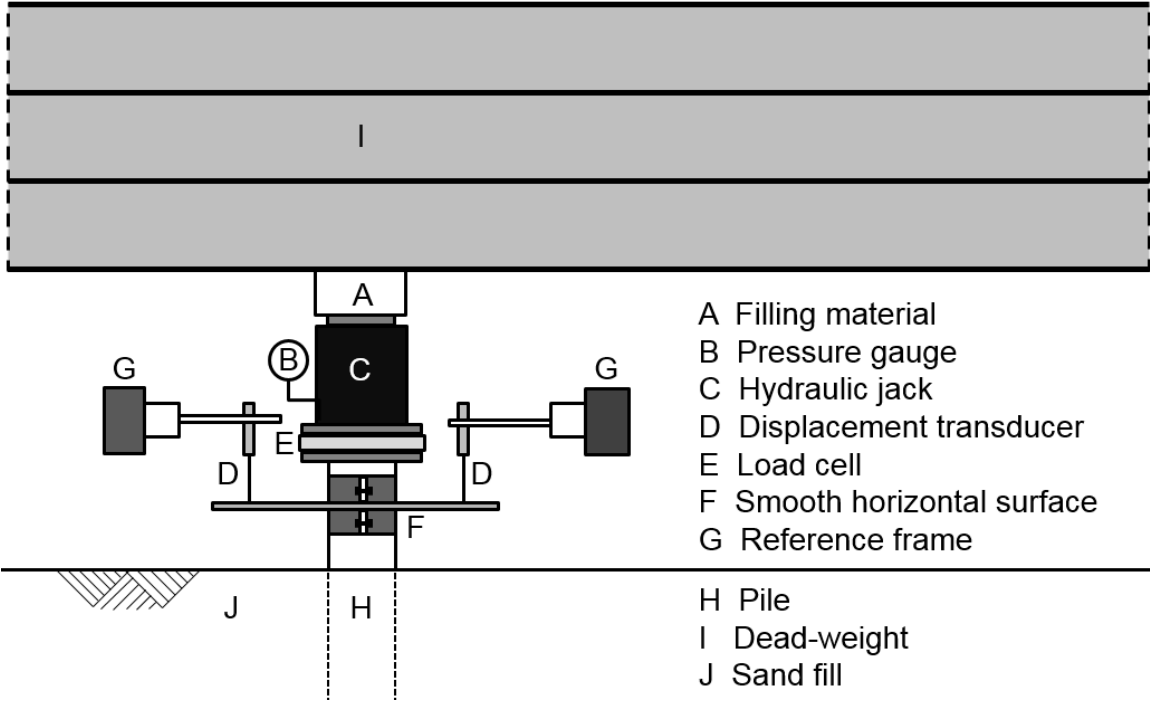
Figure 6.10: Static load test setup

7 | Results Test Program

This chapter covers the test results of the 4 closed-ended displacement piles tested. A virgin test was conducted 2, 16, 31 and 70 days after installation, see Table 7.1. First the load-, displacement- and strain measurements are discussed before the time-dependent capacity is discussed.

	Pile 1	Pile 4	Pile 5	Pile 8
Pile age at virgin test moment	2 days	31 days	16 days	70 days

Table 7.1: Test occasions

7.1 Load Measurements

The load applied at the pile head was recorded by an electric pressure gauge at the hydraulic jack and by a calibrated load cell. Piles 1, 4 and 5 were pressure controlled tests, the load at the pile head was adjusted based on the pressure gauge at the pump which was used to increase the pressure in the jack. From the results of these piles it was found that the recorded load deviated between the pressure gauge and the load cell. The jack contained a spring that increased the resistance linear with the extension of the hydraulic cylinder. The absolute deviation between the pressure gauge and load cell measurement increased with pile displacement and thereby the deviation between aimed and true load increased. From the fourth load test (pile 8) the protocol was changed (see section 6.4), from this test the applied load was controlled based on load cell measurements instead of pressure gauge measurements.

The loads provided in this chapter are the loads measured by the calibrated load cell. The load was zeroed at the start of the test. The load steps summarized in Table 7.2 are visualized in Figure 7.1. The capacity of the piles is determined from the load-displacement curves (Figure 7.2) and equaled the load at $0.1 * D$ displacement.

	Aim pile 1-4-5 [kN]	Pile 1 [kN]	Pile 4 [kN]	Pile 5 [kN]	Aim pile 8 [kN]	Pile 8 [kN]
Zero load	10.0	2.9	9.0	9.0	10.0	6.9
Load step 1	34.4	10.9	27.3	29.8	28.8	25.3
Load step 2	68.8	23.4	56.5	63.0	57.5	53.9
Load step 3	103.1	36.3	83.3	96.6	86.3	82.8
Load step 4	137.5	42.0	109.0	127.5	115.0	111.7
Load step 5	171.9	53.9	134.7	158.5	143.8	140.4
Load step 6	206.3	66.7	160.6		172.5	169.0
Load step 7	240.6	76.5			201.3	
Load step 8	275.0	87.2			230.0	
Load step 9	309.4	98.2			258.8	
Load step 10	342.8	108.9			287.8	
Load step 11		120.0				
Load step 12		131.4				
Load step 13		143.2				
0.1*D displacement		**153**	**166**	**173**		**188**

Table 7.2: Loads applied per load step
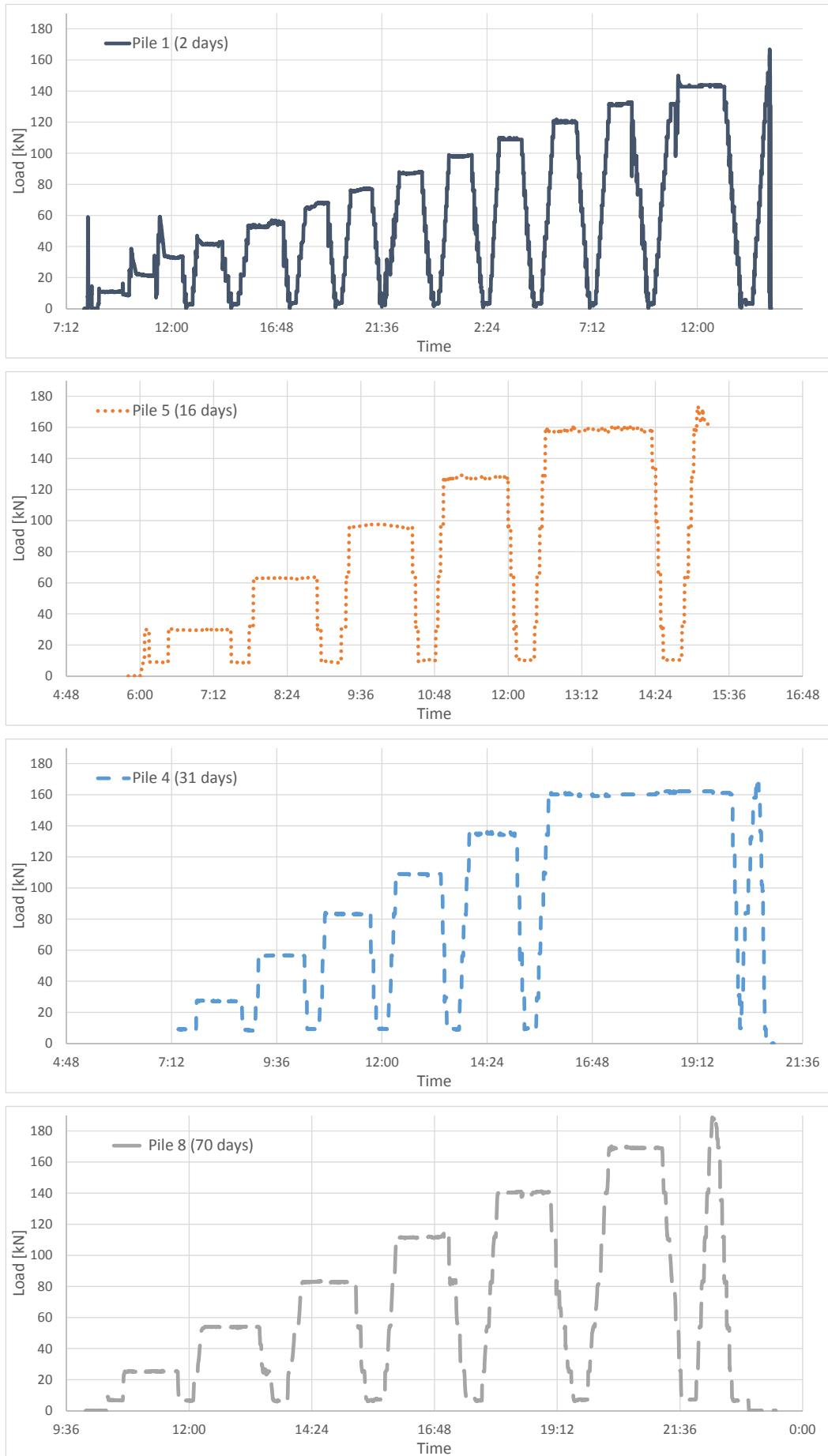
Figure 7.1: Loads applied at pile heads

Pile 1 - 2 days

Pile 1 was tested 2 days after installation. For this test both an electric pump and a hand pump were used to increase the pressure in the jack. When using the electric pump the loading rate was far higher and therefore harder to control. This caused the sloppy start of the test where a load of almost 60 kN was reached, see Figure 7.1. The electric pump was used at the start of the load test and after the last stable load step. The high loading rate at the start and end of the test is also visible in Figure 7.2. The response to the load was stiffer with a high loading rate. In the succeeding tests (piles 4, 5 and 8) only the hand pump was used.

During the load test of pile 1 the jack was wrongly connected, therefore the measured pressure did not represent the applied load. Smaller loads were applied than expected, this resulted in a test with 13 load cycles that lasted more than 31 hours. During build up to a 14th load cycle the pile failed at a capacity of 153 kN. In Figure 7.1 a peak load over 160 kN is visible. This load was recorded at a large displacement (>20 mm) and is caused by the stiff response of the pile to the high loading rate applied at the end of the test.

Pile 5 - 16 days

At the start of the test on pile 5 the load was directly built up to the first load step but was quickly corrected to follow the prescribed protocol. At the end of the load test, just after failure, the recording stopped at the peak of the load cycle.

Load step 5 was extended due to the creep limit which prescribes less than 0.1 mm creep over a 20 minute period. The pile failed during build up to load step 6. The pile capacity at failure equaled 173 kN and the load test took only about 10 hours.

Pile 4 - 31 days

Pile 4 was tested 31 days after installation, and failed at a load of 166 kN. Recording of the load data started when the zero load (10 kN) was already applied. Therefore the recorded data was zeroed with the load measured at the end of the test after the pile had failed and all pressure in the jack was released.

During load step 6 the pile had a high creep rate which was more or less constant to 0.12 mm per 20 minutes for more than 4 hours straight. Just after 4 hours the creep rate reached the limit of 0.1 mm creep over a 20 minute period. The protocol proceeded to the next load step where the max capacity was reached, see Figure 7.1. Due to the long extension of load step 6 the total test duration equaled about 14 hours.

Pile 8 - 70 days

The load test on pile 8 was the last virgin load test, 70 days after installation. The pile was tested considering the same protocol as the previous tested closed-ended steel piles but with smaller load steps since non of the previous tested piles had reached the average theoretical capacity. In contrast to the previous tests this test was controlled based on load cell measurements. In a very neat test the pile failed during build up to load step 7 at a capacity of 188 kN. The total test duration was about 13.5 hours.

Considering the measured capacities of the 4 virgin load tests at different moments after installation the lowest capacity was measured for the first pile, tested after 2 days. The highest capacity was measured for the last pile tested 70 days after installation. However, for pile 5, tested after 16 days, a higher capacity was found compared to pile 4, tested 31 days after installation. The load displacement curves of all 4 piles are provided in Figure 7.2. Time-dependent capacity of the piles was discussed later in this chapter.
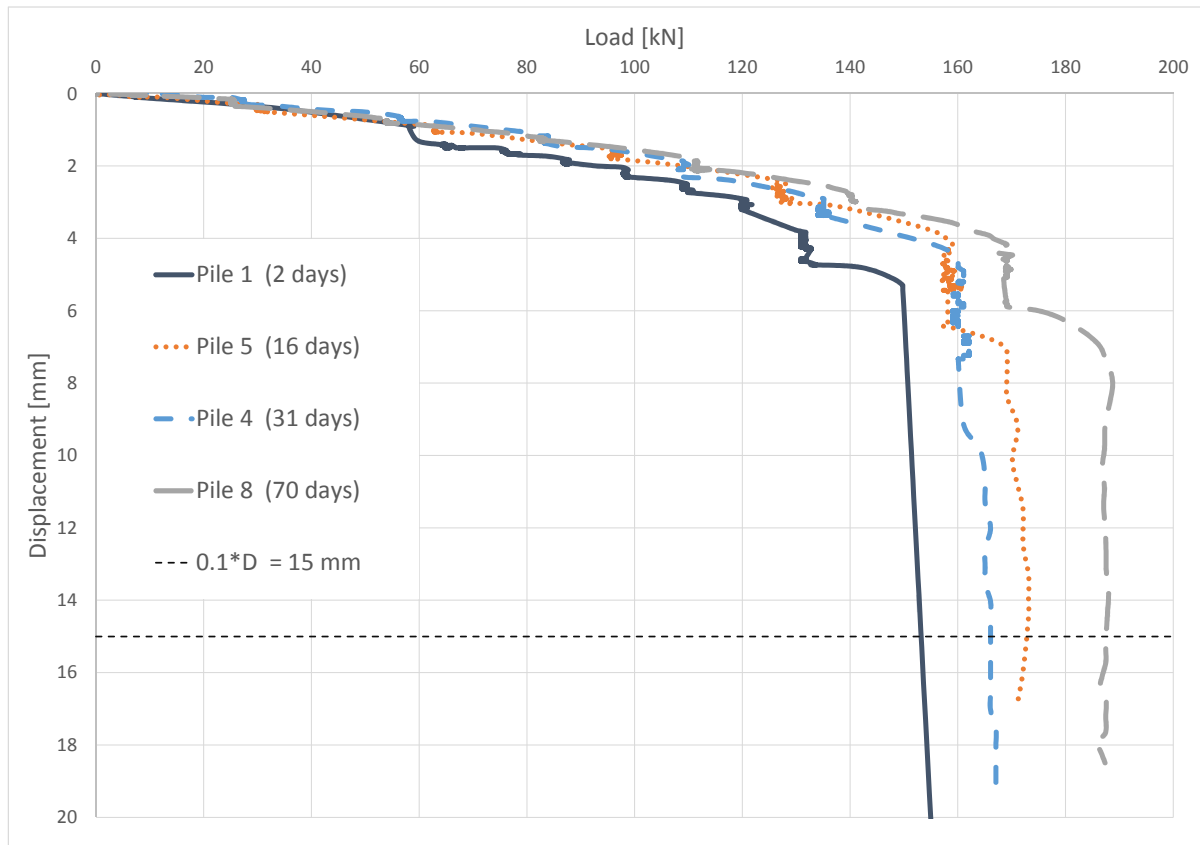
Figure 7.2: Summary of load-displacement curves

7.2 Displacement Measurements

Pile head displacement relative to the reference frame was measured with 3 displacement probes of which only two are displayed in Figure 6.10. Accurate displacement measurements were required since the capacity of the pile was determined by a set displacement of $0.1 * D$, see section 6.4. Due to the small pile diameter (0.15 m) only a small displacement was required causing the measuring error to be relatively large. The displacement of the pile head was determined as the average displacement measured by the 3 probes. Movement of the reference frame was monitored for all tests except the first. Minor frame movements were observed, mainly caused by temperature influences of direct sun on the frame. No compensation for frame movement or elastic shortening has been applied in any of the tests. Compensation was not considered since the movement was limited and the piles displaced significant when they approached failure, see Figure 7.2. The significant displacement at failure indicates the failure criterion of $0.1 * D$ displacement to be suitable for the piles tested.

7.3 Strain Measurements

Each pile was equipped with 10 strain sensors. The sensors were located on opposite sides of the pile and equally distributed between 0 and 2 m height relative to the pile tip (see Figure 6.8). Figure 7.3 demonstrates the measured strain during the tests for the sensors located at different heights (h) relative to the pile tip. The strain measurements were zeroed at the start of the load test. No measurements were recorded for the sensors that are not displayed in the legends of Figure 7.3.

The strain measurements on opposite sides of the pile were averaged in the analysis of strain development over the pile. A difference in strain was found between the A and B side measurements due to eccentric loading, bending and the piles being installed not perfectly vertical. The average strain development with pile displacement is presented in Figure 7.4. The averaged strain distribution over the piles for the different load steps is provided in Figure 7.5.

Significant creep was observed for the piles when they approached failure. This is also visible in Figure 7.2 where significant displacement is visible without any change in load. Creep causes local redistribution of forces over the pile and thereby local redistribution of strain, see the last complete load steps in Figure 7.3.
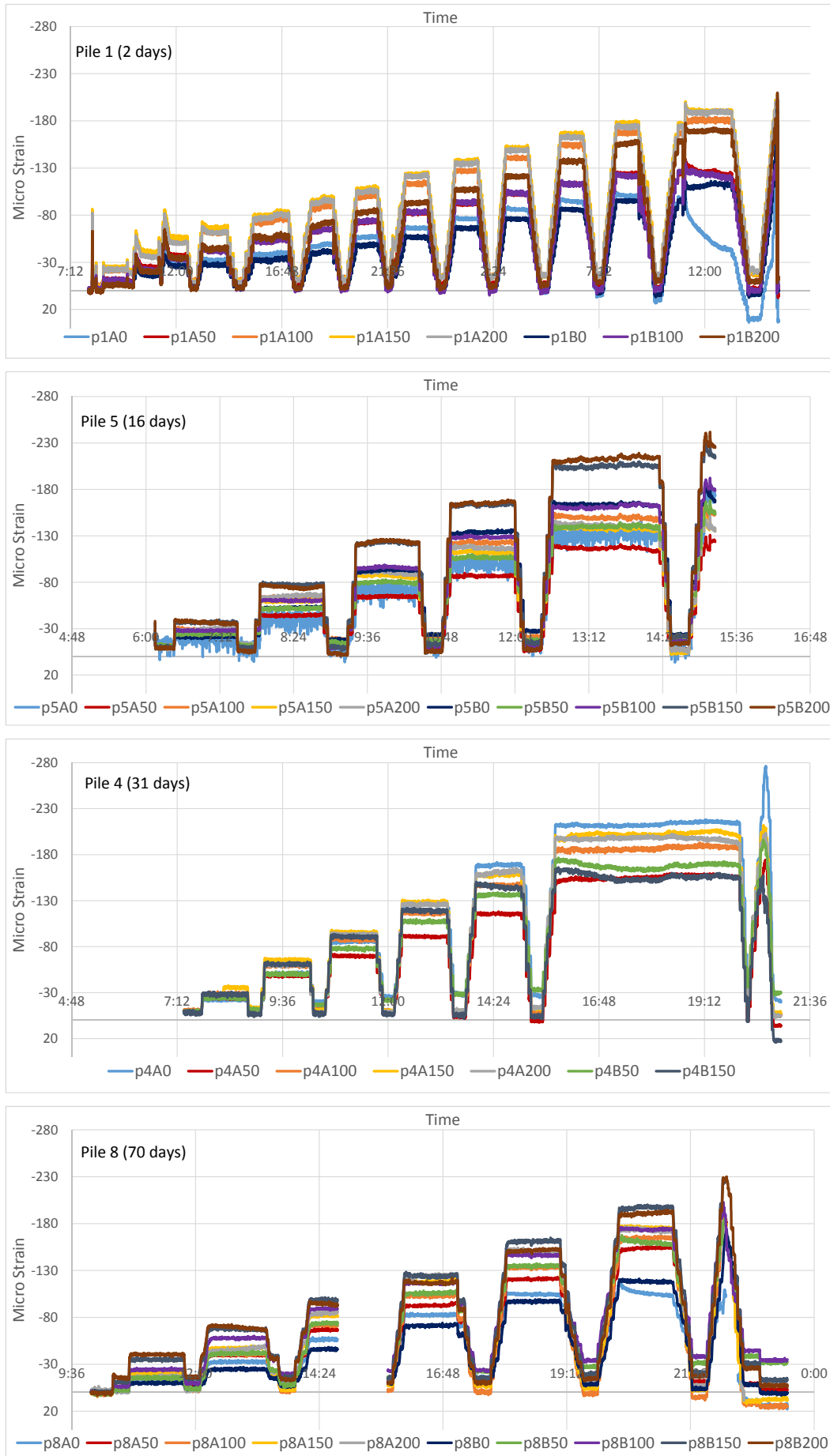
Figure 7.3: Strain measured at different levels relative to the pile tip

Pile Tip Measurements

Prior to installation the response of the strain sensors was tested by axially pressurizing the piles in a horizontal test frame. The sensors at the pile tips behaved different from the sensors further on along the shaft. At the pile tips larger negative strains were found compared to the other sensor locations when a normal force was applied. During the pile load tests the deviant behavior of the pile tip sensors was also found, see Figure 7.4 and Figure 7.5. The foot plate was welded to the pile and the edges were grinded off to create a smooth connection with the pipe. Thereafter, the small trenches were cut along the pile length and the fibre optics were glued in. The tip sensors were located 25 to 30 mm above the pile tip, see Table 6.2. This distance included the thickness of the footplate. Different effects were anticipated to be the cause of the larger negative strain found at the pile tip:

- The cross-sectional area is not constant over the length of the pile. The piles were made from old drill-pipes and used to have coupling pieces at both ends. The middle section of a drill-pipe was supposed to have a constant wall thickness. The wall thickness increased towards one end of the pipe and decreased towards the opposite end. When the drill-pipes have not been cut correct the wall thickness of a pile could deviate towards one or both ends of the pile. This could explain why the effect was not observed with all piles. At the moment of publishing the piles were still in the test pit. Eventually the piles will be extracted and the geometry will be checked to confirm or disprove this theory.
- Welding of the footplate caused stress concentrations just above the pile tip. The stress concentrations cause local strain variations when a pile is loaded. Grinding off part of the weld might reduce the stress concentration. The fact that the deviant behaviour of the tip sensor was not observed for all piles could be explained by the inconsistency of the welding and grinding process.
- The footplate tends to bend under the applied load. This could explain why the effect increased with the load. However, bending of the footplate is likely to cause a tensile force close to the sensor instead of an increased compressive force. Also, when bending caused the deviant behaviour it would have been present for all piles.

Residual Loads

The strain measurements were zeroed at the start of the load test, therefor residual loads were ignored. The residual load of a pile is the locked-in axial force at the start of the pile test caused by pile installation (Fellenius, 2002). The test program was designed to account for residual loads, strain was measured during installation and during the load test. The residual load of a pile could be determined from the difference between the strain measured at the start of installation and the strain measured at the start of the load test. However, for 2 of the 4 piles (piles 4 and 5) strain recording started too late to determine the strain distribution over the pile at the start of the load test. For the remaining piles (piles 1 and 8) the distributions found did not match the examples found in literature. Two effects were considered to be the cause of this discrepancy:

- A deviant strain distribution was found due to unconsidered temperature effects. Considering the expansion rate of steel, the strain along the pile will deviate about 12 micro strain for every centigrade temperature difference. The piles were installed on a sunny day and significant local differences in temperature were found along the piles. Temperature was measured manually prior to installation but was not recorded. Therefore, local temperature was not taken into account when the difference in strain between start of installation and start of load test were determined.
- It was difficult to determine the benchmark where the strain measurements had to be zeroed to set the reference load in the pile. The pile were placed vertical while hanging from a strap and installed with a casing and hammer on the pile, see section 6.3. From the recorded strain data is was difficult to determine to what forces the piles were exposed and where to zero the measurements.

The strain measurements presented in Figure 7.3 do not return to an equal strain level compared to the start of the load test. This is in contrast to the load measurements (Figure 7.1) that do return to the zeroed values at the start of the load test. The difference in strain at the start and end of the load test might be due to temperature variations during the test. However, the difference varies per side and level with respect to the pile tip. The difference might also be explained by locked-in stresses that were released during the load test.

Considering Fellenius (2002) the shaft resistance along the upper portion of the pile would be overestimated and along the lower portion of the pile would be underestimated when ignoring residual loads. Also, the total shaft resistance would be overestimated and, correspondingly, the pile toe resistance would be underestimated.
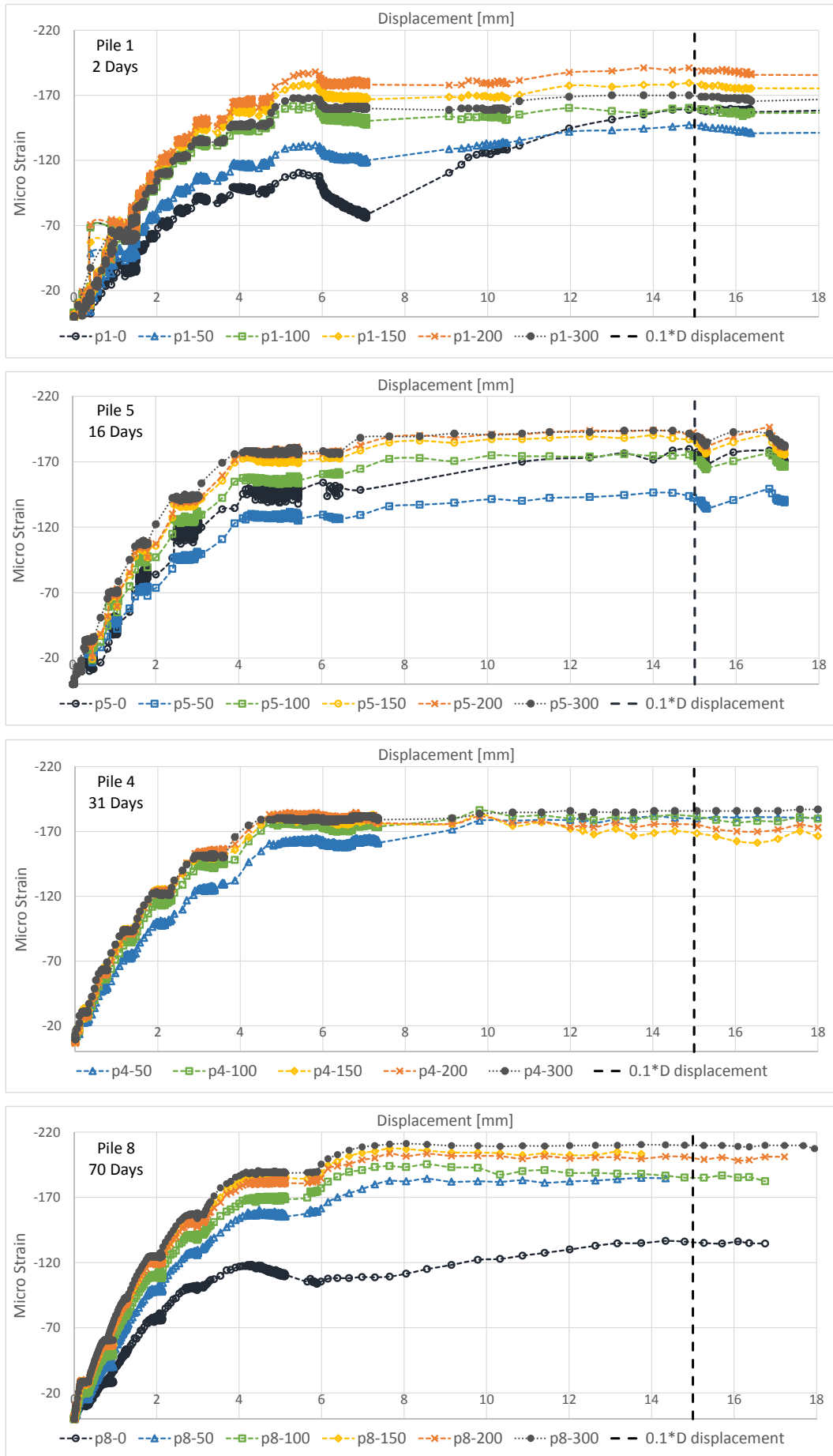
Figure 7.4: Average strain development at different heights (h) relative to the pile tip
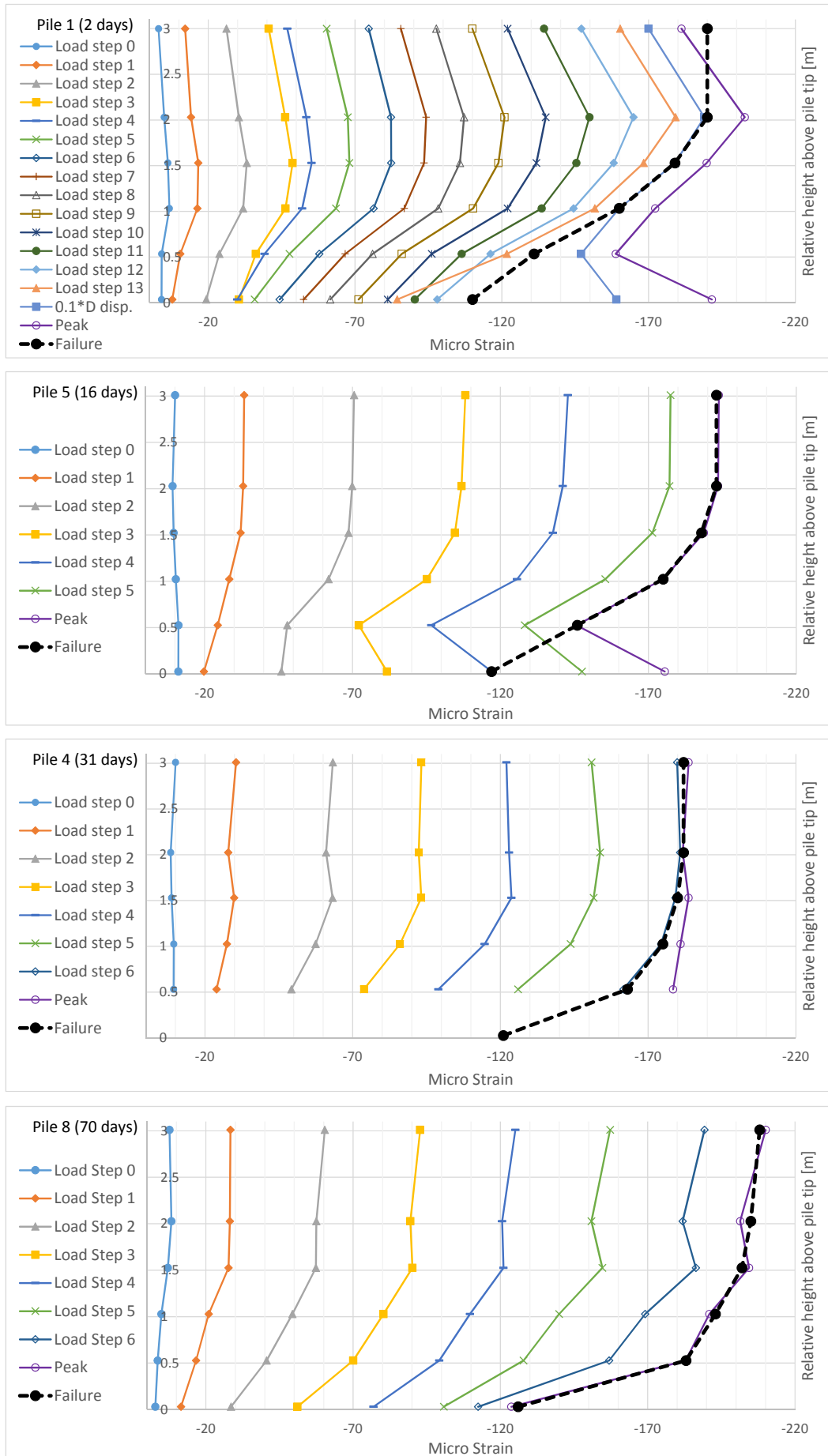
Figure 7.5: Strain distribution over the pile length

Figure 7.4 presents the development of strain with displacement of the pile head. The strain displayed for the levels 0 to 200 is the average strain measured with the strain sensors installed on opposite sides of the pile. The strain presented at the pile head (level 300) was back calculated from the load cell measurements using Equation 6.1. No negative shaft resistance was expected since the pile was fully embedded in sand. Therefore the largest negative strain was expected at the pile head and the smallest negative strain at the pile tip. Figure 7.5 illustrates the average strain measured at each load step as well as the peak in the strain data. In this figure it is clearly visible that some distributions are not in accordance with the expectation that the compression in the pile reduces from pile head to pile tip.

A corrected strain distribution at failure has been determined based on the development of strain over the pile shaft (Figure 7.3, 7.4 and 7.5) with an increasing load and displacement. In Figure 7.5 the approximated distributions are indicated by the thick dashed lines and the distributions at failure are summarized in Figure 7.6. In the sections below the strain measurements are further discussed per pile test.

Pile 1 - 2 days

During instrumentation of pile 1 a fibre optic string on the B-side got damaged, therefore no recordings were available for sensors B50 and B150. The strain at the B50 and B150 locations was interpolated from the measurement at the locations B0, B100 and B200.

The back-calculated strain at the level $h \approx 3$ m does not match the strain measurements at the other levels towards the pile tip. The strain at the pile head ($h \approx 3$ m) was back calculated from the load cell data with Equation 6.1. An incorrect cross-sectional area is probably the cause. The potential variable cross-section towards one or both ends of the pile was already covered in this section when the deviant pile tip measurements were discussed. Another option considered was a too large offset for the load cell. In that case the pile would have been fixed under the dead-weight before the measurements were zeroed. The deviation increased with the load therefore the incorrect cross-sectional area is more probable. With an incorrect offset the deviation would have been constant. The pile geometry will be checked when the piles are excavated.

During build up of load step 13 the pressure in the jack was shortly released and the load dropped rapidly. After the drop sensor A0 gave faulty measurements as visible in Figure 7.3 and from the strain distribution found for load step 13 (Figure 7.5).

At the end of the test the pressure in the jack was increased by means of an electric pump which caused the pile to displace rapidly and an unrealistic large strain to develop at the pile tip. This is clearly visible in Figure 7.5 as the peak distribution measured. The peak was measured when the displacement already exceeded $0.1 * D$.

The approximated strain distribution at failure was corrected for the peculiar measurements found at the head and tip of pile 1. This distribution is indicated by the thick dashed line in Figure 7.5. The strain at the level $h \approx 0.5$ m was determined from the measurements at the pile tip and the level $h \approx 1$ m. When the distribution started to deflect at the pile tip the interpolated strain at $h \approx 0.5$ m was also affected.

Pile 5 - 16 days

In the load test of pile 5 the recording of the strain data started too late and stopped too early as visible in Figure 7.3. In the load test on pile 4 the recording also started after the test had started. A reference strain was determined for the first zero load applied after the strain recording started. The strain at the zero load applied was set to 10 micro strain at all sensor levels based on Equation 6.1 and a 9 kN zero load. Looking at the strain measurements of pile 8 in Figure 7.3, the strain already varied at the different sensor levels when the zero load was applied at the start of the test. The largest compression was found in the top of the pile and decreased towards the pile tip. Thus, the strain along the bottom section of piles 4 and 5 might be slightly overestimated by using a constant correction of 10 micro strain at all sensor levels and the deviation increases towards the pile tip.

Stable recordings were found for all sensors. The signal of sensor p5A0 was not as smooth as the other sensors but still workable since the average strain per load step was used to determine the strain for each load step.

Both pile tip sensors gave improbable values for the strain at the pile tip. Potential causes of the deviant measurements at the pile tip were already covered in this section. The strain distribution over the bottom section of the pile was extrapolated from the average reduction in strain between $h \approx 1$ m and $h \approx 0.5$ m to approximate the strain distribution at failure.

Pile 4 - 31 days

During the load test on pile 4 the data recording started when the zero load was already applied. For this reason it was not possible to zero the strain and load measurements at the start of the test. The offset for the load recordings was determined at the end of the test when all the load was taken off the pile. Zeroing the strain recordings at the end of the test was not possible since the strain measured at the end of the test differs from the strain measured at the start of the test. The drifting strain measurements during the test was already covered in this section when residual loads were discussed.

The correction described for the strain data of pile 5 was also applied to the strain data of pile 4. The zero load measured for pile 4 was equal to the zero load of pile 5. Therefore, the set strain at the first zero load was also set to 10 micro strain for pile 5.

A fibre optic string on the B side got damaged prior to the load test. No recordings were available from the sensors B0, B100 and B200. The strain at the B100 and B200 locations was interpolated from the measurements at the locations B150 and B300.

It was not possible to receive reliable strain measurements at the pile tip since the pile tip sensor on the B side was lost and the sensor on the A side gave improbable values. The strain distribution at failure indicated by the thick dashed line in Figure 7.5 is highly approximate for the bottom section of the pile. The strain distribution in this section was approximated based on the distributions found for the other piles.

Pile 8 - 70 days

Pile 8 was the only pile where the strain was measured for a significant period prior to pile loading and after the load had been taken off. Connection to the sensors was lost for some periods during the test, see the gap in the data in Figure 7.3. The gaps had no negative influence on the results of the test.

A drop of the strain at the pile p8A0 tip sensor was observed during load step 6. The strain data of pile 8 required little correction to determine the strain distribution at failure. This distribution is indicated by the thick dashed line in Figure 7.5.

The strain distributions at failure are combined in Figure 7.6. The distributions at failure for the piles tested at different moments after installation are compared in the next section.
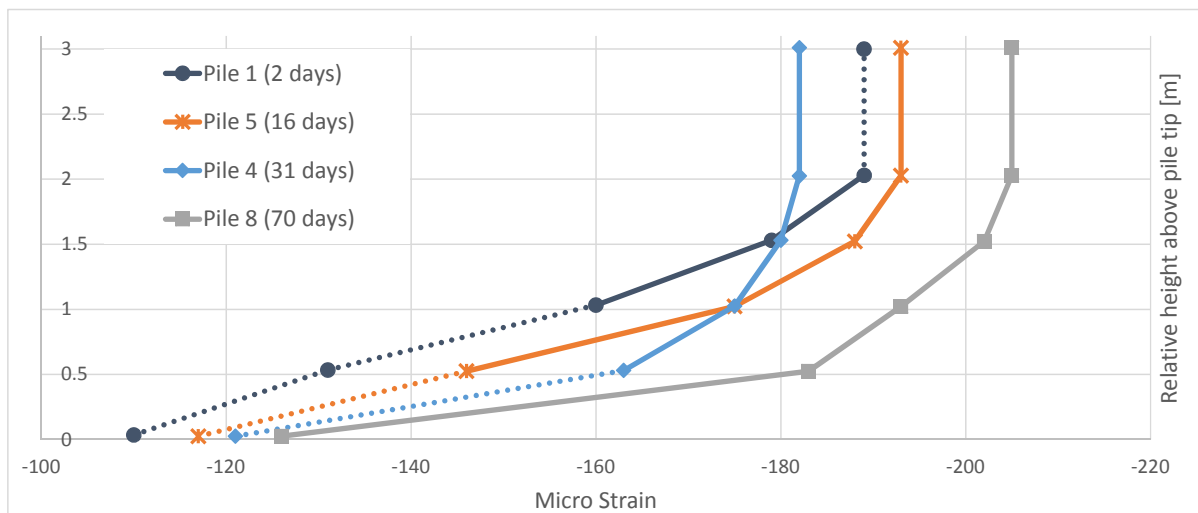
Figure 7.6: Strain distributions at pile failure

7.4 Time-Dependent Capacity

The virgin pile capacities were determined from the load-displacement curves, where the capacity was defined as the load at $0.1 * D$ displacement. The load-displacement curves are summarized in Figure 7.2 and the capacities are presened in Table 7.3.

A trend for time-dependent capacity increase was found for the 4 piles tested. The smallest capacity was found for the first pile tested, 2 days after installation. The largest capacity was found for the last pile tested, 70 days after installation. However, for the pile tested 16 days after installation a larger capacity was found compared to the pile tested 31 days after installation. An average increase in total capacity of 15% was found compared to the reference capacity determined 2 days after installation. When fitting a trend line for the normalized capacity over the logarithm of normalized time (Figure 7.7), a 13% increase per log cycle of time was found. This is just below the lower boundary set by Axelsson (2000) which equaled 15% per log cycle of time as visualized in Figure 3.3. The rate of capacity increase was expected at the higher end of the range set by Axelsson (2000) since staged test results were also included in Figure 3.3.

The contribution of the pile tip and pile shaft was determined from the approximated strain distributions at failure, see Figure 7.6. Equation 6.1 was used to calculate the force at the pile tip. The shaft contribution was determined by the total capacity minus the pile tip contribution. The tip and shaft contributions are presented in Table 7.4 and Table 7.5.

	Age [days]	Calculated capacity [kN]	Measured capacity [kN]	Q_m/Q_c	Rate of increase
Pile 1	2	221	153	0.69	1.00
Pile 5	16	210	173	0.82	1.13
Pile 4	31	217	166	0.76	1.08
Pile 8	70	185	188	1.02	1.23

Table 7.3: Measured and calculated pile capacity

	Age [days]	Calculated tip capacity [kN]	% of total calculated capacity	Measured tip capacity [kN]	% of total measured capacity	Q_m/Q_c	Rate of increase
Pile 1	2	153	69	98	64	0.64	1.00
Pile 5	16	140	67	104	60	0.74	1.06
Pile 4	31	145	67	108	65	0.74	1.10
Pile 8	70	116	63	113	60	0.97	1.15

Table 7.4: Measured and calculated tip capacity

	Age [days]	Calculated shaft capacity [kN]	% of total calculated capacity	Measured shaft capacity [kN]	% of total measured capacity	Q_m/Q_c	Rate of increase
Pile 1	2	68	31	55	36	0.81	1.00
Pile 5	16	70	33	69	40	0.99	1.25
Pile 4	31	72	33	58	35	0.81	1.05
Pile 8	70	70	38	75	40	1.07	1.36

Table 7.5: Measured and calculated shaft capacity

The shaft capacity increased on average 22%. On a log time scale the increase equaled 18.5% per log cycle of time, see figure Figure 7.7. A gentle average increase of 10% was found for the pile tip capacity with time. This equaled 9% increase per log cycle of time and is in contrast with the relation found in literature where the tip capacity is generally found to be constant in time and only the shaft resistance to increase. The strain distribution determined over the bottom sections of piles is highly approximate, especially for pile 4 and 5 where the tip sensors gave deviant measurements throughout the complete load test. Therefore the division between tip and shaft has a low reliability.

The variable tip capacity might also be explained by spatial variability of soil properties. Prior to installation CPTs had been conducted at the exact pile locations. To account for local variations in soil properties the measured capacities were compared with the calculated capacities at the exact pile locations. The piles were calculated according to the method available in the Dutch Design code, see Appendix A. The results are presented in the forelast columns of Table 7.3, 7.4 and 7.5. The relation between the calculated and measured capacity was visualized in Figure 7.8.
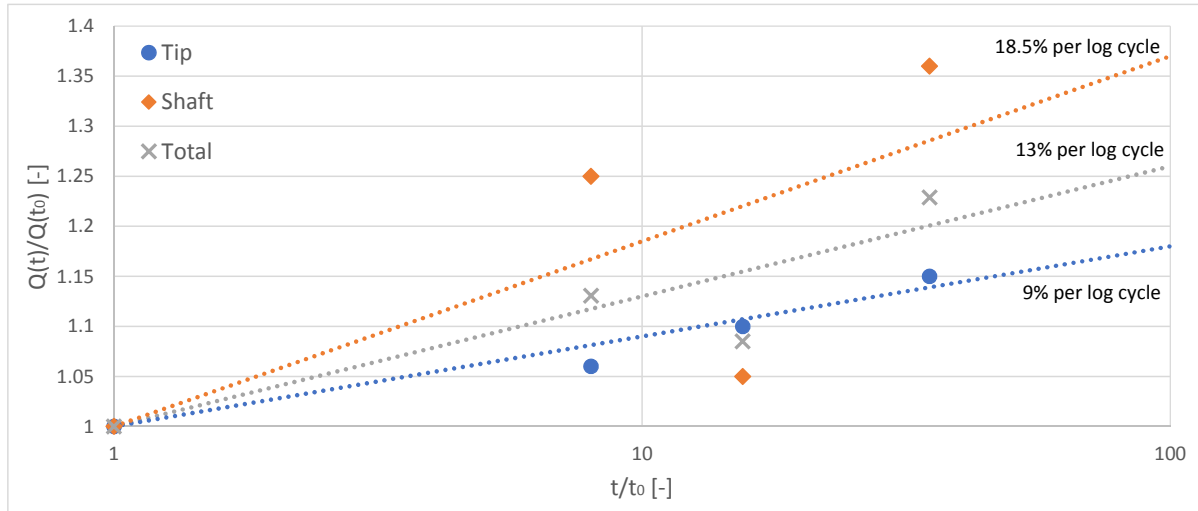
Figure 7.7: Capacity development compared to reference capacity

Considering the total measured capacity normalized by the total calculated capacity a trend for set-up was found. The pile tip capacity increase was larger than the shaft capacity increase considering the measured capacity normalized by the calculated capacity. The first pile, tested 2 days after installation, only reached 70% of the calculated total capacity where the last pile tested, 70 days after installation, reached 100% of the calculated total capacity. The same trend was found for the pile tip capacity. The first pile tested had the highest calculated tip capacity but the lowest measured tip capacity. Contrary, the last pile tested had the lowest calculated tip capacity but the highest measured tip capacity. The measured shaft capacity normalized by the calculated capacity showed a more gentle trend for capacity increase with pile age.
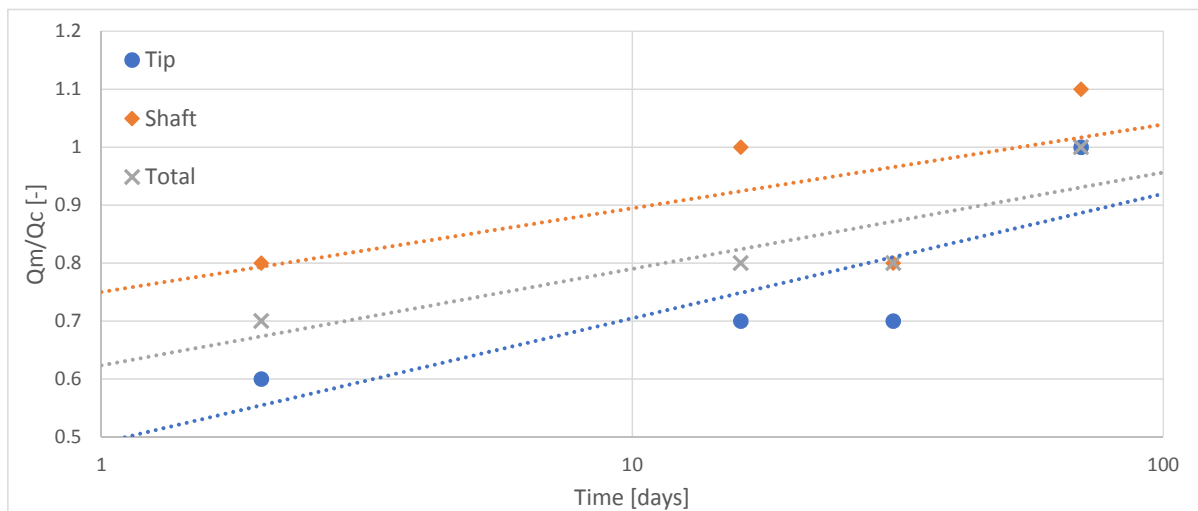
Figure 7.8: Calculated and measured capacity in time

The low accuracy of the Koppejan method was covered in chapter 4 which makes normalizing the measured capacity by the calculated capacity doubtful. On the other hand, when the rate of capacity increase is based on the capacity relative to a reference capacity the reliability of the test program is based on the quality of the reference capacity. The first load test of a test program generally has the lowest quality due to the lack of experience with the test location and response of the piles.

A useful example was the first pile tested for this research where the jack was wrongly connected, no frame movement was recorded and the protocol was designed for a too large average design capacity. As a result pile 1 had more than double the amount of load cycles compared to the other piles. The capacity of a pile is thought to be related to the test protocol. Due to the wrongly connected jack in the first load test the protocol was accidentally changed. Generally a lower shaft resistance is found for piles subjected to cyclic loads due to stress rotations caused by the cyclic movement of the pile.

The pile capacity was determined based on the recordings by the calibrated load cell. Considering the load cell data the capacity of pile 1 is the lowest. Looking at the strain data and considering a constant pile geometry this is not the case. It was assumed that the sand did not provide any resistance over the top meter of the pile due to the low cone resistances measured. For 3 piles the back calculated strain at the pile head was about equal to the strain measured at $h \approx 2.0$ m. For pile 1 the back calculated strain was lower than the strain measured at the level $h \approx 2.0$ m, see Figure 7.4. This indicated a negative shaft resistance over the top section of the pile which was not feasible with the test settings. Since the cross-sectional area is expected to differ from pile to pile and even within a pile the measurements of the calibrated load cell were considered leading. When the approximated strain distributions at failure (Figure 7.6) were considered leading the pile order sorted for increasing capacity would change to 4, 1, 5 and 8, tested respectively 31, 2, 16 and 70 days after installation. This emphasizes the need to check the pile geometries.

The increase in capacity found in the test program is not comparable to the increases found in literature or for the test programs considered in the database study, see Figure 5.4. Prior model studies also indicated far less impressive set-up rates compared to full scale field tests (Rimoy and Jardine, 2015). Potential causes identified by Rimoy and Jardine (2015) included mismatches with field stress conditions, physiochemical effects, multiple re-testing, scale effects including the test setup boundaries within the influence zone of the pile, a too large grain size and interaction with neighbouring test piles.

The low rate of capacity increase in this test program is expected to be related to the age of the sand deposit. The sand had only been in place for less than 2 weeks prior to pile installation. Formation of a stress arch is expected to be less prone for fresh deposits due to a relative low stiffness. The displaced soil will move into the soil body without forming a stress arch. Research on land reclamation projects revealed increased CPT resistance with time for newly deposited or densified hydraulic fills. Also, laboratory tests on aged samples have displayed increases in stiffness, dilation, and strength with time compared to non-aged samples (Chow et al., 1998).

Alpha-Values

Alpha (α) values are used in the Dutch design code NEN9997-1 (2016) to calculate the tip and bearing shaft capacity of piles, see Appendix A. The α-values are material and installation method dependent. For driven closed-ended steel piles loaded in compression the prescribed α_s and α_p are 0.010 and 0.7 respectively.

The strain sensors along the shaft of the piles divided the shaft length in 5 sections. For each section an α-value was back-calculated from the strain distribution and the CPT profile in order to asses the development of resistance over the pile shaft in time. Figure 7.9 provides the development of the back calculated α_p and α_s with the displacement measured at the pile head for pile 1 and 8. Pile 1 was the first pile tested, 2 days after installation, and pile 8 was the last pile tested, 70 days after installation. From Figure 7.9 it was found that pile 8 developed both higher α_p and α_s values with the displacement. From 5.9 mm displacement the tip sensor p1A0 gave deviant measurements, see Figure 7.3, 7.4 and 7.5. The back calculated α-values for pile 1 are incorrect from this displacement which is indicated by the vertical dotted line in Figure 7.9. Pile 4 and 5 were not included in Figure 7.9 since the pile tip sensors of these piles gave deviant measurements from the start of the tests.
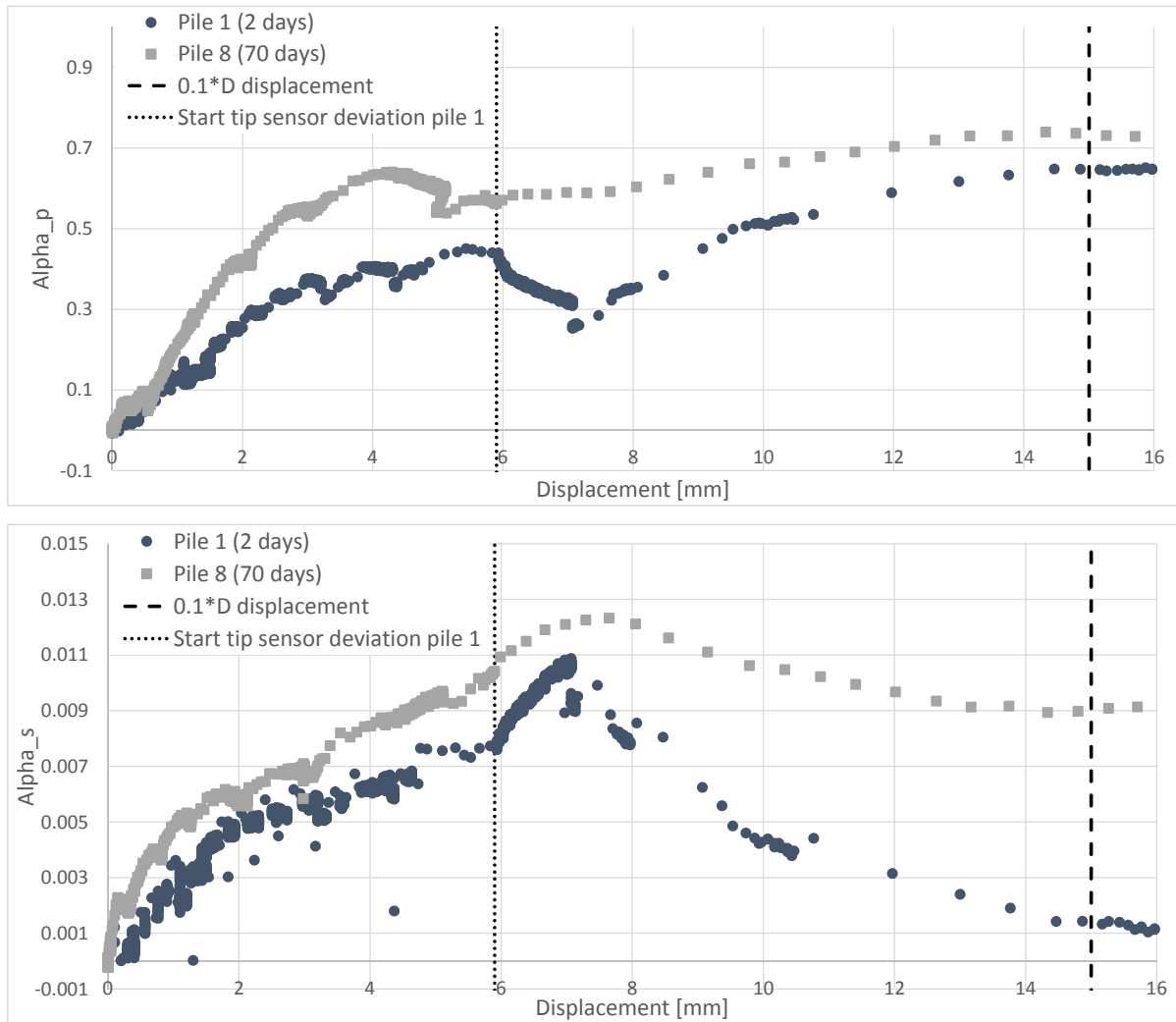
Figure 7.9: Back calculated α values for pile 1 and pile 8

Instead of the development of α with the displacement of each pile only the α-values at pile failure were assessed. The α-values at failure were back calculated from the distributions presented in Figure 7.6. The results are presented in Table 7.6. The strain distributions at failure were approximate, especially the distribution over the bottom section. Thereby the α_p and α_s values determined have a relative low accuracy.

		Pile 1 (2 days)	Pile 5 (16 days)	Pile 4 (31 days)	Pile 8 (70 days)	Average
α_s	total length	0.010	0.009	0.008	0.010	0.009
	200-300	0.000	0.000	0.000	0.000	0.000
	150-200	0.018	0.004	0.003	0.004	0.008
	100-150	0.015	0.012	0.005	0.007	0.010
	50-100	0.018	0.023	0.011	0.011	0.016
	0-50	0.006	0.009	0.011	0.014	0.010
α_p		0.45	0.52	0.52	0.68	0.54

Table 7.6: Back calculated α values from corrected strain distributions

From Figure 7.9 it is visible that for pile 8 both higher α_p- and α_s-values developed with the displacement. For the strain distribution approximated at failure no difference was found in the α_s value of both piles. While a large difference in α_p was found. The α_p was expected constant in time and the α_s was expected to increase with the age of the pile. This effect was not observed from the results of the test program. Also, the highest α_s values were expected at the bottom section of the piles. The most reliable test and α-values were found for pile 8. The average α-values found for the scaled closed-ended steel piles were $\alpha_p = 0.54$ and $\alpha_s = 0.009$ considering the full embedded length. The code prescribes an α_p of 0.70 and α_s of 0.010.

Concluding Remarks Test Program

The influence of time on the capacity of driven displacement piles was examined in a field test. The virgin capacity of 4 scaled closed-ended steel piles was determined at different moments after installation. A pile was statically loaded to failure 2, 16, 31 and 70 days after installation. Strain was measured at multiple locations along the shaft. The applied load and pile displacement were measured at the pile head.

A small trend for time-dependent capacity increase was found from the results of the load tests. On average the increase in total capacity equaled 13% per log cycle of time. The rate of set-up was not as convincing as the average 40% increase per log cycle of time reported in literature. The age of the sand deposit is likely related to the set-up potential of the deposit.

The tip capacity increased on average 9% per log cycle of time and the average shaft capacity increase was 18.5% per log cycle of time compared to the reference capacity assessed 2 days after installation. An increase in tip resistance with time is in discrepancy with previous research where the increase in capacity was only attributed to an increase in shaft resistance.

Considering the measured capacity normalized by the calculated capacity the influence of time is even stronger on the tip capacity than on the shaft capacity. CPTs had been conducted at the pile center line locations prior to pile installation. Thereby normalizing the measured capacity by the calculated capacity at the exact pile location was anticipated to reduce the effect of local variability of soil characteristics.

It was not possible to determine a direct relation between shaft and tip resistance from the strain measurements due to deviant measurements from pile tip sensors or defect pile tip sensors. The shaft and tip contribution to the total resistance were determined from approximated strain distributions over the pile length.

The increase in total capacity is based on the measurements of a calibrated load cell. The tip and shaft contribution to the total pile capacities are approximate and thereby less reliable.

8 | Conclusions and Recommendations

The objective of the research was to expand knowledge on time-dependent bearing capacity of driven displacement piles and make way for a pile design method that incorporates time dependency of pile capacity. The general view on time-dependent capacity of driven displacement piles in sand was evaluated in an extensive literature review. Hereafter a database with pile test results was compiled to assess time-dependent capacity and the accuracy of CPT-based design methods. The last and main part of the research consisted of a test program on 4 scaled piles. Each pile was tested at a different moment after installation where the capacity of the pile and the contribution of the pile tip and shaft to the total resistance was determined.

Literature Review

A time-dependent increase in bearing capacity is often observed for driven displacement piles in sand. The magnitude differs strongly per site and even within one site with homogeneous soil properties and constant pile geometry, installation- and test method. The set-up rate in sand is generally in the range of 15 to 75% per log cycle of time. Non linear relations with the logarithm of time have also been proposed but stagnation of capacity increase over time was always observed. Time-dependent capacity increase is predominantly attributed to shaft capacity increase, the influence of time on the base capacity was found to be limited.

Depending on the pile geometry, soil characteristics and installation method set-up will start within 2 days after installation and will continue for several weeks up to years after installation. In particular the installation method is thought to have a strong influence on the set-up rate of a pile.

The rate of set-up is determined as the capacity increase with respect to a reference capacity. How and when the reference capacity is determined is of strong influence on the rate of increase. Short-term capacity increase caused by dissipation of excess pore pressure is included when the reference capacity is determined by PDA or a dynamic load test shortly after driving. Also, interpretation of dynamic test results is not straightforward. The most reliable reference capacity is found with a static load test approximately 1 day after installation when all excess pore pressures have dissipated.

Capacity increase after dissipation of excess pore pressure in sand is expected to be related to a change in stress state and soil properties. An increased horizontal stress is related to creep-induced breakdown of a driving-induced stress arch. When present, chemicals or salts establishing inter-particle bindings or bindings between particles and pile shaft are also anticipated to contribute to set-up. These potential mechanisms elaborated in Section 3.3 lack experimental evidence.

Generally CPT-based design methods are used to calculate pile capacity. The current design codes do not recognize time-dependency of the bearing capacity. Multiple methods have been proposed to quantify time-dependent behaviour. The Skov and Denver (1988) method is most common used, this method predicts capacity increase on the assumption that the rate of increase is linearly proportional to the logarithm of time. In general, all calculation methods exhibit significant uncertainty without site-specific calibration and a specified reference time.

Database Study

A large amount of pile test results was available in literature. However, the requirements for assessing time dependency of virgin pile capacity strongly reduced the available data.

At homogeneous sites different pile types and geometries were installed which made the assessment of time-dependent capacity less convenient. By normalizing the measured capacity by the calculated

capacity it was attempted to reduce the influence of different pile types and geometries. A general trend for capacity increase with time was found for the normalized capacity. However, the trend was not consistent for sites where different pile geometries were used.

Only 4 test sites were identified where multiple piles with a constant geometry were installed and tested to failure at different moments after installation. At all sites open-ended steel piles were used that were tested statically in tension. Convincing increases in capacity with time were found at these test sites. The capacity increase with respect to a measured reference capacity was not evaluated since the first tests were 2, 9, 29 and 30 days after installation.

The accuracy of the available CPT-based design methods was determined by comparing the measured capacity with the calculated capacity. The accuracy of the assessed CPT-based design methods was disturbingly low. No single method predicted the capacity well. The calculated capacity exceeded the measured capacity up to 3 times. It should be noted that each test site came with 1 representative CPT for the complete site. Therefore, some variation was to be expected. A more comprehensive database study is recommended to determine the accuracy of the methods. The data must be selected carefully since the wide range of soil, installation and test variables makes comparison of test results inaccurate.

Test Program

The influence of time on the bearing capacity of driven displacement piles was examined in a field test. The virgin capacity of 4 scaled closed-ended steel piles was determined at different moments after installation. A virgin test was conducted 2, 16, 31 and 70 days after installation. Strain was measured at multiple locations along the shaft. The applied load and pile displacement were measured at the pile head. The recorded data was processed after the third load test. It is recommended to process the data as soon as it comes available, thereby it is possible to adjust the test setup or protocol.

A small trend for time-dependent capacity increase was found from the results of the load tests. On average the increase in total capacity equaled 13% per log cycle of time. The rate of set-up was not as convincing as the average 40% increase per log cycle of time reported in literature. The age of the sand deposit is likely related to the set-up potential of the deposit. The sand, although compacted, had only been in place for less than 2 weeks prior to installation of the piles. Set-up is thought to be more prone with aged deposits due to a higher stiffness of the aged sand body.

The tip capacity increased on average 9% per log cycle of time and the average shaft capacity increase was 18.5% per log cycle of time compared to the reference capacity assessed 2 days after installation. An increase in tip resistance with time is in discrepancy with previous research where the increase in capacity was only attributed to an increase in shaft resistance. All piles in the test programs on time-dependent bearing capacity found in literature were tested in tension. Tension tests were conducted since only a time dependency of the shaft capacity was expected. However, in the test program on the scaled piles a relation between pile tip capacity and pile age was found. New virgin compression tests are recommended to further investigate the effect of time on the pile tip capacity.

Considering the measured capacity normalized by the calculated capacity it was found that the influence of time is even stronger on the tip capacity than on the shaft capacity. CPTs had been conducted at the pile center line locations prior to pile installation. Thereby normalizing the measured capacity by the calculated capacity at the exact pile location was anticipated to reduce the effect of local variability of soil characteristics.

It was not possible to determine a direct relation between shaft and tip resistance from the strain measurements due to deviant measurements from pile tip sensors or defect pile tip sensors. The shaft and tip contribution to the total resistance were determined from approximated strain distributions over the pile length. For the current piles it is recommended to check if the wall thickness is constant over the pile length and potentially calibrate the tip sensors in the test frame. For future closed-ended piles with a welded footplate it is recommended to increase the distance between the pile tip and the sensor or update the welding procedure.

The increase in total capacity was based on the measurements of a calibrated load cell. The tip and shaft contribution to the total pile capacities were approximated from the development of strain over the pile and thereby less reliable. All measurements were zeroed at the start of the load test. Temperature compensated strain sensors are recommended for future test programs in order to assess residual loads.

General Conclusions and Recommendations

Time-dependent capacity increase is a potential mechanism to incorporate in designs of axially loaded driven displacement piles. A time-dependent increase in capacity was found for all the test results considered in literature as well as for the test program conducted. However, the rate of capacity increase was highly variable. More research is required on the mechanism(s) for a better understanding of time-dependent capacity increase. Understanding of the mechanisms will also help understand what factors, and how these factors, influence the rate of increase. It would be interesting to research the influence of the installation method on the capacity. Also, the influence of loading type and rate on the capacity of a pile is a relatively undiscovered topic. The test pit constructed for this research provides the perfect location to assess installation and/or loading effects on pile bearing capacity due to the limited spatial variability in soil properties. The fresh deposit in the test pit is less suitable to validate full scale pile capacities in aged deposits. Re-use of the test pit and potentially the piles will save costs in future tests and thereby make (generally expensive) field tests more attractive.

Conducting new, standardized test programs on time-dependent bearing capacity is expected to increase the accuracy of the database study. The scatter caused by different test methods and/or test protocols is anticipated to be reduced with a guideline or standardization for pile testing. Advised is to conduct a CPT in the pile center line prior to installation to account for local variation in soil characteristics. Also, all results of pile load test that are published should be accompanied with the site investigation data available. A guideline on reporting of load tests like the Dutch guideline on pile tests NPR7201 (2017) are recommended to follow.

For research on time-dependent bearing capacity a reference capacity measured in a static load test is favorable. Normalizing by a measured reference capacity asks for strict requirements on the window where the reference capacity is determined.

When time-dependent capacity is to be implemented in a design method a calculated reference capacity is favorable. Normalizing by a calculation method corrects for different pile geometries and local variations in soil characteristics. However, the database study indicated a low accuracy of the CPT-based calculation methods. Only one representative CPT was available for multiple piles and the amount of pile tests considered was limited. More research is required on the accuracy of CPT-based design methods to determine the practicability of the Koppejan method or any other design method to assess time-dependent bearing capacity.

Bibliography

Alawneh, A. S., Nusier, O. K., and Awamleh, M. S. (2009). Time dependent capacity increase for driven pile in cohesionless soil. *Jordan Journal of Civil Engineering*, 3(1):1–31.

American Petroleum Institute (2014). Recommended Practice for Planning , Designing and Constructing Fixed Offshore Platforms - Working Stress Design.

Axelsson, G. (2000). *Long-term set-up of driven piles in sand*. PhD thesis, Kungliga Tekniska högskolan Stockholm.

Bogard, J. D. and Matlock, H. (1990). Application of Model Pile Tests to Axial Pile Design. In *Offshore Technology Conference*, pages 271–278, Housten, Texas.

Bullock, P., Schmertmann, J., McVay, M., and Townsend, F. (2005). Side Shear Setup. I: Test Piles Driven in Florida. *Journal of Geotechnical and Geoenvironmental Engineering*, 131(3):292–300.

Chow, F. C., Jardine, R. J., Brucy, F., and Nauroy, J. F. (1998). Effects of Time on Capacity of Pipe Piles in Dense Marine Sand. *Journal of Geotechnical and Geoenvironmental Engineering*, 124(March):254–264.

Chun, B. S., Cho, C. W., and Lee, M. W. (1999). Prediction of Increase in Pile Bearing Capacity With Time After Driving. In *Eleventh Asian Regional Conference on Soil Mechaniscs and Geotechnical Engineering*, number 11, pages 171–174, Rotterdam. Balkema.

CUR B&I (2010). Axiaal draagvermogen van palen. Technical report, Stichting CURNET, Gouda.

De Lange, D. A., Stoevelaar, R., and Van Tol, A. F. (2015). Onderzoek naar 'set-up' bij palen in zand in de geo-centrifuge. *GEO techniek*, 19(1):38–43.

Fellenius, B. H. (2002). Determining the True Distributions of Load in Instrumented Piles. *Geotechnical Special Publication No.116*, 2(116):1455–1470.

Gavin, K. G., Igoe, D. J. P., and Kirwan, L. (2013). The effect of ageing on the axial capacity of piles in sand. *Proceedings of the Institution of Civil Engineers-Geotechnical Engineering*, 166(2):122–130.

Gavin, K. G., Jardine, R. J., Karlsrud, K., and Lehane, B. M. (2015). The effects of pile ageing on the shaft capacity of offshore piles in sand. In *3rd International Symposium on Frontiers in Offshore Geotechnics*.

Gunaratne, M. (2006). *The foundation engineering handbook*. CRC/Taylor & Francis, Boca Raton, FL :.

IJnsen, P. and Admiraal, B. (2017). Onderzoek naar gedrag paalpunten met schaalproef. *Cievele Techniek nummer 7*, pages 14–16.

Jardine, R. J., Standing, J. R., and Chow, F. C. (2006). Some observations of the effects of time on the capacity of piles driven in sand. *Géotechnique*, 56(4):227–244.

Karlsrud, K., Jensen, T. G., Wensaas Lied, E. K., Nowacki, F., and Simonsen, A. S. (2014). Significant Ageing Effects for Axially Loaded Piles in Sand and Clay Verified by New Field Load Tests. In *Offshore Technology Conference*.

Komurka, V. E., Wagner, A. B., and Tuncer, E. (2003). Estimating Soil / Pile Set-up. Technical report.

Lehane, B. M., Jardine, R. J., Bond, A. J., and Frank, R. (1993). Mechanisms of Shaft Friction in Sand from Instrumented Pile Tests. *Journal of Geotechnical Engineering*, 119(1):19–35.

Lim, J. and Lehane, B. (2014). Characterisation of the effects of time on the shaft friction of displacement piles in sand. *Geotechnique*, 64(6):476–485.

Long, J. H., Kerrigan, J. A., and Wysockey, M. H. (1999). Measured time effects for axial capacity of driven piling. *Transportation Research Record: Journal of the Transportation Research Board*, pages 8–15.

NEN9997-1 (2016). NEN 9997-1 Geotechnical design of strucutres.

NPR7201 (2017). Praktijkrichtlijn Geotechniek - Bepaling van het axiaal draagvermogen van funderingspalen door middel van proefbelastingen.

Reddy, S. C. and Stuedlein, A. W. (2014). Time-dependent Capacity Increase of Piles Driven in the Puget Sound Lowlands. In *From Sol Behaviour to Innovations inGeotechnical Engineering*, volume 233, pages 464–474.

Rimoy, S. P. and Jardine, R. J. (2015). Axial capacity ageing trends of piles driven in silica sands. *Frontiers in Offshore Geotechnics III*, (2000):637–642.

SBRCURnet (2010). *Handboek funderingen - Deel A (volgens Eurocode 7)*.

Skov, R. and Denver, H. (1988). Time-Dependence of Bearing Capacity of Piles. In Fellenius, B. H., editor, *3rd International Conference on Application of Stress-Waves to Piles*, pages 879–888, Ottawa, Canada.

Stoevelaar, R., Bezuijen, A., Nohl, W., Jansen, H., Hoefsloot, F., and Hannink, G. (2012). Werkdocument Verborgen Veiligheden.

Svinkin, M. R. (1996). Setup and Relaxation in Glacial Sand - Discussion. *Journal of Geotechnical Engineering*, 122(4):319–321.

Tan, S. L., Cuthbertson, J., and Kimmerling, R. E. (2004). Prediction of Pile Set-Up in Non-Cohesive Soils. In DiMaggio, J. A., Hussein, M. H., and Goble, G. G., editors, *Current practices and future trends in deep foundations*, pages 50–65. American Society of Civil Engineers, Reston.

Tavenas, F. and Audy, R. (1972). Limitations of the Driving Formulas for Predicting the Bearing Capacities of Piles in Sand. *Canadian Geotechnical Journal*, 9(1):47–62.

Tomlinson, M. J. and Woodward, J. (2015). *Pile Design and Construction Practice*. Sixth edit edition.

Van Tol, A. (2012). Draagkracht funderingspalen, een up-date. *GEO Techniek*, pages 14–18.

Van Tol, A., Stoevelaar, R., and Rietdijk, J. (2010). Draagvermogen van geheide palen in internationale context. *GEO Techniek*, pages 4–9.

Winterkorn, H. F. H. F. and Fang, H.-Y. (1975). *Foundation engineering handbook,*. Van Nostrand Reinhold, New York.

Xu, X., Schneider, J. a., and Lehane, B. (2008). Cone penetration test (CPT) methods for end-bearing assessment of open- and closed-ended driven piles in siliceous sand. *Canadian Geotechnical Journal*, 45:1130–1141.

Yan, W. M. and Yuen, K. V. (2010). Prediction of pile set-up in clays and sands. *IOP Conference Series: Materials Science and Engineering*, 10.

Yang, Z., Jardine, R. J., Guo, W., and Chow, F. C. (2016). *A Comprehensive Database of Tests on Axially Loaded Piles Driven in Sand*.

York, D. L., Brusey, W. G., Clemente, F. M., and Law, S. K. (1994). Setup and Relaxation in Glacial Sand. *Journal of Geotechnical Engineering*, 120(9):1498–1513.

Zhang, Z. and Wang, Y. (2014). Examining Setup Mechanisms of Driven Piles in Sand Using Laboratory Model Pile Tests. *Journal of Geotechnical and Geoenvironmental Engineering*, 141(3).

A | Pile Design Methods

In this appendix the following pile design methods are elaborated:

- Method provided by the Dutch code (NEN 9997-1), also known as Koppejan method
- American Petroleum Institute (API) method
- Imperial College Pile (ICP) method
- University of Western Australia (UWA) method
- Norwegian Geotechnical Institute (NGI) method
- Fugro method

The symbols used in the equations are listed below. The original equations have been adapted to harmonize the use of symbols. The pile design methods presented calculate the expected max resistance of a pile at $0.1 * D$ pile displacement.

The Fugro and ICP method use an average cone resistance $(q_{c,avg})$ to calculate q_b. The cone resistance is averaged over an area $1.5 * D$ above and below pile the tip. The UWA and Koppejan method use the $4D - 8D$ method which is elaborated in section A.1. The NGI method employs the relative density (D_r) at pile tip level to calculate the tip resistance.

a, b and β appear in multiple methods where the parameters have a different meaning. The meaning of these parameters is provided with each method.

Nomenclature Appendix A

q_b	=	Tip resistance	kPa
q_s	=	Shaft resistance	kPa
q_c	=	Cone resistance	kPa
$q_{c,avg}$	=	Average cone resistance	kPa
p_{ref}	=	Reference pressure (100 kPa)	kPa
A_r	=	Area ratio $(1 - (D_i/D)^2)$	-
$A_{r,eff}$	=	Effective area ratio $(1 - IFR(D_i/D)^2)$	-
h	=	relative height above pile tip	m
R^*	=	Equivalent pile radius $(R_o^2 - R_i^2)^{0.5}$	m
R_o	=	Radius of outer diameter	m
R_i	=	Radius of inner diameter	m
N_q	=	Dimensionless tip capacity factor	-
β	=	Method dependent dimensionless factor	-
σ'_v	=	Local effective vertical stress	kPa
D	=	Pile diameter	m
D_{CPT}	=	Diameter of standard CPT cone (0.036 m)	m
D_{eq}	=	Equivalent pile diameter	m
D_i	=	Inner pile diameter	m
D_r	=	Relative density	%
a	=	Method dependent	-
b	=	Method dependent	-
w	=	Pile wall thickness	m
$\Delta\sigma_{rd}$	=	Change in radial stress during pile loading	kPa
δ	=	Interface friction angle	°
L	=	Embedded pile length	m
K	=	Coefficient of lateral earth pressure	-
z	=	Depth	m
IFR	=	Incremental Filling Ratio	
FFR	=	Final Filling Ratio	

A.1 Dutch (Koppejan) Design Method

The Dutch code, NEN 9997-1 **"Geotechnical design of structures - Part 1: General rules"**, describes multiple methods to determine the ultimate bearing capacity for axial loaded piles. Including guidelines to determine pile capacity from the results of static load tests, dynamic load tests, driving analysis, based on wave equations, restrike results and on in-situ obtained data. The method most often used is the latter, calculation of capacity with a direct CPT method based on Koppejan (NEN9997-1, 2016).

Piles Loaded in Compression

For closed-ended piles in compression the capacity is determined by the tip resistance and outer shaft resistance. For open-ended piles in compression there is also an inner shaft or plug contribution to the total capacity.
An open-ended pile might plug during installation, the soil plug closes the bottom end of the pile and the pile will behave like a closed-ended pile. Following the code, both the potential inner shaft contribution and the capacity of a plugged pile should be determined. The smallest contribution of these two is added to the base and outer shaft capacity to determine total capacity.
For long piles the potential contribution of the inner shaft often exceeds the potential contribution of a plugged pile. For open-ended piles with a large L/D ratio fully embedded in sand the shaft resistance largely exceeds the base resistance of the pile.

The max bearing capacity of a pile in compression near CPT i is determined by calculating its shaft and tip resistance as presented below (NEN9997-1, 2016).

$$R_{c;cal;i} = R_{b;cal;max;i} + R_{s;cal;max;i} \tag{A.1}$$

with:

$$R_{b;cal;max;i} = A_b * q_{b;max;i} \tag{A.2}$$

and:

$$R_{s;cal;max;i} = O_{s;\Delta L;avg} * \int_{\Delta L} q_{s;max;z;i} * dz \tag{A.3}$$

with:

$R_{c;cal;i}$	=	Calculated pile capacity in CPT i	kN
$R_{b;cal;max;i}$	=	Calculated tip capacity in CPT i	kN
$R_{s;cal;max;i}$	=	Calculated shaft capacity in CPT i	kN
A_b	=	Pile tip surface	m^2
$q_{b;max;i}$	=	Pile tip resistance determined for CPT i	kPa
$O_{s;\Delta L;avg}$	=	Average circumference of the pile section installed in the bearing stratum	m
Δ_L	=	Length over which shaft resistance is considered when determining the max capacity, with: • In case the soil layers above the pile tip consist of sand and/or clay with CPT values above 2 MPa, ΔL is equal to the total pile length. • In case a prefab pile with an enlarged footing is used where the footing stretches more than 10 mm outside the pile shaft, ΔL may not exceed the length of the enlarged footing.	m
$q_{s;max;z;i}$	=	Max shaft friction at depth z for CPT i	kPa
z	=	Indication of vertical direction	-

Tip Resistance

The calculated base capacity of a pile is determined by the cone resistance near pile tip level and by the size and shape of the tip. The characteristic value of the cone resistance at the location of the pile tip is determined by the $4D - 8D$ method, often referred to as 'the Dutch method'.

The max tip resistance for CPT i is determined by:

$$q_{b;max} = \frac{1}{2} * \alpha_p * \beta * s * (\frac{q_{c;I;avg} + q_{c;II;avg}}{2} + q_{c;III;avg}) \tag{A.4}$$

with:

$q_{b;max}$	$=$	Tip capacity with a limit value of 15 MPa	kPa
α_p	$=$	Pile class factor	-
β	$=$	Factor determined by the shape of the pile tip	-
s	$=$	Factor determined by the shape of the pile tip cross section	-
$q_{c;I;avg}$	$=$	Average of CPT values found in section I which consist of a length of at least $0.7 * D_{eq}$ and at most $4 * D_{eq}$ below the pile tip. The correct length between $0.7 * D_{eq}$ and $4 * D_{eq}$ is determined such that the value for $q_{b;max}$ is smallest	kPa
$q_{c;II;avg}$	$=$	Average of CPT values found in section II, the length of section II is equal to the length of section I. Considering the route from the deepest point of the section up to pile tip level the considered CPT values are limited by the lowest preceding value	kPa
$q_{c;III;avg}$	$=$	Average of CPT values found in section III, the length of section III is $8 * D_{eq}$. From pile tip to the top of section III the considered CPT values are limited by the lowest preceding value and starts with the lowest value found in section II	kPa

See Figure A.1 for a visualization of the sections described above. To determine the max tip resistance of rectangular piles the equivalent pile tip center line is required which is calculated by Equation A.5 (NEN9997-1, 2016).

$$D_{eq} = \sqrt{\frac{4}{\pi}} * a * \sqrt{\frac{b}{a}} \tag{A.5}$$

with:

D_{eq}	$=$	Equivalent pile tip center line	m
a	$=$	Smallest side of a pile with a rectangular cross-section	m
b	$=$	Largest side of a pile with a rectangular cross-section	m
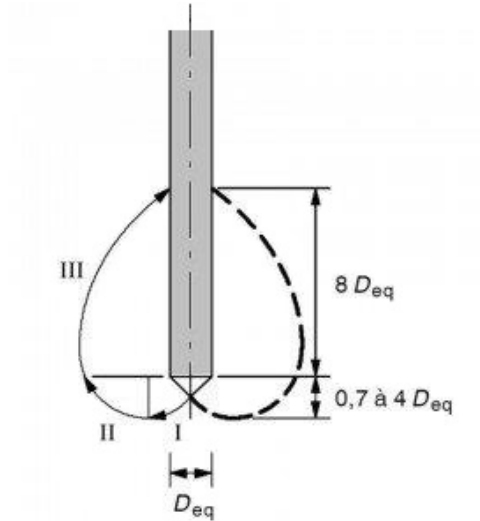
Figure A.1: Zones specified by Kopppejan to determine tip resistance

If $b > 1.5 * a$ then $D_{eq} = a$ for section I & II and the top of section III is at a length of $8 * a$ instead of $8 * D_{eq}$. For circular piles D_eq is equal to the (outer) diameter. There are five options for the β-factor in Equation A.4 which are equally distributed between 0.6 and 1.0. For piles with a constant cross-section β is equal to 1.0. s is determined by Equation A.6 for circular and square piles s equals 1.0 (NEN9997-1, 2016).

$$s = \frac{1 + \frac{\sin \varphi}{r}}{1 + \sin \varphi} \tag{A.6}$$

with:

φ	$=$	Angle of internal friction, it is allowed to use $\varphi = 40°$ if the pile tip is installed in a densely packed sand layer	°
r	$=$	Ratio $\frac{b}{a}$, $r = 1$ for circular piles	-
b	$=$	Largest side of a pile with a rectangular cross-section	m
a	$=$	Smallest side of a pile with a rectangular cross-section	m

The tip capacity of a pile is calculated by multiplying the tip resistance by the tip surface, see Equation A.2.

Shaft Resistance

The calculated shaft resistance of a pile is determined by the cone resistance over the length of the pile in the bearing stratum and pile type.
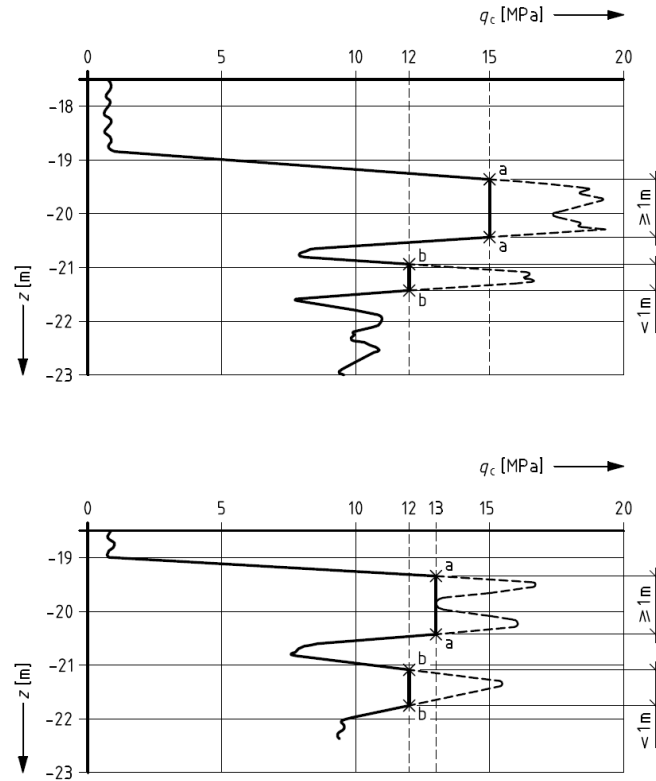
Figure A.2: Setting limit values to q_c-diagram

The max shaft resistance for CPT i is determined by:

$$q_{s;max;z} = \alpha_s * q_{c;z;a} \tag{A.7}$$

with:

$q_{s;max;z}$	=	Shaft capacity at depth z (z in m)	kPa
α_s	=	Pile class factor	-
$q_{c;z;a}$	=	Average of CPT values found over the shaft length with a limit value of 12 MPa. A limit value up to 15 MPa is applicable if the CPT values over a length of 1 m or more exceed the 12 MPa limit value, see Figure A.2. More reductions apply for determining $q_{c;z;a}$, see section end of this section	kPa

The shaft capacity of a pile is calculated by multiplying the shaft resistance by the shaft surface embedded in the bearing stratum, see Equation A.3.

Piles Loaded in Tension

The capacity of a pile in tension is determined by the outer shaft resistance to the tensile force. In tension the max capacity measured is often compensated for the self-weight of the pile. Less common is compensation for the self-weight of the soil in the pile.

The method presented in the Dutch code to determine shaft capacity in tension is presented in Equation A.8. This method is only valid for single piles with a length between 7 and 50 m and a length/center-line ratio of at least 13.5. If a pile does not fit the requirements additional safety or tests are required. The method is not applicable for piles exposed to dynamic loads (NEN9997-1, 2016).

The tensile capacity of a pile near CPT i is determined by:

$$R_{t;d} = \int_0^L O_{s;avg} * q_{s;z;d} * dz \tag{A.8}$$

$R_{t;d}$	=	Calculated tensile pile capacity	kN
$O_{s;avg}$	=	Average circumference of the pile	m
L	=	Length over which shaft resistance is considered	m
$q_{s;z;d}$	=	Shaft friction at depth z	kPa
z	=	Indication of vertical direction	-

The max shaft resistance for CPT i is determined by:

$$q_{s;z;d} = \alpha_t * q_{c;z;d} \tag{A.9}$$

with:

$q_{s;z;d}$	=	Shaft friction at depth z	kPa
α_t	=	Pile class factor	-
$q_{c;z;d}$	=	design value of the CPT value at depth z	kPa

where $q_{c;z;d}$ is $q_{c;z;a}$ divided by a partial factor, a correlation factor and a factor taking into account variation is static load states. For the comparison with the measured pile capacity the characteristic value is determined.

The contribution of cohesive layers to the total tensile capacity may be considered in case of a layered soil profile where the majority of the tensile resistance is provided by sand. However, in this case the α_t's for the cohesive layers are divided by a factor 2. This reduction is required since sand and cohesive layers have different stress-strain behaviour (NEN9997-1, 2016).

For displacement piles in sand the values of α_p, α_s and α_t vary with pile type. For driven closed-ended concrete and steel piles the values equal 0.7, 0.010 and 0.007. For driven open-ended steel piles α_p, α_s and α_t equal 0.7, 0.006 and 0.004 (NEN9997-1, 2016).

The design value of a pile is determined by dividing the calculated value by a correlation factor (ξ) and a partial resistance factor (γ). The correlation factor accounts for the amount of CPTs and the consistency in soil characteristics in the surrounding of the pile. This factor also accounts for the ability of the superstructure to spread loads. The partial resistance factor adds safety, the magnitude depends on installation method and the way soil parameters are determined.

In the Dutch code specific conditions are described for which the q_c-profile needs to be reduced. Reduction must be applied for a certain particle size distribution, overconsolidation and/or excavation of top-layers. The q_c-profile is reduced prior to cutting of the peaks at their limit values (NEN9997-1, 2016).

A.2 API Design Method

The API method assumes the shaft and tip resistance to increase with local effective vertical stress.

Tip resistance

$$q_b = N_q \sigma'_v \leq q_{b,lim} \tag{A.10}$$

Shaft resistance

$$q_s = \beta \sigma'_v = K \tan(\delta) \sigma'_v \leq q_{s,lim} \tag{A.11}$$

The β factor in Equation A.11 is equal to $K \tan(\delta)$ where K is the coefficient of lateral earth pressure and δ the interface friction angle. β, N_q and the limit values depend on soil type description and relative density. Parameters intended as guidelines for open-ended piles are presented in Table A.1. For closed-ended or fully plugged pipe piles the β values are considered 25% higher (American Petroleum Institute, 2014; Yang et al., 2016).
The API method tends to be conservative for relatively short piles in dense sand and non-conservative for relatively long piles driven into loose sands.

Relative density[a]	Soil description	Shaft friction factor β [-]	Limiting shaft friction values $q_{s,lim}$ [kPa]	Tip resistance factor N_q [-]	Limiting tip resistance values $q_{b,lim}$ [Mpa]
Very loose	Sand	Not	Not	Not	Not
Loose	Sand	applicable[b]	applicable[b]	applicable[b]	applicable[b]
Loose	Sand-silt[c]				
Medium dense	Silt				
Dense	Silt				
Medium dense	Sand-silt[c]	0.29	67	12	3
Medium dense	Sand	0.37	81	20	5
Dense	Sand-silt[d]				
Dense	Sand	0.46	96	40	10
Very dense	Sand-silt[c]				
Very dense	Sand	0.56	115	50	12

Note: The parameters listed in this table are intended as guidelines only. Where detailed information such as in situ cone tests, strength tests on high quality samples, model tests, or pile driving performance is available, other values may be justified.

[a] The definitions for the relative density percentage are as follows:

• Very loose: 0-15 %
• Loose: 15-35 %
• Medium dense: 35-65 %
• Dense: 65-85 %
• Very dense: 85-100 %

[b] In previous versions of the API 2A-WSD parameters for all soil types and relative densities in the table were provided. For the combinations indicated with not applicable in this table it is recommended to use CPT-based methods since the parameters provided were considered non-conservative.

[c] Sand-silt includes those soils with significant fractions of both sand and silt. Strength values generally increase with increasing sand fractions and decrease with increasing silt fractions.

Table A.1: API design parameters for cohesionless siliceous soil (Yang et al., 2016), *modified*

A.3 ICP Design Method

Tip resistance

Closed-ended piles:

$$q_b = q_{c,avg} * \max[1 - 0.5\log(D/D_{CPT}), 0.3] \tag{A.12}$$

The calculated tip resistance of open-ended piles is based on the ability of a soil plug to form in the pile. Open-ended piles are considered unplugged for an inner diameter (D_i):

$$D_i \geq 2.0(D_r - 0.3) \tag{A.13}$$

or when

$$D_i \geq 0.083(q_{c,avg}/p_{ref})D_{CPT} \tag{A.14}$$

where D_r is the relative density, D_i is the inner diameter and p_{ref} the absolute atmospheric pressure which equals 100 kPa. When the inner diameter complies with Equation A.13 or Equation A.14 the tip resistance (q_b) is equal to the area ratio ($A_r = 1 - (D_i/D)^2$). When a pile has plugged the tip resistance is calculated by:

$$q_b = q_{c,avg} * \max[0.5 - 0.25\log(D/D_{CPT}), 0.15, A_r] \tag{A.15}$$

Shaft resistance

The ICP method provides two ways to calculate the shaft resistance. A full version and a "simplified" version where the change in effective radial stress during pile loading (Δ'_{rd}) is ignored and parameters are rounded up or down. Parameter a is 0.9 for open-ended piles in tension and 1.0 for other conditions. In tension b is 0.8 and in compression b equals 1.0.

Full version:

$$q_s = a[0.029bq_c(\frac{\sigma'_v}{p_{ref}})^{0.13}(\max[\frac{h}{R^*}, 8])^{-0.38} + \Delta\sigma'_{rd}]\tan(\delta) \tag{A.16}$$

"Simplified" version:

$$q_s = a[0.023bq_c(\frac{\sigma'_v}{p_{ref}})^{0.10}(\max[\frac{h}{R^*}, 8])^{-0.40}]\tan(\delta) \tag{A.17}$$

The equivalent pile radius (R^*) is $(R_o^2 - R_i^2)^{0.5}$ for open-ended piles and equal to the pile radius (R) for closed-ended piles.

A.4 UWA Design Method

The UWA method provides 2 options to calculate the pile capacity. Just like the ICP method there is a full version and a "simplified" version, also referred to as offshore version.
The difference between the full version and the offshore version is inclusion of the Final Filling Ratio (FFR).The FFR is the average value of the Incremental Filling Ratio (IFR) recorded over the last $3 * D$ length pile penetration. Where IFR is the ratio between the increment of the soil plug length and the increment of the pile penetration. Equation A.18 is used when no IFR is recorded during pile driving.

$$IFR = \min[1, (D_i/1.5)^{0.2}] \tag{A.18}$$

Tip resistance
For closed-ended piles both versions use the same equation (Equation A.19) to calculate tip resistance. For open-ended piles the method differs for the 2 versions, see Equation A.20 and Equation A.21.
Closed-ended piles:

$$q_b = 0.6q_{c,avg} \tag{A.19}$$

Open-ended piles:

In the full version the tip resistance is calculated with an effective area ratio $(A_{rb,eff} = 1.0 - FFR(D_i/D)^2)$ and the offshore version is calculated with the area ratio equal to A_r as presented in the ICP method.

Full version:

$$q_b = q_{c,avg} * (0.15 + 0.45A_{rb,eff}) \tag{A.20}$$

Offshore version:

$$q_b = q_{c,avg} * (0.15 + 0.45A_r) \tag{A.21}$$

Shaft resistance
Full version:

$$q_s = a(0.03q_c A_{rs,eff}^{0.3}(\max[\frac{h}{D}, 2]^{-0.5}) + \Delta\sigma'_{rd})\tan(\delta) \tag{A.22}$$

Offshore version:

$$q_s = a(0.03q_c A_r^{0.3}(\max[\frac{h}{D}, 2]^{-0.5}))\tan(\delta) \tag{A.23}$$

Parameter a is 1.0 for piles loaded in compression and 0.75 for piles loaded in tension.

A.5 NGI Design Method

Tip resistance
Closed-ended piles:

$$q_b = F_{D_r}q_{c,tip} = 0.8q_{c,tip}/(1 + D_r^2) \tag{A.24}$$

Open-ended piles:

$$q_b = \min[\text{plugged}(q_b), \text{unplugged}(q_b)] \tag{A.25}$$

where:
plugged$(q_b) = F_{D_r}q_{c,tip} = 0.7q_{c,tip}/(1 + 3D_r^2)$
unplugged$(q_b) = q_{c,tip}A_r + q_{b,plug}(1 - A_r)$
$q_{b,plug} = 12q_{s,avg}L/(\pi D_i)$

Shaft resistance

$$q_s = \max[z/Lp_{ref}F_{D_r}F_{sig}F_{tip}F_{load}F_{mat}, q_{s,min}] \tag{A.26}$$

where:
$F_{D_r} = 2.1(D_r - 0.1)^{1.7}$

$D_r = 0.4\ln(q_{c1N}/22)$
$F_{sig} = (\sigma'_v/p_{ref})^{0.25}$
$q_{s,min} = 0.1\sigma'_v$
$F_{tip} = 1.0$ for open-ended piles and 1.6 for closed-ended piles
$F_{load} = 1.0$ for tension and 1.3 for compression
$F_{mat} = 1.0$ for steel and 1.2 for concrete

A.6 Fugro Design Method

Tip resistance:

$$q_b = 8.5(p_{ref} * q_{c,avg})^{0.5} A_r^{0.25} \tag{A.27}$$

Shaft resistance:
For piles loaded in compression with $h/R^* \geq 4$

$$q_s = 0.08q_c\left(\frac{\sigma'_v}{p_{ref}}\right)^{0.05}\left(\frac{h}{R^*}\right)^{-0.90} \tag{A.28}$$

For piles loaded in compression with $h/R^* \leq 4$

$$q_s = 0.08q_c\left(\frac{\sigma'_v}{p_{ref}}\right)^{0.05}(4)^{-0.90}\left(\frac{h}{4R^*}\right) \tag{A.29}$$

For piles loaded in tension

$$q_s = 0.045q_c\left(\frac{\sigma'_v}{p_{ref}}\right)^{0.15}(\max[\frac{h}{R^*},4])^{-0.85} \tag{A.30}$$

This design method is valid for driven steel pipe piles in the following field of application:

- Pile in silica sand
- $\frac{w}{D} > \frac{1}{60}$
- Single open and closed piles
- Static and quasi-static loads
- Open piles with and without a driving shoe
- Loads applied within 10 to 50 days after installation (before 10 days the capacity can be less; after 50 days the capacity can be greater)

The Fugro method was designed from the results of a limited amount of load tests. The method has only been validated for a specific range of pile diameters, pile lengths and soil conditions. The Fugro method is expected to apply to the following ranges:

Pile diameter:	0.25 - 3.00 m
Pile length:	5 - 80 L/D
Sand conditions:	Silica sand with relative densities (D_r) from 10 to 100%

B | Test Methods

Pile load tests can be classified in three groups; static load tests, dynamic load tests and statnamic/statrapid load tests. The latter are seldom used in test programs on set-up and will not be elaborated in this appendix.

B.1 Static Load Test

A static load test can be either in compression or in tension. Static load tests are often used to test a pile's ultimate capacity, generally the load is axially applied to failure. The load can be applied cyclic or with a constant rate. There are top-loaded and bottom-loaded static load tests.

Bottom-loaded static load test use an Osterberg cell (O-cell) at the bottom of the pile. The cell is a cylindrical hydraulic jack. The soil below the toe of the pile is loaded with the pile's shaft resistance taking the reaction force, contrary the pile shaft is loaded (upward) with the end-bearing resistance of the soil below the O-cell providing the reaction force. Bottom-loaded static load tests are not common and generally only piles in a dedicated test program are equipped with an O-cell (Komurka et al., 2003). In a top-loaded static test the force is applied to the pile head, in compression tests the counter force is generally provided by a large dead-weight and/or tension piles. In tensile tests the reaction force is distributed by a pile or strip footing. Depending on instrumentation it is possible to determine shaft and base capacity separately for a static load test in compression.

Setup of a static load test often requires one to several days due to the logistics accompanied (Komurka et al., 2003).

The main advantages of a static load test:
- Static behaviour
- Maintained load
- No pile damage
- Direct load measurement (calibrated load cell)
- Direct displacement measurement

The main disadvantages of a static load test:
- Expensive
- Time consuming

B.2 Dynamic Load Test

Dynamic tested piles are instrumented with accelerometers and strain transducers. Dynamic testing consists of a ram hammering the pile head while the propagation of the wave induced by the ram impact is measured. Processing the signals of the accelerometers and strain transducers during pile installation is done by a Pile Driving Analysis (PDA) program. With this data the combined shaft and toe resistance can be predicted. By further processing the data by a CAse Pile Wave Analysis Program (CAPWAP) it is possible to predict residual stresses and distinguish between toe and shaft resistance.

The main advantages of a dynamic load test:
- Economic
- Fast

The main disadvantages of a dynamic load test:
- Indirect load measurements
- Indirect displacement measurements
- Calibration to static load test
- Interpretation requires experienced engineers
- Chance of pile damage
- Full capacity often not mobilized

C | Set-Up Calculation Methods

Numerous methods have been proposed to quantify set-up, the methods are often based on the results of test programs. Test programs differ in soil conditions, pile type, pile geometry and test equipment. All methods found in literature for calculating time-dependent capacity of driven piles in sand are presented in this appendix.

C.1 Skov & Denver (1988)

Skov and Denver (1988) were one of the first to propose an equation for estimating long-term capacity based on measured short-term capacity. Even though the method was designed from a limited amount of tests, it is still most commonly used.

At 4 different locations divided over Denmark and Germany tests were performed. At 3 sites prefab concrete piles were tested and at the remaining location a steel pipe pile was used. The soil profile at 2 of the 4 sites consisted of sand, there was 1 clay site and the last site consisted of calcareous soil. The piles were tested between 0.5 and 23 days after installation. Pile capacities were determined by both dynamic and static load tests.

Equation C.1 was proposed based on the results of the 21 tests conducted. By changing parameters A and t_0 the equation can be adjusted for sand or clay conditions.

$$Q_t = Q_0(1 + A * \log \frac{t}{t_0}) \tag{C.1}$$

With:

Q_t	$=$	Pile capacity at time t	kN
Q_0	$=$	Pile capacity at reference time t_0	kN
A	$=$	Set-up factor	-
t	$=$	Time elapsed since the end of initial driving	days
t_0	$=$	Time elapsed since the end of initial driving from which the increase in capacity is linear with the logarithm of time	days

The observed time-dependent increase in capacity stabilized after initial driving as a logarithmic function of t/t_0, where t_0 is a function of soil type. Skov and Denver (1988) determined a set-up factor (A) equal to 0.2 and a reference time (t_0) equal to 0.5 day for piles installed in sand. In other words, for piles in sand the capacity increases with 20% per log cycle of time compared to the capacity half a day after installation. Skov and Denver (1988) explicitly stated that the advised set-up factor and reference time should be used with caution at other locations.

The Skov and Denver (1988) method has been employed by Chow et al. (1998) and Axelsson (2000) for the database studies presented in section 3.1. Although different values for A were determined the semi log linear relation was confirmed (Axelsson, 2000; Chow et al., 1998). Chow et al. (1998) found an average set-up factor (A) of 0.5 and Axelsson (2000) found a set-up factor (A) of 0.4 ± 0.25 in his research on prefab concrete piles in silty sand. Based on test results Long et al. (1999) stated that A ranged between 0.2 and 1.0.

Set-up is affected by various factors and thereby A is most likely not only a function of soil type but also on pile geometry (Stoevelaar et al., 2012). (Alawneh et al., 2009) assessed the reliability of A on soil and pile characteristics based on a database study and proposed an equation for A as presented in Equation C.2.

$$A = 0.005(\frac{L}{D}) \exp(0.6 \tan \phi) \tag{C.2}$$

Considering Equation C.2 the set-up factor (A) is a function of pile length/diameter ratio ($\frac{L}{D}$) and friction angle (ϕ).

Chun et al. (1999) reported the limitations of the Skov and Denver (1988) method for calculating time dependent capacity increase. Considering Chun et al. (1999) the method overestimates the long-term capacity. Skov and Denver (1988) assume the capacity increase linear with the logarithm of time, Chun et al. (1999) state that the capacity should converge to a constant value. There will be a maximum capacity and the increase in capacity will not be linear with the logarithm of time (Chun et al., 1999). Recent research by Karlsrud et al. (2014) also found a non-linear relation with the logarithm of time where the capacity tends to a constant capacity in time.

The Skov and Denver (1988) method was developed for time-dependent increase of total capacity, no distinction was made between shaft capacity and tip capacity. Various researchers validated the Skov and Denver (1988) method but there is no common agreement on what set-up factor (A) and reference time (t_0) should be used. A is critically dependent on the reference time (t_0). When for the same case a different reference time is considered a different Q_0 will be found and thereby a different value for A (Stoevelaar et al., 2012).

C.2 Svinkin (1996)

Svinkin et al. (1994) tested 5 square pre-stressed concrete piles at different moments in time. The 20 m long piles were driven at a site consisting of dense silty sand. The water table was 0.6 m below ground surface and pile capacities were determined by both dynamic and static load tests. From the results of this study Svinkin (1996) determined an upper and lower limit values for capacity increase over the first 25 days after installation.

The results from the dynamic analysis and the static load tests were normalized by the EOID capacity of the piles. Svinkin (1996) found that the normalized capacity of the piles gradually increased during approximately 10 days after installation. The rate of set-up varied from pile to pile. After approximately 10 days a more or less constant set-up rate was observed. All 5 piles revealed the same tendency for capacity increase with time which could be expressed by the power law function of Equation C.3. This equation was designed to calculate the pile capacities up to 25 days after installation.

$$Q_t = B * Q_{EOID} * t^{0.1} \tag{C.3}$$

With:

Q_t	=	Pile capacity at time t	kN
Q_{EOID}	=	Pile capacity at End Of Initial Driving	kN
B	=	Set-up factor	-
t	=	Time elapsed since the end of initial driving	days

Svinkin (1996) found a lower boundary value for set-up factor B of 1.025 and an upper boundary value of 1.4.

Notice that short-term capacity increase due to dissipation of excess pore water pressure was most certainly included in this method. Excess pore water pressures generated during pile installation will take at least several hours to dissipate in a saturated dense silty sand. Equation C.3 is designed for very specific data set and appears to under-predict long term pile capacity of most other published case histories (Tan et al., 2004).

C.3 Chun et al. (1999)

Chun et al. (1999) had a different approach to describe time-dependent capacity increase. Equation C.4 was proposed based on the idea that the pile capacity converges to a long-term capacity over time. As visualized in Figure C.1, the ratio of bearing capacity gain can be calculated by subtracting D_t from the normalized long-term capacity ((Q_t/Q_{EOID}). It is also shown that there is a linear relationship between the ratio of bearing capacity gain (D_t) and the rate of capacity gain ($\frac{d}{dt}(Q_t/Q_{EOID})$) (Gunaratne, 2006).
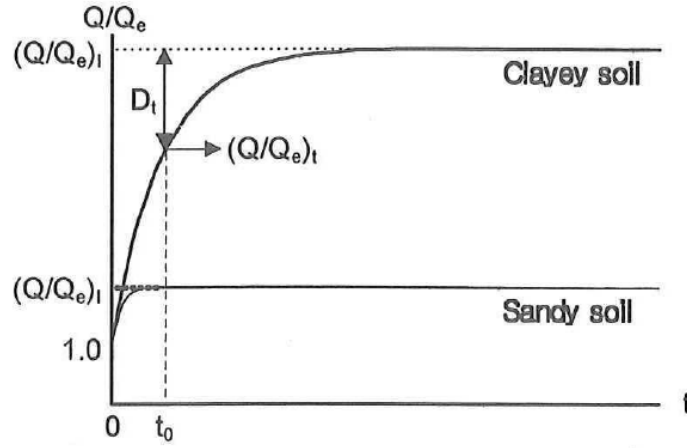
Figure C.1: Ratio of bearing capacity gain with time (Chun et al., 1999)

Considering Chun et al. (1999) the trend found in Figure C.1 is equal for all soil types but the shape may differ depending on the rate of capacity gain. Chun et al. (1999) state that the rate of capacity gain dependent on soil conditions and not on soil type. The following general relationship to estimate the capacity gain regardless of the soil type was proposed:

$$\frac{Q_t}{Q_{EOID}} = C - B\frac{d}{dt}(Q_t/Q_{EOID}) \tag{C.4}$$

With:

Q_t	=	Pile capacity at time t	kN
Q_{EOID}	=	Pile capacity at End Of Initial Driving	kN
C	=	Q_u/Q_{EOID} which is the long-term ratio of capacity gain	kN
B	=	Constant ($= G/K$), K is the dissipation factor while G is the ageing factor	-

Constant B in Equation C.4 is a constant for converting the rate of capacity gain to D_t. The constant is equal to the ratio of the degree of ageing (G) over the degree of dissipation (K). Concerning Chun et al. (1999) dissipation and ageing are the main factors contributing to set-up. Where, K is depending on the permeability of soil while G is depending on the aging potential that could be associated with soil properties. Note, the prior excluded contribution to set-up due to dissipation of excess pore pressure is included in this calculation method.

A higher B value could be expected for sandy soils, where the aging effect is predominant, and a lower value of B could be associated with clayey soils as the pore pressure dissipation is predominant.

The ratio of capacity gain can be obtained by solving Equation C.4 resulting in:

$$Q_t = C(1 - (\frac{C-1}{C})e^{-\frac{t}{B}}) * Q_{EOID} \tag{C.5}$$

Constant C is the long-term gain ratio which is obtained by matching the measured with the predicted values of capacity gain ratio. 4 case studies of piles in sand have been analyzed by Chun et al. (1999). The values obtained for parameter B and C are summarized in Table C.1.

Parameter B	Parameter C
0.57	2.08
4.33	1.41
0.11	2.02
0.21	1.60

Table C.1: Available values of parameters B and C for Chun et al. (1999) method (Gunaratne, 2006)

For 3 of the 4 case studies analyzed the long-term capacity was reached within 7 days after installation. This is very unlikely considering section 3.2 where respected researchers found set-up periods of at least several months. It is impossible to determine the long term capacity since the exact duration of set-up is unclear.

C.4 Tan et al. (2004)

Tan et al. (2004) reviewed case histories of driven piles in sand and found a trend for capacity development in time that was very similar to the trend found by Bogard and Matlock (1990) for capacity development in time of piles in clay. Tan et al. (2004) proposed an equation that described setup by a hyperbolic function and was based on the method of Bogard and Matlock (1990) describing ultimate capacity development in time for piles installed in clay. The modified method is presented in Equation C.6.

$$Q_t = Q_u(\alpha + (1 - \alpha)(\frac{\frac{t}{T_{50}}}{1 + \frac{t}{T_{50}}})) \tag{C.6}$$

With:

Q_t	=	Pile capacity at time t	kN
Q_u	=	Ultimate pile capacity with 100% of set-up realized	kN
α	=	Empirical coefficient	-
t	=	Time after the end of initial driving	days
T_{50}	=	Time required to realize 50% of pile set-up	days

Tan et al. (2004) selected case histories of piles individually tested by either dynamic or static load tests to validate Equation C.6. Parameter α and T_{50} were determined by fitting the equation with the test results. The values of α and T_{50} varied for the different case histories analyzed. For α Tan et al. (2004) found values ranging between 0.2 and 0.5. For piles in sand it was advised to work with the lower bound of α equal to 0.2. For T_{50} values ranging between 0.7 and 10 days were found for the case histories analyzed.

C.5 Yan & Yuen (2010)

Skov & Svinkin adjusted the Skov and Denver (1988) equation (Equation C.1) to Equation C.7. Adjustment was done for cohesive soils and the equation is basically equal to the old one with a reference time t_0 of 0.1 day and the set-up parameter A is renamed as parameter B. Other parameters are equal to Equation C.1.

$$Q_t = Q_0(1 + B(1 + \log t)) \tag{C.7}$$

Considering Yan and Yuen (2010) a limitation of Equation C.1 and Equation C.7 is that it contains t_0 (either explicit or implicit) and thereby a decrease in capacity is predicted for $t < t_0$. Yan and Yuen (2010) slightly adjusted Equation C.7 to avoid this limitation. The proposed new equation by Yan & Yuen (2010) is presented in Equation C.8. In this equation the C parameter describes the rate of set-up. For Equation C.8 $Q_t = Q_0$ when $t = 0$.

$$Q_t = Q_0(1 + C \log(1 + t)) \tag{C.8}$$

For sand Yan and Yuen (2010) determined the value of B for Equation C.7 and C for Equation C.8 based on a database study. A mean B value of 0.232 was found with a standard deviation of 0.0115. Which equaled a 90% confidence interval between 0.213 and 0.251. A mean C value of 0.418 was found with a standard deviation of 0.0196. Which equaled a 90% confidence interval between 0.385 and 0.451. The database consisted of driven steel, concrete and wooden piles in various lengths and cross sections. The smaller standard deviation of parameter B compared to parameter C indicates Equation C.7 to provide a better indication of time-dependent capacity.

C.6 Reddy & Stuedlein (2014)

Reddy and Stuedlein (2014) analyzed the resistance from initial driving and restrike dynamic testing of 76 piles in the Puget Sound Lowlands of Oregon, USA. The database consisted of driven pre-stressed concrete piles and both closed and open ended steel pipe piles. Restrike periods varied between 5.5 and 312.5 hours, pile diameters ranged from 356 to 914 mm and pile lengths ranged from 8.4 to 48.4 m. Like Tan et al. (2004), Reddy and Stuedlein (2014) approximated the increase in pile capacity due to set-up using a hyperbolic curve and applied this approach to the Skov and Denver (1988) method which resulted in Equation C.9 (Reddy and Stuedlein, 2014).

$$Q_t = \frac{Q_0 * A \log \frac{t}{t_0}}{k_1 + k_2 * Q_0 * A \log \frac{t}{t_0}} + Q_0 \tag{C.9}$$

With:

Q_t	=	Pile capacity at time t	kN
Q_0	=	Pile capacity at reference time t_0	kN
A	=	Constant based on pile type	-
t	=	Time elapsed since the end of initial driving	days
t_0	=	Time elapsed since the end of initial driving	days
k_1	=	Fitting parameter	-
k_2	=	Fitting parameter	-

A is the average setup factor determined per pile type analyzed. Fitting parameters k_1 and k_2 were determined using least squares regression and govern the rate of gain in capacity. The parameters found for the pile database analyzed are presented in Table C.2.

Pile type	A	k_1	k_2
Pre-stressed concrete pile	1.72	0.17	0.00044
Open ended steel pipe pile	0.77	0.15	0.00060
Closed ended steel pipe pile	0.70	0.12	0.00078

Table C.2: Set-up factor and fitting parameters for the Reddy and Stuedlein (2014) method

The shape of the hyperbolic curve is affected by Q_0, where a larger Q_0 indicates a higher initial setup rate. In this research pre-stressed concrete piles exhibited the largest average setup ratio, this pile type also exhibited the largest variability (Reddy and Stuedlein, 2014).

C.7   Karlsrud et al. (2014)

Karlsrud et al. (2014) performed tests at two sand sites in Norway as part of an extensive research on time-dependent pile capacity. Piles with an embedded length of approximately 20 m were tested at a fine sand site in Larvik. At this site 6 of the 7 piles were virgin tested at different moments in time. At a coarse sand site in Rygkollen 6 piles were installed with an embedded length of approximately 15 m. Here 5 piles were statically loaded to failure in a virgin test. The tests moments were roughly 1, 2, 6, 12 and 24 months after installation.
The results found in Norway were compared with the results found by Gavin et al. (2013) and Jardine et al. (2006) who conducted comparable tests in Blessington and Dunkirk respectively. Karlsrud et al. (2014) tried to fit the Skov and Denver (1988) equation (Equation C.1 to the results with a reference time (t_0) of 10 days and found a wide spread in set-up factor (A) for the different sites (respectively 2.4 at Larvik, 5.0 at Ryggkollen and 0.6 at Dunkirk and Blessington). Also, the log-linear fit tended to unreasonable low capacities at the set reference time of 10 days.

The data found at the Norwegian test sites suggest that the capacity gain levels off after approximately 12 months. An alternative approach was suggested by fitting the results to a tanh-fit which described the ultimate shaft capacity in time by a S-shaped curve. The proposed relation is presented in Equation C.10. Since the test were in tension there is only a shaft resistance contribution to the total capacity (Karlsrud et al., 2014).

$$Q_t = Q_0 + a * \tanh(b * (t - t_0)) \tag{C.10}$$

With:

Q_t	=	Shaft capacity at time t	kN
Q_0	=	Shaft capacity at reference time t_0	kN
Q_{10}	=	Shaft capacity at $t_0 = 10$ days (calculated with fitting parameter)	kN
Q_u	=	Ultimate capacity with 100% of setup realized (calculated with fitting parameter)	kN
a	=	Fitting parameter which corresponds to (Q_u - Q_{10})	kN
b	=	Fitting parameter	1/months
t	=	Time elapsed since the end of initial driving	months
t_0	=	Time elapsed since the end of initial driving	months

Karlsrud et al. (2014) determined the best fit of the hyperbolic equation to the results found at the 4 test sites. The values of the parameters giving the best fit are provided in Table C.3.

Test Site	a [kN]	b [1/months]	t_0 [months]	Q_0 [kN]
Larvik (Karlsrud et al., 2014)	260	0.4	2.4	780
Ryggkollen (Karlsrud et al., 2014)	540	0.2	7.0	1280
Dunkirk (Jardine et al., 2006)	1150	0.3	2.0	2100
Blessington (Gavin et al., 2013)	500	0.2	2.0	600

Table C.3: Best-fit values for Equation C.10 per test site

D | Database

The load test results collected for the database study on time-dependent virgin capacity of driven displacement piles are tabulated in this appendix. More information on the test sites and pile tests are available with Yang et al. (2016).

Site ID	Location	Pile ID	Pile type	Length [m]	Width/Diameter [mm]	Inner diameter [mm]	Pile age [days]	Test type	Capacity [kN]	Shaft capacity [kN]	Base capacity [kN]
ZJU-ICL 1	Wuhu, China	K24-1	Circular open-ended concrete	33.0	600	340	5	Compression	2400	Not isolated	Not isolated
		K24-2	Circular open-ended concrete	39.8	600	340	14	Compression	4400	Not isolated	Not isolated
		K24-3	Square open-ended concrete	39.8	500	310	13	Compression	4450	Not isolated	Not isolated
ZJU-ICL 4	Rio de Janeiro, Brazil	PI-1	Square concrete	37.2	500	-	64	Compression	3590	Not isolated	Not isolated
		PI-2	Square concrete	21.4	500	-	72	Compression	1950	Not isolated	Not isolated
ZJU-ICL 5	Rio de Janeiro, Brazil	PI-3	Square concrete	35.6	700	-	89	Compression	6010	3680	550 (Not fully mobilized)
		PI-4	Square concrete	26.5	500	-	86	Compression	4532	2732	1800
ZJU-ICL 6	Blessington Dublin, Ireland	S2	Open-ended steel	7.0	340	312	2	Tension	344	344	-
		S3	Open-ended steel	7.0	340	312	13	Tension	665	665	-
		S5	Open-ended steel	7.0	340	312	220	Tension	990	990	-
ZJU-ICL 7	Horstwalde, Germany	P2D	Open-ended steel	17.69	711	661	34	Tension	1400	1400	-
		P5B	Open-ended steel	17.71	711	686	36	Tension	1420	1420	-
		P5D	Open-ended steel	17.76	711	686	29	Tension	950	950	-
		P4B	Open-ended steel	17.67	711	686	37	Tension	1550	1550	-
		P4D	Open-ended steel	17.66	711	686	32	Tension	1250	1250	-
		P3B	Open-ended steel	17.63	711	686	116	Tension	1900	1900	-
		P3D	Open-ended steel	17.74	711	686	30	Tension	1120	1120	-
ZJU-ICL 24	Larvik, Norway	L1-1	Open-ended steel	21.5	508	495.4	43	Tension	980	980	-
		L2-1	Open-ended steel	21.5	508	495.4	135	Tension	990	990	-
		L3-1	Open-ended steel	21.5	508	495.4	218	Tension	1160	1160	-
		L4-1	Open-ended steel	21.5	508	495.4	365	Tension	1065	1065	-
		L5-1	Open-ended steel	21.5	508	495.4	730	Tension	1080	1080	-
		L6-1	Open-ended steel	21.5	508	495.4	730	Tension	900	900	-
		L7-1	Open-ended steel	21.5	508	495.4	30	Tension	600	600	-

Table continues on next page

Site ID	Location	Pile ID	Pile type	Length [m]	Width/ Diameter [mm]	Inner diameter [mm]	Pile age [days]	Test type	Capacity [kN]	Shaft capacity [kN]	Base capacity [kN]
ZJU-ICL 29	Hoogzand, The Netherlands	1-C	Open-ended steel	7	356	324	37	Compression	2270	1310	1130
		1-T	Open-ended steel	7	356	324	37	Tension	820	820	-
		3-C	Open-ended steel	5.3	356	316	19	Compression	1850	Not isolated	Not isolated
		3-T	Open-ended steel	5.3	356	316	19	Tension	530	530	-
ZJU-ICL 32	Hound Point, Scotland	P(O)-C	Open-ended steel	26	1220	1171.6	21	Compression	7000	4000	3000
		P(O)-T1	Open-ended steel	34	1220	1171.6	4	Tension	3860	3860	-
		P(O)-T2	Open-ended steel	41	1220	1171.6	4	Tension	3740	3740	-
ZJU-ICL 34	Baghdad, Iraq	P1-C	Square concrete	11	253	-	88	Compression	950	580	370
		P1-T	Square concrete	11	253	-	200	Tension	580	580	-
		P2-C	Square concrete	15	253	-	42	Compression	1610	1251	359
ZJU-ICL 35	Dunkirk CLAROM, France	CL-T	Open-ended steel	11.3	324	298.6	175	Tension	444	444	-
		CS-T	Open-ended steel	11.3	324	298.6	187	Tension	400	400	-
ZJU-ICL 36	Dunkirk GOPAL, France	R1-T	Open-ended steel	19.31	457	430	9	Tension	1450	1450	-
		C1-C	Open-ended steel	10.02	457	430	68	Compression	2820	2820	Not isolated
		C1-T	Open-ended steel	10.02	457	430	69	Tension	820	820	
Jardine et al. (2006)		R2-T	Open-ended steel	18.85	457	430	235	Tension	3210	3210	-
Jardine et al. (2006)		R6-T	Open-ended steel	18.9	457	430	80	Tension	2400	2400	-
ZJU-ICL 37	Euripides, The Netherlands	Ia	Open-ended steel	30.5	763	691.8	7	Compression	7400	3400	4000
		Ib	Open-ended steel	38.7	763	691.8	2	Compression	13000	9500	3500
		Ic	Open-ended steel	47	763	691.8	12	Compression	18800	14050	4750
		Ia-T	Open-ended steel	30.5	763	691.8	7	Tension	1660	1660	-
		Ib-T	Open-ended steel	38.7	763	691.8	2	Tension	8400	8400	-
		Ic-T	Open-ended steel	47	763	691.8	12	Tension	12500	12500	-

Table continues on next page

Site ID	Location	Pile ID	Pile type	Length [m]	Width/ Diameter [mm]	Inner diameter [mm]	Pile age [days]	Test type	Capacity [kN]	Shaft capacity [kN]	Base capacity [kN]
ZJU-ICL 39	Locks and Dam, USA	3-1	Closed-ended steel	14.2	305	-	35	Compression	1170	Not isolated	Not isolated
		3-4	Closed-ended steel	14.4	356	-	27	Compression	1150	Not isolated	Not isolated
		3-7	Closed-ended steel	14.6	406	-	28	Compression	1620	Not isolated	Not isolated
		3-2	Closed-ended steel	11	406	-	35	Tension	540	540	-
		3-5	Closed-ended steel	11.1	305	-	27	Tension	610	610	-
		3-8	Closed-ended steel	11	406	-	35	Tension	900	900	-
ZJU-ICL 46	Shanghai, China	ST-1	Open-ended steel	79	914	874	23	Compression	15560	11460	4100
		ST-2	Open-ended steel	79.1	914	874	35	Compression	17080	14570	2510
ZJU-ICL 49	Fittja Straits, Sweden	D-5	Square concrete	12.8	235	-	5	Compression	340	Not isolated	Not isolated
		D-1	Square concrete	13	235	-	1	Compression	310	Not isolated	Not isolated

E | Pile Tests Program Illustration

This appendix provides a photographic visualization of the test program.

Test Pit

Test Frame

Pile Installation

Load Test